LSU Doctoral Dissertations   Graduate School

2007

Chiral analyses using molecualr micelles and multiple regression modeling in chromatographic and spectroscopic methods

Alicia Williams Snearl
Louisiana State University and Agricultural and Mechanical College, awill56@lsu.edu

CHIRAL ANALYSES USING MOLECULAR MICELLES AND MULTIPLE REGRESSION
MODELING IN CHROMATOGRAPHIC AND SPECTROSCOPIC METHODS

A Dissertation

Submitted to the Graduate Faculty of the
Louisiana State University and
Agricultural and Mechanical College
in partial fulfillment of the
requirements for the degree of
Doctor of Philosophy

in

The Department of Chemistry

by
Alicia Williams Snearl
B.S. Xavier University of Louisiana, 2002
December, 2007

*To my parents, Paul and Pam, for their guidance and
my husband, Dedrick, for his continuous support.*

ACKNOWLEDGEMENTS

The completion of this work would not have been possible without the generosity and support of many people.

Dr. Isiah M. Warner, for his guidance, patience, wisdom, and knowledge. It has been an honor and a privilege working with one of the greatest mentors in my field. Most of all, I appreciate the toughness which encouraged me to realize my potential.

Committee Members, for their time, helpful comments, and especially for making sure my data analysis is statistically correct.

Dr. Sayo O. Fakayode, for introducing me to the world of chemometrics. I will always be grateful for the endless hours we spent working together.

Dr. Kristin Fletcher, for taking her time to review my manuscripts. I will never be able to repay you for your exceptional editing skills.

Dr. Mark Lowry, for his help understanding fluorescence concepts and for teaching me to have an appreciation for excel spreadsheets.

Dr. Onur Alptürk, for our collaborations with characterization techniques.

Candace Luces, for helping me prepare thousands of samples and for keeping me company many evenings while completing my experiments. You are truly an amazing friend.

Christina Jones, the smartest undergraduate freshmen I have ever known, for the time dedicated to understanding my research work and all of the hours spent synthesizing molecular micelles.

Warner Research Group, for your friendship and support through the years, especially during the loss of many family members.

TABLE OF CONTENTS

LIST OF ABBREVIATIONS

Abbreviation	Name
BENZ	benzoin
BGE	background electrolyte
BNA	1,1′-binaphthyl-2,2′-diamine
BNP	1,1′-bi-2-naphthyl-2,2′-dihydrogen phosphate
BOH	1,1′-bi-2-naphthol
CD	circular dichroism
CDs	cyclodextrins
CE	capillary electrophoresis
CEC	capillary electrochromatography
CGE	capillary gel electrophoresis
CIEF	capillary isoelectric focusing
CIT	citramalic acid
CITP	capillary isotachophoresis
CMC	critical micelle concentration
CME	chloromethyl menthyl ether
COUM	coumachlor
CPL	4-chlorophenol
CZE	capillary zone electrophoresis
CZP	clonazepam
DCC	dicyclohexylcarbodiimide
DZP	diazepam

EOF	electroosmotic flow
FCMM	fluorescent chiral molecular micelle
GC	gas chromatography
HB	hydrobenzoin
HCl	hydrochloric acid
HPLC	high performance liquid chromatography
MEKC	micellar electrokinetic chromatography
LIM	limonene
LZP	lorazepam
MLR	multivariate linear regression
MS	mass spectrometry
NaOH	sodium hydroxide
NHS	*N*-hydroxysuccinimide
NMR	nuclear magnetic resonance
NPRX	naproxen
ORD	optical rotary dispersion
PC	principal component
PCL	pentachlorophenol
PCR	principal component regression
PLS-1	partial-least-squares regression
Poly-L-SUL	poly(sodium *N*-undecanoyl-L-leucinate)
Poly-L-SUILV	poly(sodium *N*-undecanoyl-L-isoleucylvalinate)
Poly-L-SULV	poly(sodium *N*-undecanoyl-L-leucylvalinate)

Poly-L-SUV	poly(sodium N-undecanoyl-L-valinate)
Poly-SUF	poly(sodium N-undecanoyl-phenylalaninate)
Poly-SUS	poly(sodium N-undecylenic sulfate)
Poly-SUW	poly(sodium N-undecanoyl-tryptophanate)
Poly-SUY	poly(sodium N-undecanoyl-tyrosinate)
PROP	propranolol
RMS%RE	root-mean-square percent relative error
SiO$^-$	deprotonated silanol groups
TAR	tartaric acid
THF	tetrahydrofuran
TFA	2,2,2-trifluoroanthrylethanol
TRIS	tris(hydroxymethyl)aminomethane
TZP	temazepam
WAR	warfarin
Xe	xenon

ABSTRACT

Multiple regression modeling techniques allow for rapid and accurate prediction of migration times and resolution values for micellar electrokinetic chromatography (MEKC) as well as the development of quick screening methods using steady-state fluorescence spectroscopy. All studies reported in this dissertation include optimization of calibration models and predictions of dependent variables by the use of validation samples. The root-mean-square percent relative error (*RMS%RE*) is used as a figure of merit for characterizing the performance of the calibration models. MEKC separations of achiral and chiral analytes were performed using an achiral molecular micelle, poly(sodium *N*-undecylenic sulfate), and chiral molecular micelles, poly(sodium *N*-undecanoyl-L-leucylvalinate) or poly(sodium *N*-undecanoyl-L-isoleucylvalinate), at various operating temperatures, applied voltages, pH, and molecular micelle concentrations in the background electrolyte. The *RMS%RE* values of predicted migration time, resolution, and resolution per unit time of the chiral as well as the achiral analytes ranged from 8.78 to 37.73% for all MEKC studies. Chiral analysis using steady-state fluorescence spectroscopy was employed to investigate the use of chiral molecular micelles as chiral selectors by multivariate regression modeling of spectral data. PLS-1 was used to correlate changes in the fluorescence emission intensity of several fluorescent analytes in the presence of non-fluorescent molecular micelles and fluorescent chiral molecular micelles (FCMMs) in the presence of non-fluorescent analytes. In terms of *RMS%RE*, the ability of the model to accurately predict the enantiomeric composition of future samples was dependent on the chiral analyte, molecular micelle, as well as the solvent medium, and ranged between 1.21 and 6.10 %.

CHAPTER 1

INTRODUCTION

1.1 Chirality

Optical activity was first observed by the French physicist, Jean Baptiste Biot, in 1813 when he studied the behavior of the vibrational plane of polarized light.[1] He discovered that certain liquids rotate the plane of polarization in equal magnitude but opposite direction. Clockwise rotation, rotation to the right, is considered to be dextrorotary and is designated by a (+) sign. Likewise, counterclockwise rotation, rotation to the left, is levorotary and is designated by a (-) sign. A chiral compound is optically inactive if it is a racemic mixture and there is no rotation of the plane of polarized light.

Optical isomers or enantiomers exist because they are chiral compounds. Chirality was discovered by Louis Pasteur in 1848 when he demonstrated the optical inactivity of a racemic sample of tartaric acid. In addition, he separated the enantiomers and observed that the crystals rotated polarized light in opposite directions with the same magnitude.[2] As a result, Pasteur concluded that optically active molecules are due to asymmetric atoms. In 1874, Jacobus Henricus van't Hoff related the chemical bonds of the carbon atom in optically active compounds to a three-dimensional tetrahedron.[3] He discovered that enantiomers differ in their three-dimensional spatial arrangement. Two enantiomers have the same physical properties, i.e. boiling point, melting point, density, dipole moment, and refractive index, and the same chemical properties unless in the presence of other chiral molecules.

The word chiral originates from a Greek word meaning hand, and one of the most universal examples of chirality is the human hands (Figure 1.1).[4] Any molecule lacking a plane, center, or axis of symmetry, and having a non-superimposable mirror image is a chiral

molecule.[5] Two most common classes of chiral compounds are molecules that have point (asymmetric atom) or axial chirality (asymmetric plane) and are illustrated in Figure 1.2. A molecule with point chirality has a carbon atom with four different substituents. Although most chiral molecules have point chirality, a stereogenic carbon is not necessary for a molecule to exist in enantiomeric form. Many compounds have an axis of chirality where there is restricted rotation around a bond and a non-superimposable spatial arrangement exists. The enantiomers of these molecules are usually named by use of the *R/S* configuration system which is based on the geometry of each enantiomer.
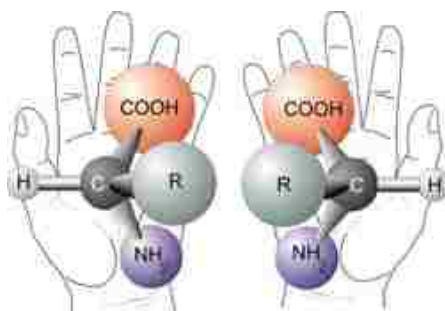
Figure 1.1   Universal example of chirality (reproduced from reference 4).

point chirality
(asymmetric atom)

axial chirality
(asymmetric plane)
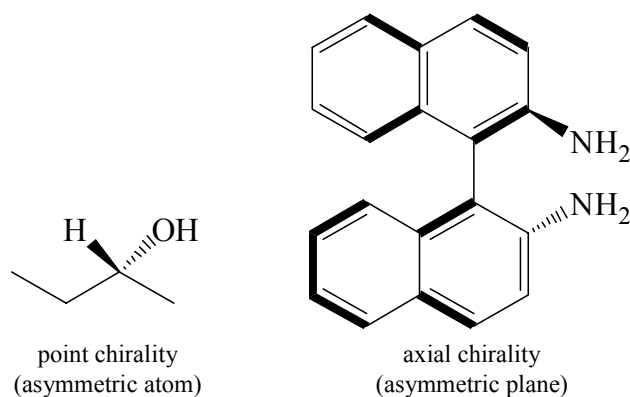
Figure 1.2   Structures of two types of chiral molecules.

Molecules having point chirality may also use the *R/S* naming system based on the Cahn-Ingold-Prelog priority rules.[6]   There are four basic rules for naming an enantiomer using this system: 1)

identify the asymmetric carbon, 2) assign the priority to each group (higher atomic number is given priority and higher atomic mass is given priority) using the sequence $1 > 2 > 3 > 4$, 3) the lowest priority group [4] is viewed so that it is positioned away from the viewer, and 4) the remaining three groups are counted in the direction from the highest priority. If the direction is clockwise, the enantiomer is designated *R* or *rectus* (meaning right in Latin). Likewise, if the direction is counterclockwise, the enantiomer is designated *S* or *sinister* (meaning left in Latin). An example of this process is illustrated in Figure 1.3. The substituents are prioritized, and the direction of decreasing priority number is counterclockwise. Thus, the molecule as illustrated in Figure 1.3 is the *S*-enantiomer. Other naming systems include the *D/L* and (+)/(-) naming conventions and are unrelated to the *R/S* naming convention. As previously noted, the (+)/(-) system is based on optical activity. Similar to the *R/S* system, the *D/L* naming convention is based on configuration.
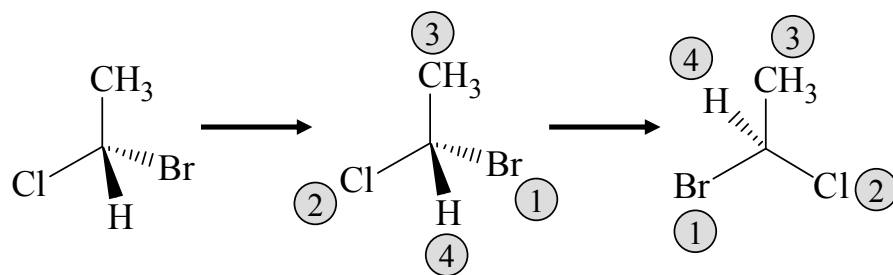
Figure 1.3   Cahn-Ingold-Prelog sequence rules for the *S*-enantiomer configuration of a chiral molecule.

Chirality is important in many industries including the pharmaceutical industry due to differences in pharmacological and physiological properties of enantiomers. One enantiomer of a chiral drug may have therapeutic effects and the other enantiomer may be ineffective or toxic.[7-13] A well known occurrence that demonstrated the importance of enantiomeric activity was the thalidomide tragedy of the 1960s.[5] This chiral drug is a classical example of the different

pharmacokinetic characteristics of individual isomers. Thalidomide was prescribed in racemic form as a sedative to pregnant women to treat morning sickness. As a result, many babies suffered from birth defects and some were even stillborn. This was due to the different pharmacological activity of each enantiomer of thalidomide. The *R*-enantiomer is the therapeutic form of the drug that was responsible for the desired treatment and the *S*-enantiomer is the teratogenic form responsible for the birth defects.[14]

In an effort to eliminate potential toxic side effects, many drugs are marketed as a single enantiomer. In addition, the Food and Drug Administration is demanding the accurate determination of purity for the production of single enantiomer drugs.[15] This is an ongoing challenge because 80% of the chiral market is found in the pharmaceutical industry and the number of chiral drugs and drug sales continues to increase every year.[16,17] Figure 1.4 illustrates the increase in chiral drug sales and the increase of the amount of chiral drugs marketed as single enantiomers from 1996 to 2002.
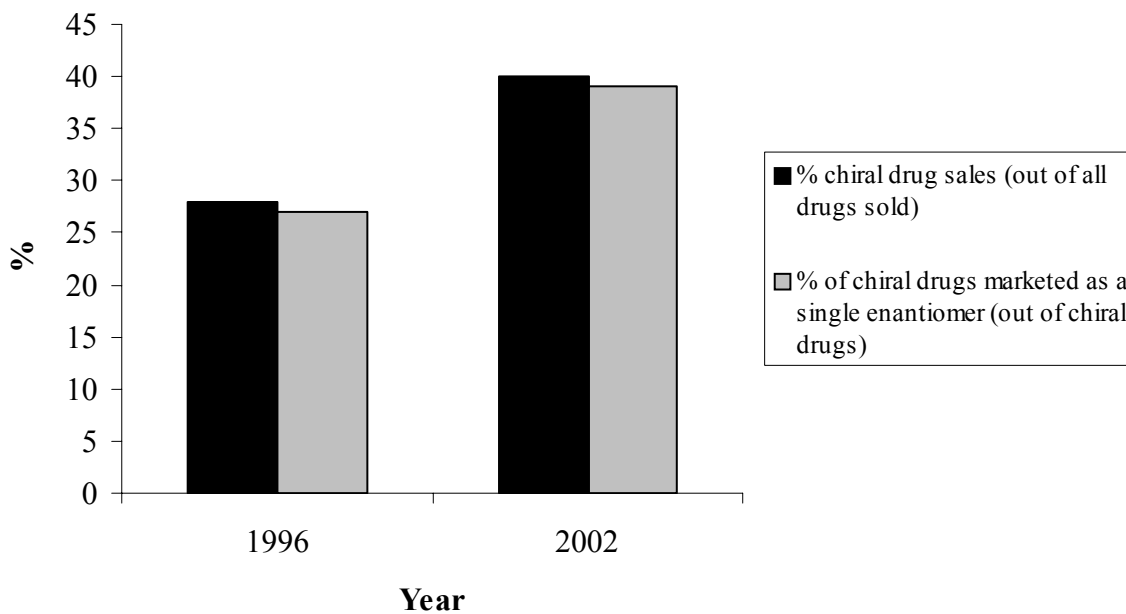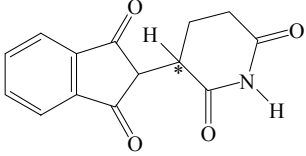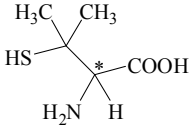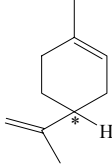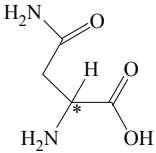
Figure 1.4 The chiral market worldwide.[16,17]

Chirality also plays an important role in the agricultural, fragrance, and food industries. Some chiral pesticides and herbicides may have different insecticidal or herbicidal effects where one form can be harmful to our environment or to humans while the other form is responsible for controlling pests or weeds. In the food and fragrance industries, chiral compounds have been found to have different tastes and smells.[12] Table 1.1 summarizes the different activities of some chiral molecules found in the pharmaceutical, agricultural, fragrance, and food industries.

Table 1.1   Enantiomeric activity of chiral compounds.[12,13]

Compound	Enantiomeric Activity	Structure
Thalidomide	R – sedative S – teratogen	
Penacillamine	R – mutagen S – antiarthritic	
Limonene	R – lemon smell/taste S – orange smell/taste	
Asparagine	D – sweet taste L – bitter taste	

1.2 Methods of Chiral Analysis

Chiral discrimination of two enantiomers requires the formation of a diastereomeric complex between the enantiomer and a chiral selector. A chiral selector is a chiral auxiliary agent capable of interacting enantioselectively with a pair of enantiomers. Once this complexation occurs, the diastereomers can be analyzed using several analytical techniques. Unlike enantiomers, diastereomers are not mirror images and have different physical and chemical properties which allow for discrimination between a diastereomeric pair. Additional studies are needed to understand the exact mechanism of chiral recognition, however, the "three-point interaction rule" provides some insight into the complex formation.[18,19] Figure 1.5 illustrates the interaction between a chiral selector and an enantiomer. This model depicts the mechanism that requires the interaction of at least three points on one enantiomer with the chiral selector for chiral recognition to occur. Spatial restraints prevent the other enantiomer from interacting in the same way with the chiral selector.
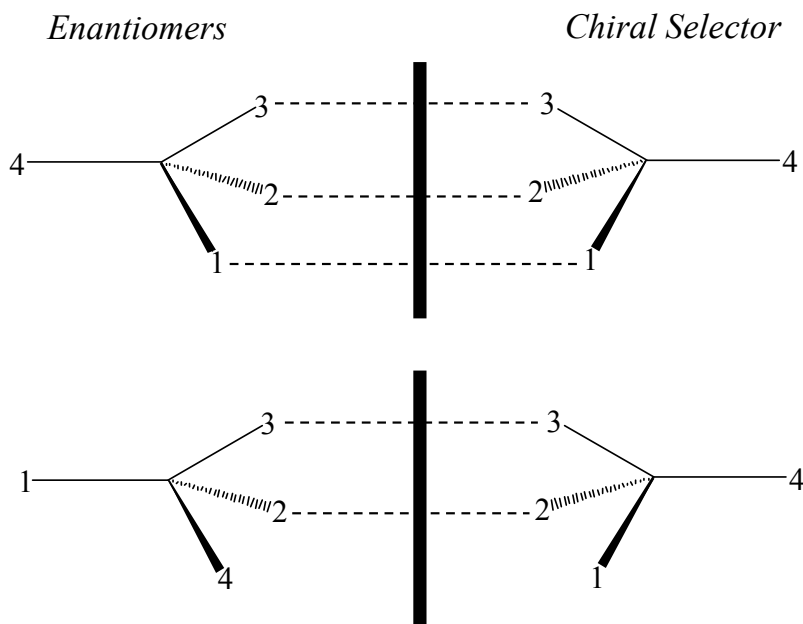
Figure 1.5 Three-point interaction rule.

1.2.1 Capillary Electrophoresis

Gas chromatography (GC) and high performance liquid chromatography (HPLC) have been some of the most widely used chromatographic techniques for chiral separation.[20] As previously noted, separation is achieved due to the formation of a diastereomeric complex between an enantiomer and a chiral selector. These diastereomers have a different boiling point, volatility, and polarity, which allows for separation using GC and HPLC. In general, a column contains a sample which is dissolved or suspended in a gas or liquid mobile phase that interacts with a stationary phase. The sample components have different solubilities in the mobile and stationary phases. As a result, the components separate while traveling through a column due to varying mobilities. While GC and HPLC are unquestionably effective, there are some major drawbacks, including the analysis time and sample consumption using HPLC and the requirement that the analytes are volatile for GC.

The use of capillary electrophoresis (CE) addresses some of the disadvantages encountered with HPLC and GC. CE is a separation technique capable of the high resolution of diverse analytes while consuming small amounts of sample and reagents. Some of the first CE experiments were performed by Hjerten in 1967.[21] Years later, Mikkers *et al*.[22] and Jorgenson and Lukacs[23] demonstrated that CE could achieve high resolution of small pharmaceutical analytes and polymers. The electrophoresis occurs in a narrow-bore silica capillary, and the separation is based upon the differences in the electrophoretic mobility of solutes dissolved in buffer under an applied electric field. CE instrumentation is simple and consists of a capillary, buffer reservoirs, a sample reservoir, a high-voltage power supply, two electrodes (anode and cathode), a detector, and a data output and handling device (see Figure 1.6). The ends of the capillary are positioned in the buffer reservoirs which contain the two electrodes used to supply

7

current from the high voltage supply. The capillary is filled with buffer prior to sample injection. The migration of the analytes occurs when the buffer reservoir replaces the sample reservoir and an electric field is applied.[20]
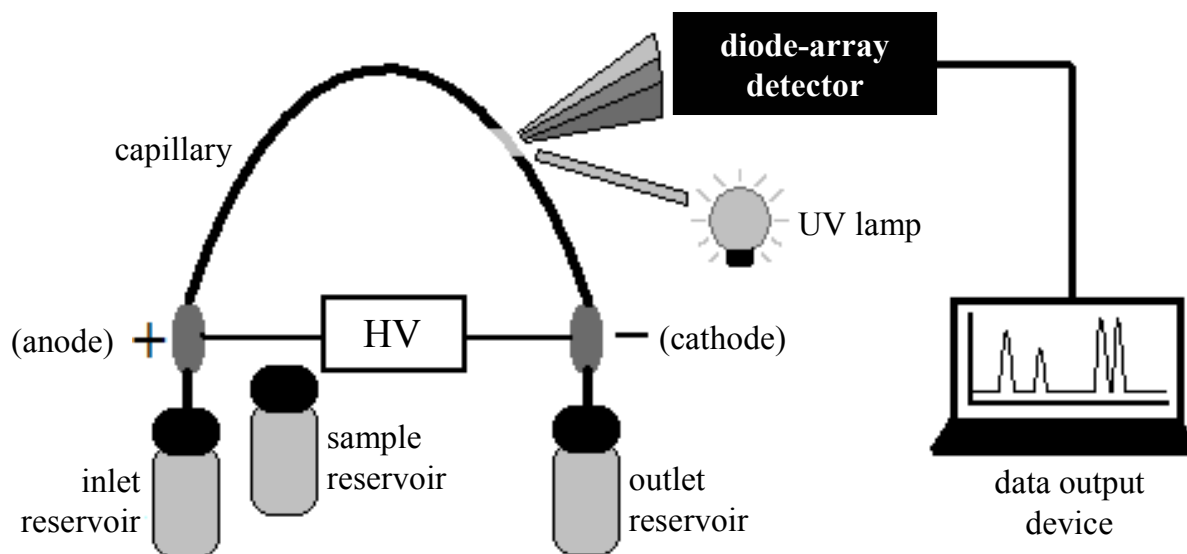
Figure 1.6   Schematic of CE instrumentation.

There are numerous modes of CE including capillary zone electrophoresis (CZE), micellar electrokinetic chromatography (MEKC), capillary isoelectric focusing (CIEF), capillary gel electrophoresis (CGE), capillary isotachophoresis (CITP), and capillary electrochromatography (CEC).[20] Table 1.2 lists a brief description of each mode, which all have different mechanisms of separation; however, the same fundamental theory and principles. This family of CE techniques has a wide application range and is capable of separating several different classes of analytes including small ions, small achiral and chiral molecules, peptides, proteins, oligo-nucleotides, and DNA.[20]

Table 1.2   Modes of CE.[20]

Mode	Brief Description	Class of Analytes
CZE	separation performed in buffer, also known as free solution CE	Small ions, small charged molecules, peptides, proteins
MEKC	CZE with the addition of surfactants serving as pseudostationary phase	Small charged/uncharged molecules, peptides, oligonucleotides
CIEF	CZE with the addition of ampholines	Peptides, proteins
CGE	CZE with the addition of a sieving matrix	Peptides, proteins, oligo-nucleotides, DNA
CITP	On-capillary pre-concentration technique	Small ions, small charged/uncharged molecules, peptides, proteins
CEC	Separation performed using an immobilized stationary phase	Small ions, small molecules, peptides, proteins, oligonucleotides

The driving force for flow in many CE modes, including MEKC, is electroosmotic flow (EOF). In normal mode, the EOF causes the bulk flow of the components (ionic and neutral) from anode to cathode as a result of the formation of an electric double layer or Stern layer on the inner capillary wall. Figure 1.7 illustrates the formation of the Stern layer and the development of the EOF which occurs in several steps:[24]

1. The deprotonation of the capillary wall forms silanol groups (SiO^-).

2. Counterions (cations) are attracted to the SiO^- groups in order to maintain a charge balance

3. A voltage is applied across the capillary and the cations are attracted toward the cathode.

Step 1. Deprotonation of the capillary wall.
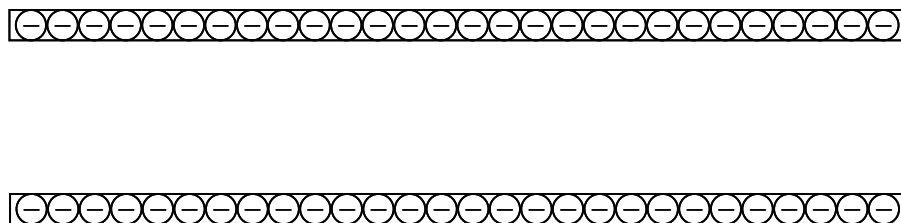
Step 2. Cations are attracted to capillary wall, Stern layer formation

Stern layer

diffuse layer

+ anode
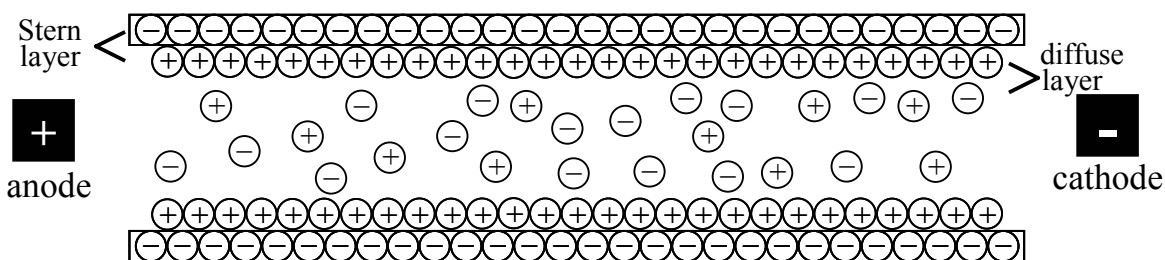
- cathode

Step 3. Applied voltage causes cations to migrate toward cathode

+ anode

- cathode

deprotonated capillary wall (SiO⁻)

$\ominus$ anion

$\oplus$ cation

electrophoretic mobilities

net flow
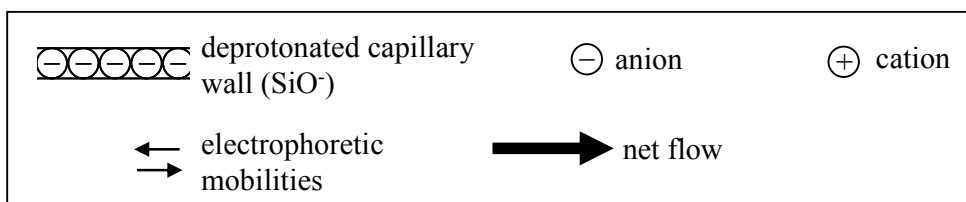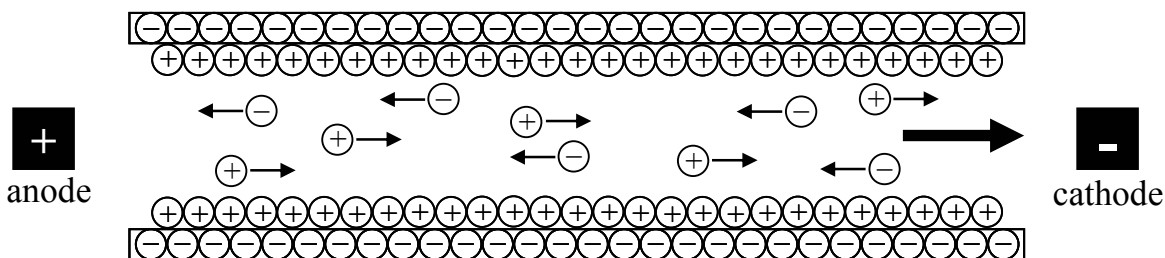
Figure 1.7   Development of the EOF.

The overall movement of all charged and neutral species to the cathode occurs because the cations are solvated. In CEC the magnitude of the EOF is calculated by:

$$\nu_{EOF} = (\varepsilon \, \zeta \, / \, \eta) \, E \qquad\qquad 1.1$$

$$\mu_{EOF} = (\varepsilon \, \zeta \, / \, \eta) \qquad\qquad 1.2$$

where ν is the velocity of the EOF, μ is the mobility of the EOF, ε is the dielectric constant, ζ is the zeta potential, η is the solvent viscocity, and E is the applied electric field. It is interesting to observe that the mobility of the EOF is independent of the applied electric field. The zeta potential occurs in the diffuse layer inside of the capillary and is determined by the extent of the charge on the capillary wall, which is pH dependent.[20,24] Therefore, higher buffer pH values will increase the number of SiO⁻ groups and increase the EOF. Likewise, lower buffer pH values will decrease the number of SiO⁻ groups and decrease the EOF.

The separation of ions is based upon the solute velocity while neutral species migrate with the EOF. The ion velocity is the product of the electrophoretic mobility and the applied electric field. As the applied electric field is increased, the velocity increases. The electrophoretic mobility depends on the electric force, which is the product of the charge of the ion and the applied electric field, and the counteracting frictional force. The two forces are opposite and result in the electrophoretic mobility being dependent on the charge and size of the ions. This relationship is given in the following equation:

$$\mu_e = q \, / \, (6 \, \pi \, \eta \, r) \qquad\qquad 1.3$$

where q is the charge of the ion, η is the solution viscosity, and r is the radius of the ion. In a given sample, the charge-to-size ratio will determine the elution order of ionic species. From equation 1.3, it can be concluded that larger solutes will have higher electrophoretic mobilities than smaller solutes of the same charge. The elution order of solutes is determined by the

apparent mobility (μ_{app}), which is simply the sum of the electrophoretic mobility of the ion and the mobility due to the EOF. Figure 1.8 illustrates the elution order of ions of different charge and size in CZE.
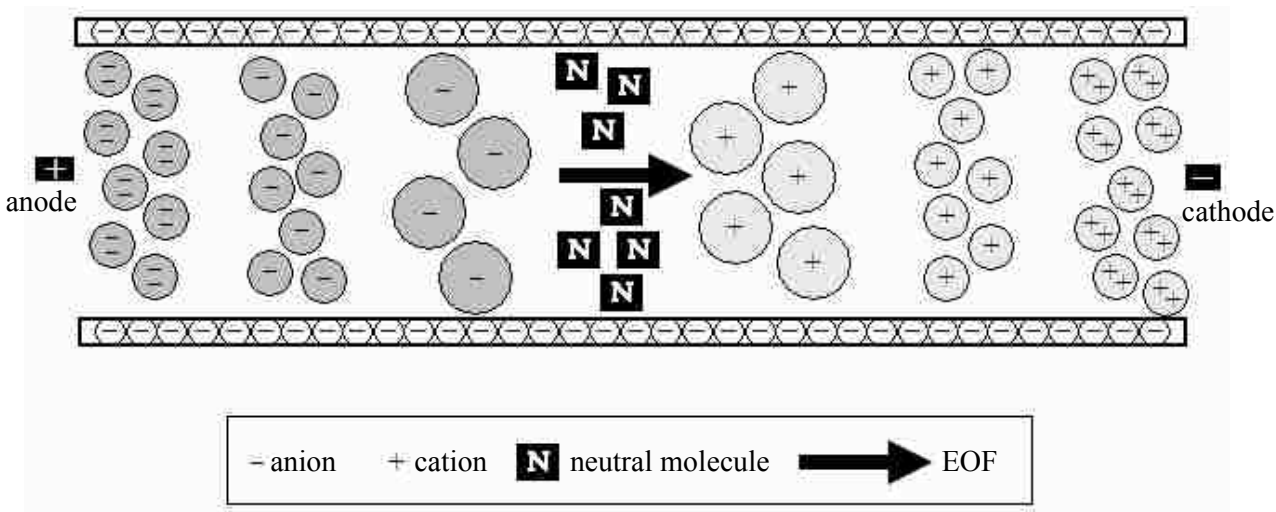
Figure 1.8   Solute elution order in CZE.

As illustrated in Figure 1.8, neutral molecules migrate with the EOF because they have no electrophoretic mobility. Therefore, it is not possible to separate neutral species by use of CZE. In the mid 1980s, Terabe introduced MEKC, a mode of CE capable of separating neutral species with the addition of charged species to the running buffer.[25,26] Separation of neutral and charged species for both achiral and chiral analytes can be accomplished by MEKC due to several factors including differences in electrophoretic mobility of the complex formed, hydrophobicity, ionic interactions, and hydrogen bonding between the charged selector and the analyte.[20]

The most widely used additives for the separation of neutral species are molecular aggregates known as micelles. Surfactant monomers consist of a hydrophobic tail and a charged hydrophilic head group. As the concentration of monomers increases in aqueous solution,

aggregates self assemble to form hydrophobic pockets. This phenomena occurs for all types of surfactants, including nonionic, anionic, cationic, and zwitterionic. At a certain concentration known as the critical micelle concentration (CMC), organized assemblies of surfactant monomers are formed. Micellar aggregates consist of hydrophobic tails which are directed inside of the micelle and have limited interaction with the solvent, while the hydrophilic head groups form the outer shell of the micelle. The hydrophobic core of the micelle provides an environment that can solubilize non-polar analytes. Du-Nouy first introduced the apparatus for surface tension measurements[27] that would later be used for CMC determination of surfactants. As the concentration of surfactant monomers increase, the surface tension decreases and at concentrations above the CMC, there is no change in the surface tension (see Figure 1.9).
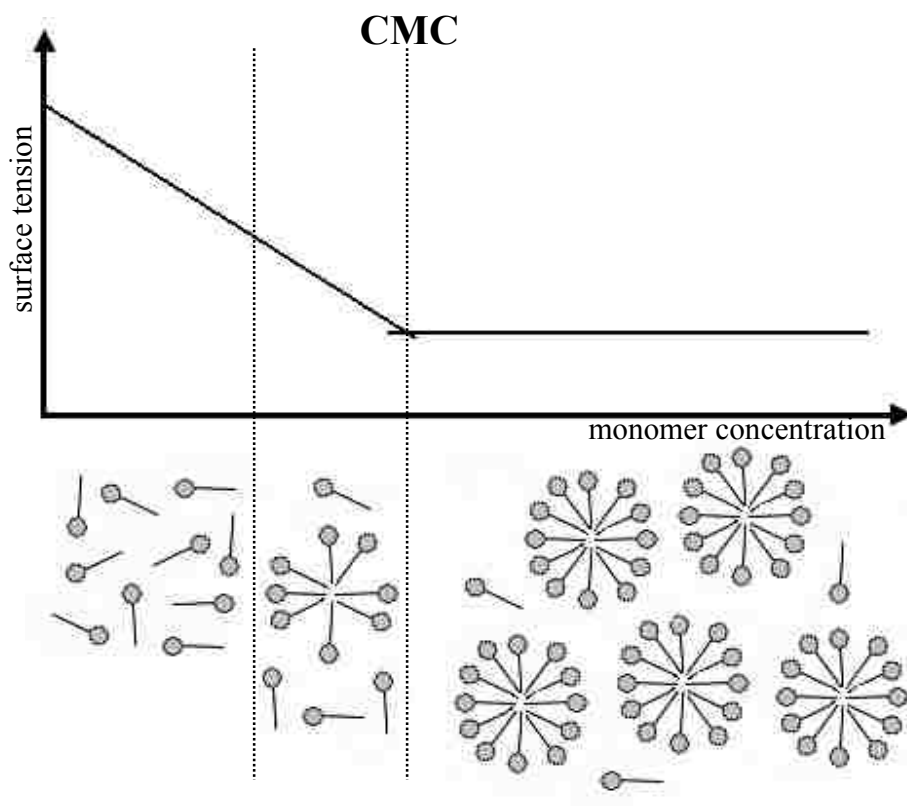
Figure 1.9 Micelle formation and CMC determination by surface tension measurements.

As previously noted, there are several conditions necessary for the separation of neutral analytes to occur using MEKC. The presence of the micelle will result in complexes formed with the analytes based on hydrogen bonding, hydrophobic interactions, and/or electrostatic interactions. The extent of the separation of all analytes can be altered by changing several experimental conditions including buffer concentration, micelle size, micelle charge, surfactant concentration, pH of the running buffer, operating temperature, mobile phase modifiers, and the applied voltage. These experimental conditions will ultimately play an important role in the migration time as well as the resolution of the analytes.

Baseline resolution (R_s = 1.5) in a reasonable migration time is the ultimate goal of any separation. The resolution depends on the efficiency of the separation, the retention of the solutes, and the selectivity of the system. Therefore, optimization studies of experimental parameters affecting these factors are important in MEKC separations. Separations with high efficiency values (N) have sharp and symmetrical peaks. Peak tailing or fronting can result in lower resolution values. Experimentally, efficiency is determined by:

$$N = 5.54 \, (t_n / w_{1/2})^2$$

$$1.4$$

where N is the number of theoretical plates, t_n is the elution time for peak n, and $w_{1/2}$ is the peak width at half height.

A solute partitions between the mobile phase and the micelle. The ratio of the molar concentration of the solute in the pseudostationary phase (or micellar phase) to the molar concentration of the solute in the mobile phase is given by the capacity factor (k`),

$$k` = \frac{(t_r - t_o)}{t_o \, (1 - t_r/t_m)} = K \, \frac{V_s}{V_m}$$

$$1.5$$

where t_r is the retention time of the solute, t_o is the retention time of the unretained solute, t_m is the retention time of the solute retained by the micellar phase. The capacity factor is related to the partition coefficient (K) which is determined by the volume of the micellar phase (V_s) and the volume of the mobile phase (V_m). Solutes that elute with the EOF at t_o do not complex with the micellar phase however solutes that are completely solubilized by the micelle will elute at t_m. All other solutes will elute between t_o and t_m. Separation of solutes is possible if the capacity factors of two solutes are not the same. The selectivity factor (α) is used to determine if two solutes have different interactions with the pseudostationary phase.

$$\alpha = k'_2 / k'_1 \text{ , where } k'_2 > k'_1 \tag{1.6}$$

A system capable of resolving two species will have $\alpha > 1$. A selectivity of 1 means there is no separation and the resolution is 0 as given in the following equation:

$$Rs = \left(\frac{N^{1/2}}{4}\right) \left(\frac{\alpha - 1}{\alpha}\right) \left(\frac{k'_2}{k'_2 + 1}\right) \left(\frac{1 - (t_o/t_m)}{1 - (t_o/t_m)\, k'_1}\right) \tag{1.7}$$

where N is the number of theoretical plates, α is the selectivity, k'_2 and k'_1 are the capacity factors for solutes, t_o is the retention time of the unretained solute, and t_m is the retention time of the solute retained by the micelle. When calculating the experimental resolution, the following equation is used:

$$Rs = \frac{2(t_2 - t_1)}{w_1 + w_2} \tag{1.8}$$

where w_1 and w_2 are the baseline widths of peaks 1 and 2, respectively.

Although many experimental factors affect the resolution during MEKC separations, the concentration of micelles, applied voltage, pH of the running buffer, and operating temperature were optimized as described in Chapter 2 of this dissertation. Generally, the capacity factor can be improved by increasing the concentration of surfactant; however, high concentrations may

lead to current problems.[24] This limitation can be eliminated by the use of molecular micelles as opposed to conventional micelles. A brief discussion of molecular micelles can be found in section 1.3. Varying the electric field (applied voltage), buffer pH, and operating temperature can affect the magnitude of the EOF. Changing the electric field will result in a change of the velocity of the EOF as given in equation 1.1. Lower applied voltages results in a slower EOF which may cause lower separation efficiency, while higher applied voltages may cause Joule heating which is the heat generated as a result of electrical current.[24] Changing the buffer pH has an affect on the magnitude of the EOF as well as the solute charge. High pH values result in a higher percent of deprotonated silanol groups and a faster EOF while low pH values protonate the silanol groups and result in a slower EOF. The operating temperature is important for reproducibility by controlling injection volume, minimizing Joule heating, and altering the viscosity of the buffer.

1.2.2 Fluorescence Spectroscopy

By definition, all spectroscopic techniques involve the interaction between radiation and matter and are used in analytical chemistry for the identification of substances.[28] Fluorescence spectroscopy is a relatively inexpensive and highly sensitive spectroscopic method for accurate and rapid chiral analysis. Fluorescence involves the absorption of light at a given wavelength followed by the emission of light at longer wavelengths.[28] This process is demonstrated by the Jablonski Diagram which was proposed by the Polish physicist Alexander Jablonski in 1935 to describe the absorption and emission of light.[28] Figure 1.10 illustrates possible transitions between electronic states of a molecule. A molecule absorbs a photon of light which promotes an electron to a higher energy level. Before relaxing back to the electronic ground state (S_0) by fluorescence emission or phosphorescence, three nonradiative deactivation processes can occur,

including collisional quenching, internal conversion, and intersystem crossing. Collisional quenching, also known as vibrational relaxation, occurs when energy is transferred from an excited molecule to another particle through collisions. Internal conversion is the result of the transition between energy states of the same spin state while conversion from a singlet state (S) to a triplet state (T) is called intersystem crossing. Phosphorescence is the emission of a photon from the triplet state instead of from the singlet state (fluorescence).
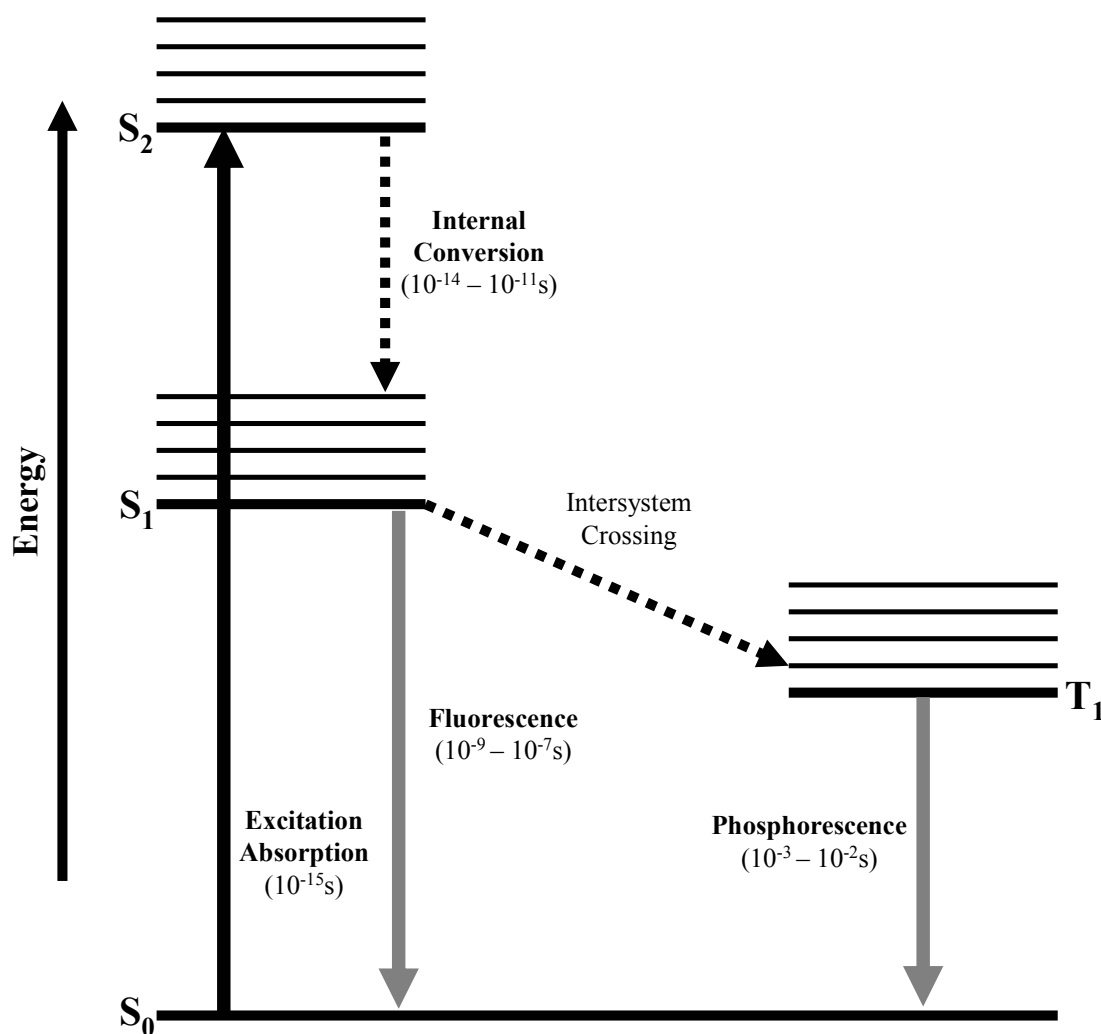
Figure 1.10 The Jablonski Diagram.[28] Molecular electronic states are represented by black horizontal lines displaced vertically, radiative transitions are indicated with solid arrows, and radiationless transitions are indicated with dashed arrows.

When a molecule returns to the ground state, the photon has a different energy and the frequency corresponding to this energy difference can be measured and recorded by a spectrometer in an emission spectrum. An excitation spectrum is measured at a single emission wavelength while an emission spectrum is measured at a single excitation wavelength. George Gabriel Stokes first observed a shift between the excitation and emission spectra due to a loss of vibrational energy (Figure 1.11).[28] This phenomena is known as the Stokes shift which states that the *wavelength of fluorescent light is always greater than the wavelength of the exciting light*.[28] Several factors may cause the Stokes shift including solvent effects, excited state reactions, energy transfer, and complex formation. In Figure 1.11, it is apparent that the emission spectrum is a mirror image of the excitation spectrum. This observation is due to the Franck-Condon principle which states that *if a particular transition probability between the zeroth and second vibrational levels is largest in absorption, the reciprocal transition is also most probable in emission*.[28] The absorption and emission spectra of most fluorescent molecules are the mirror image of each other; however, all electronic transitions are not always vertical. Thus, symmetry is broken due to a change in position of the nuclei in the excited state versus the ground state.
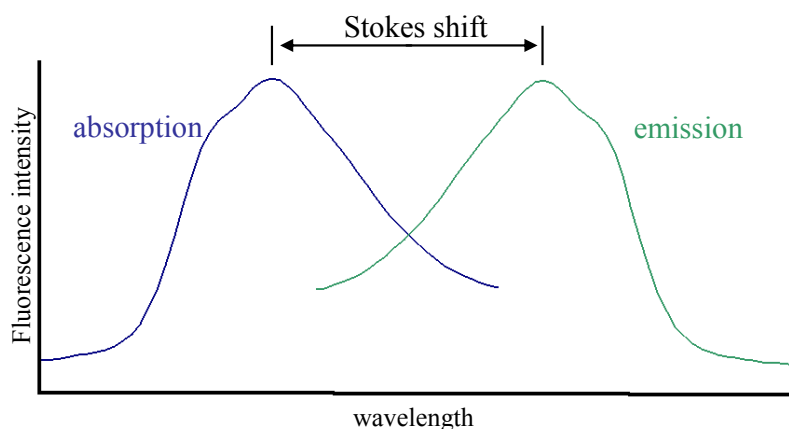
Figure 1.11   Absorption and emission spectra illustrating the mirror image rule and Stokes shift.

Two types of fluorescence measurements are steady-state and time-resolved fluorescence. Steady-state is the more commonly used measurement where the sample is exposed to a continuous beam of light. Time-resolved measurements are performed by exposing the sample to a pulse of radiation. The work presented in this dissertation is based upon steady-state fluorescence measurements and observations. The basic instrumentation consists of a light source, excitation and emission monochromators, a sample chamber, and a detector or photomultiplier tube (Figure 1.12). The excitation source produces light ranging from 200 to 900 nm.[28]

There are several light sources used in fluorescence spectroscopy including lasers, photodiodes, and lamps. A 400W xenon (Xe) arc lamp was used as the light source for all fluorescence experiments in Chapters 3-5 of this dissertation. Xe-arc lamps are the most versatile light sources because they provide continuous light output from 250 to 700 nm.[29] Monochromators decrease stray light, or light outside of the chosen excitation or emission wavelength, from the light source by the use of prisms or diffraction gratings. Transmitted light from the excitation monochromator that ranges around the specified excitation wavelength is filtered through adjustable slits before passing through the sample. The emission monochromator is at a 90° angle from the excitation light path to minimize excitation radiation detected. Excitation radiation is much more intense than emitted fluorescence; therefore, fluorescence emission would not be detectable if the emission monochromator was in a straight line with sample holder and excitation monochromator.[28] The light that exits the emission monochromator that ranges around the specified emission wavelength is filtered through adjustable slits before entering the detector. The photomultiplier amplifies the signal and the output is displayed as a spectrum.
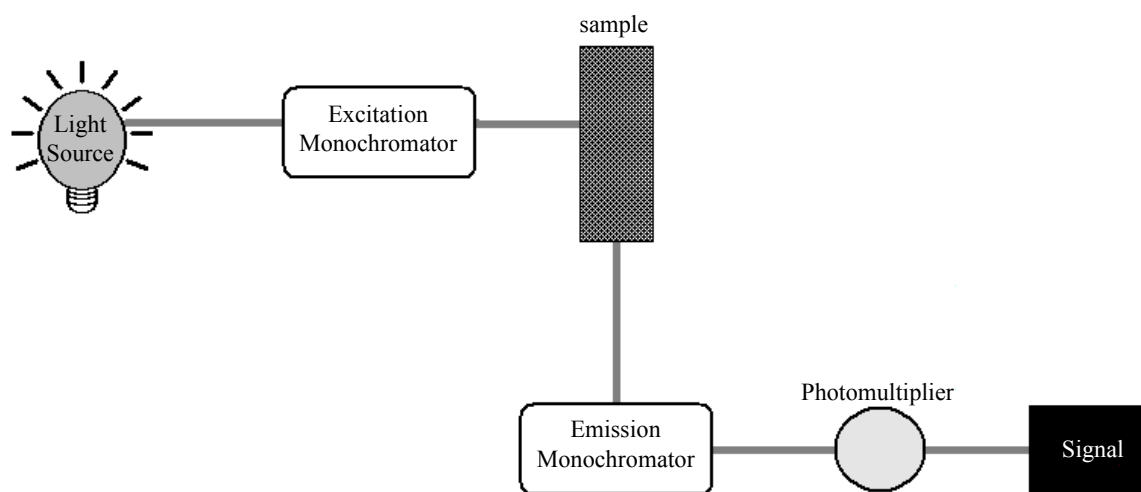
Figure 1.12   Schematic diagram of a spectrofluorometer.

Since chiral fluorescent sensors have become useful for enantioselective recognition of a variety of chiral molecules, fluorescence methods for determining the enantiomeric composition of chiral molecules have received growing interest.[30] Busch and co-workers recently reported a new rapid, accurate, and robust method for determining the enantiomeric composition of chiral molecules using fluorescence spectroscopy and cyclodextrin guest-host chemistry.[31] Subsequently, Tran and co-workers used a similar approach with a chiral ionic liquid that functions as a solvent and chiral selector.[32] In the studies reported in this dissertation, non-fluorescent and novel fluorescent molecular micelles were used to determine the enantiomeric composition of a variety of analytes, both fluorescent and non-fluorescent.

1.2.3 Other Techniques and Limitations

There are several other methods (e.g. chiroptical methods,[33,34] high performance liquid chromatography [HPLC],[35] gas chromatography [GC],[36] nuclear magnetic resonance [NMR],[37] and mass spectrometry [MS][38]) used for chiral analysis and determination of enantiomeric

20

composition of a variety of chiral molecules. These techniques have proven to be effective;
however, they have several drawbacks including analysis time, sensitivity, sample consumption,
and expensive instrumentation (see Table 1.3). As a result, development of a rapid, sensitive,
accurate, and universal technique is of considerable interest.

Table 1.3   Summary of traditional techniques and drawbacks for chiral analysis.

Method	Drawback
Polarimetry	Measured optical rotation can be solvent dependent; not sensitive
ORD	Lacks specificity in differentiation of chiral molecules
CD	Expensive instrumentation; molecules must have a chromophore
HPLC	Time consuming; reagent consumption
GC	Compounds must be readily vaporized
NMR	Expensive instrumentation; not sensitive
MS	Expensive instrumentation

Chiroptical methods use optical techniques which involve measurements of optical
rotation at a fixed wavelength. These methods include polarimetry, optical rotary dispersion
(ORD), and circular dichroism (CD). Polarimetry was one of the first analytical techniques for
chiral analysis and determination of optical purity or enantiomeric excess.[34] The two major
drawbacks of this method include low sensitivity and low tolerance of impurities. In addition,
polarimetry is not useful for near racemic mixtures and the optical purity can be solvent
dependent. ORD is the measurement of change of optical rotation and wavelength. This method
is similar to polarimetry with the exception that rotation is determined at a fixed predetermined

wavelength, while ORD is measured over a range of wavelengths. The use of ORD for chiral analysis is limited due to a lack of specificity in differentiating chiral molecules and there is high uncertainty in defining the baseline. CD is a widely used chiroptical method observed when optically active molecules absorb left and right hand circularly polarized light slightly differently. The instrumentation for this method is rather expensive and the technique is limited to molecules with a chromophore.

Chiral separation is most often performed by use of chromatographic techniques. Separations using HPLC occur by adding a chiral selector to the mobile phase or immobilizing the chiral selector on the stationary phase. Selectivity is achieved due to differences in chemical properties of the diastereomers formed between enantiomer and chiral selector. These separations require larger volumes of reagents and samples as compared to CE or spectroscopic techniques. GC methods require volatile compounds for analysis and decomposition may often occur.

The use of NMR chiral shift reagents, chiral derivatizing agents, or chiral solvating agents with enantiomers of a molecule results in diastereomeric complex formation. Although NMR can discriminate between diastereomers, it is limited due to sensitivity and the requirement of a singlet proton on the chiral molecule that can be probed. In addition, the instrumentation for NMR is expensive and the solvent for analysis is limited.

1.3 Chiral Selectors

Several chiral selectors such as micelles, cyclodextrins (CDs), crown ethers, and protein antibiodies and have been widely used for chiral discrimination and for enantio-differentiation of chiral molecules. Conventional micelles or monomeric surfactants are commercially available and are relatively inexpensive. In the studies described in Chapters 2 through 5, molecular

micelles are used for chiral analysis instead of conventional micelles. Figure 1.13 illustrates a conventional micelle and molecular micelle. Molecular micelles, first introduced by Hara and Dobashi,[39] have no CMC and can be used at much lower concentrations than conventional micelles; therefore, a wider range of concentrations can be used for chiral separations with MEKC. In addition, molecular micelles have proven to be successful chiral selectors in various applications.[40-46] Compared to other chiral selectors such as cyclodextrins, crown ethers or protein antibiotics, molecular micelles are more soluble in aqueous and organic solvents. Additionally, the polar head group as well as the number of stereogenic centers in the molecular micelle can easily be controlled and modified. In Chapter 4, novel fluorescent chiral molecular micelles (FCMMs) that allow for the chiral analysis of fluorescent and non-fluorescent chiral molecules are described. Molecular micelles, therefore, have potentially wider applications and can be used for chiral analytes of various molecular size and polarity.

monomer　　　**conventional micelle**　　　**molecular micelle**
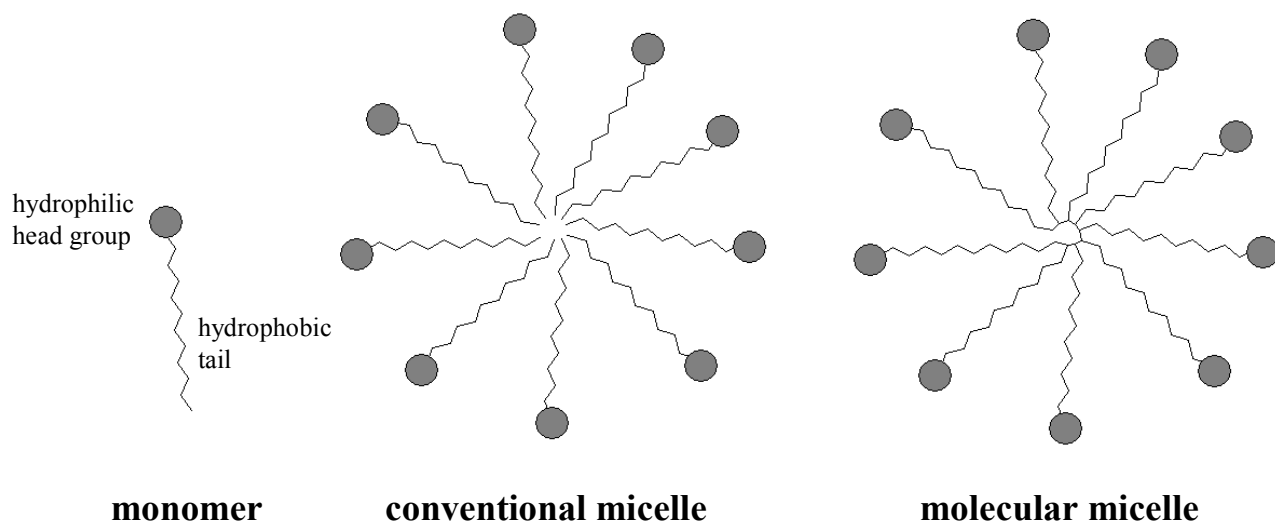
Figure 1.13　General structures of micelles.

23

CDs are naturally occurring homochiral cyclic oligosaccharides and are the most widely used chiral selectors that were first discovered by Villiers in 1891.[47,48] Figure 1.14 illustrates one of the three types of native CDs (α-, β-, and γ-) which all have hydroxyl groups at the rims of the cavity and the same cavity height (~7.9Å), but different chemical and physical properties. The cavity diameter varies as a result of the number of glucose units for α-, β-, and γ- CDs, which gives for different cavity volumes. The cavity diameters are 4.7 to 5.3Å, 6.0 to 6.5Å, and 7.5 to 8.3Å for α-, β-, and γ-CD, respectively. Poor solubility of native CDs as well as highly hydrophobic guest molecules are shortcomings that can be overcome by the use of modified CDs.[49] Modifications are possible by the substitution of hydroxyl groups and are usually designed for a specific purpose. CDs have been used in a variety of analytical techniques for chiral analysis[50-53] and are attractive chiral selectors because of availability and relatively low cost.
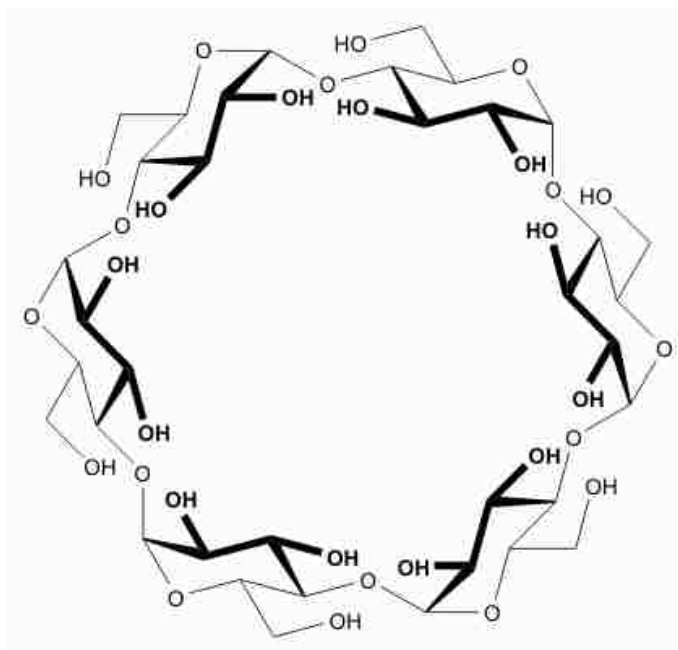
Figure 1.14　Structures of α-CD, which has 6 glucose units. The structures of β- and γ-CD have 7 and 8 glucose units, respectively.

Crown ethers and protein antibiotics (Figure 1.15) have also been used for chiral analysis. Crown ethers, which are macrocycles composed of ethylene groups, possess a central cavity and have been used for chiral analysis in HPLC,[54] CE,[55] MS,[56,57] and NMR.[58] Protein antibiotics are complex structures recently used in chiral analysis.[59,60] Although several chiral selectors have been used in a variety of analytical techniques, development of a universal chiral selector is still an area of keen interest.

18-crown-6-tetracarboxylic acid ether   vancomycin
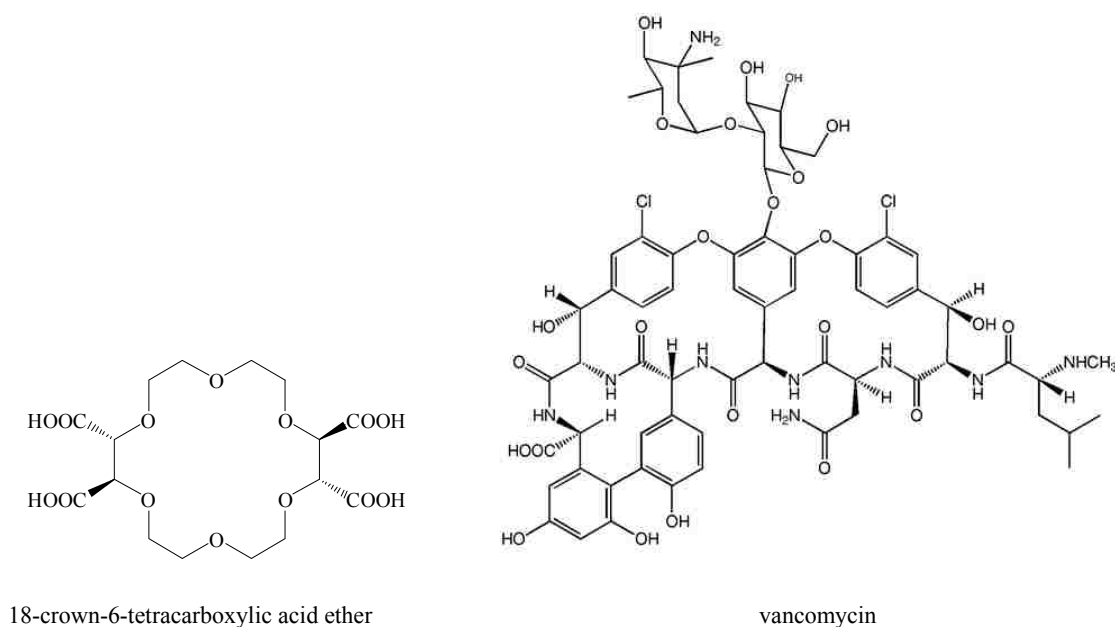
Figure 1.15   Molecular structures of a crown ether (18-crown-6-tetracarboxylic acid ether) and a protein antibiotic (vancomycin).

1.4 Chemometrics and Experimental Design

Chemometrics is the science that uses mathematical and statistical techniques for the purposes of designing or selecting optimal measurements and experiments to provide maximum chemical information from chemical data. There are two general branches of chemometrics, regression calibration and pattern recognition. The term *chemometrics* was coined in 1972 by Svante Wold and Bruce R. Kowalski.[61] In the 1960s, computers and analytical instruments

25

became more advanced and capable of generating more data in a shorter amount of time. Scientist began to have problems interpreting data until mathematical and statistical techniques were developed that were capable of extracting useful chemical information from complex data systems. Commercial statistical software simplified the complicated mathematical methods making the numerical process practical for chemists.

Regression calibration involves the formation of a regression model that will explain the experimental data. This process is possible because of a mathematical relationship between independent and dependent variables. Examples of independent variables or factors in chiral separations include operating temperature, applied voltage, buffer pH, and concentration of molecular micelle. The dependent variables are the migration time and resolution. The purpose of a regression model is to find a relationship between independent and dependent variables so that predictions of future responses can be made.

Pattern recognition is essential to science in general, and chemistry in particular. Early classification of elements in the periodic table is based upon critical observable patterns among the elements. Groups or rows of elements have similar physical and chemical properties such as ionization energy, atomic radius, number of valence electrons, electron affinity, etc. In addition, compounds with similar functional groups tend to have similar physical characteristics and, in most cases, exhibit similar chemical reactivity. Hence, the grouping of chemical compounds into different classes, such as aromatic or aliphatic compounds, alcohols, esters, amines, carbonyls, or carboxylic acids, is based on the similarity of functional groups within the compounds.

The experimental results presented in Chapters 2 through 5 were analyzed using regression calibration. There are two types of regression analysis, including univariate linear regression and multiple regression modeling. In univariate linear regression, a relationship exists

between a dependent variable (y) and a single independent variable (x) according to the following equation:

$$y = b_0 + b_1 x \qquad 1.9$$

where b_0 is the intercept and b_1 is the slope. For example, in MEKC experiments, an independent variable is applied voltage and the dependent variable is resolution. The problem with univariate linear regression is that it only allows for the affect of one experimental factor or independent variable to be studied at a time. Multi-factor systems are more common in analytical techniques and requires multiple regression modeling techniques, such as multiple linear regression (MLR), partial-least-squares regression (PLS-1), and principal component regression (PCR).[62,63]

1.4.1 Multiple Regression Modeling

The use of multiple regression modeling for correlating independent x-variables with a dependent y-variable is well known in chemistry.[61,64-67] Classical MLR is a modeling technique widely used to correlate several x-variables in a linear combination with a corresponding y-vector:[62]

$$y = b_0 + b_1 x_1 + b_2 x_2 + \ldots + b_p x_p \qquad 1.10$$

where the b_p is the coefficient of the regression model, x is the independent variable (separation parameters in Chapter 2 of this dissertation) and y is the response or dependent variable (migration time, resolution and resolution per unit time of analytes in Chapter 2 of this dissertation). The above equation can be expressed in matrix notation:

$$Y = X\mathbf{b} + f \qquad 1.11$$

where Y is the matrix data set containing the dependent variables, X is the matrix data set containing the independent variables, b is the vector containing the regression coefficients of the

model, and f is the residual error term. For MLR to have practical utility, the residual error term must be at a minimum.[62,63] In addition, there must be no colinearity among the independent variables. Once the regression coefficient vectors are determined, the model can be used for the prediction of future responses. The coefficient of the regression can be calculated using:[62]

$$b = (X^T \cdot X)^{-1} \cdot X^T \cdot Y \qquad 1.12$$

where X^T is the transpose of X. The coefficients are useful for determining the significance of the parameter. Once the coefficients are calculated, it is possible to predict future values of Y using the following equation:

$$Y = X_{fs} \cdot b \qquad 1.13$$

where X_{fs} is the matrix response of future data.

When the x-variables are reasonably uncorrelated and the number of x-variables is much less than the number of samples or experimental runs, MLR is the chemometric method of choice for the investigation of the main effects of the x-variables on the y-response.[63] Chapter 2 of this dissertation uses MLR modeling for the prediction of migration time, resolution, and resolution per unit time for a variety of chiral and achiral analytes.

1.4.2 Principal Component Regression (PCR) and Partial-Least Square (PLS-1) Modeling

Multivariate analysis in the form of PCR is widely used for pattern recognition or to study trends in analytical data. A fundamental assumption in multivariate analysis is that directions with maximum variance contain major information in the data.[63] When colinearity or correlation between the variables exists, $X^T X$ are not always invertible. To avoid problems of colinearity between variables involving a large number of independent variables (i.e. spectral data), an orthogonal basis set or coordinate system is formed to represent the data. Both PCR and PLS-1 methods employ projection techniques to obtain a series of variance-scaled

eigenvectors that serve as a new coordinate system for the data. Table 1.4 lists a response matrix

for a set of the steady-state fluorescence emission intensity at varying concentrations of sample

solutions.

Table 1.4 An example response for a set of the steady-state fluorescence emission intensities at varying concentrations of sample solutions.

Sample	Fluorescence emission intensities at different wavelengths (λ) (x-Data)								Concentration (y-Data)
1	$A_{1\lambda1}$	$A_{1\lambda2}$	$A_{1\lambda3}$	$A_{1\lambda4}$	A_{1--}	A_{1--}	A_{1--}	$A_{1\lambda m}$	y_1
2	$A_{2\lambda1}$	$A_{2\lambda2}$	$A_{2\lambda3}$	$A_{2\lambda4}$	A_{2--}	A_{2--}	A_{2--}	$A_{2\lambda m}$	y_2
3	$A_{3\lambda1}$	$A_{3\lambda2}$	$A_{3\lambda3}$	$A_{3\lambda4}$	A_{3--}	A_{3--}	A_{3--}	$A_{3\lambda m}$	y_3
4	$A_{4\lambda1}$	$A_{4\lambda2}$	$A_{4\lambda3}$	$A_{4\lambda4}$	A_{4--}	A_{4--}	A_{4--}	$A_{4\lambda m}$	y_4
5	$A_{5\lambda1}$	$A_{5\lambda2}$	$A_{5\lambda3}$	$A_{5\lambda4}$	A_{5--}	A_{5--}	A_{5--}	$A_{5\lambda m}$	y_5
6	$A_{6\lambda1}$	$A_{6\lambda2}$	$A_{6\lambda3}$	$A_{6\lambda4}$	A_{6--}	A_{6--}	A_{6--}	$A_{6\lambda m}$	y_6
7	$A_{7\lambda1}$	$A_{7\lambda2}$	$A_{7\lambda3}$	$A_{7\lambda4}$	A_{7--}	A_{7--}	A_{7--}	$A_{7\lambda m}$	y_7
8	$A_{8\lambda1}$	$A_{8\lambda2}$	$A_{8\lambda3}$	$A_{8\lambda4}$	A_{8--}	A_{8--}	A_{8--}	$A_{8\lambda m}$	y_8
9	$A_{9\lambda1}$	$A_{9\lambda2}$	$A_{9\lambda3}$	$A_{9\lambda4}$	A_{9--}	A_{9--}	A_{9--}	$A_{9\lambda m}$	y_9
10	$A_{10\lambda1}$	$A_{10\lambda2}$	$A_{10\lambda3}$	$A_{10\lambda4}$	A_{10--}	A_{10--}	A_{10--}	$A_{10\lambda m}$	y_{10}
---	---	---	---	---	---	---	---	---	---
---	---	---	---	---	---	---	---	---	---
---	---	---	---	---	---	---	---	---	---
---	---	---	---	---	---	---	---	---	---
n-1	$A_{(n-1)\lambda1}$	$A_{(n-1)\lambda2}$	$A_{(n-1)\lambda3}$	$A_{(n-1)\lambda4}$	$A_{(n-1)--}$	$A_{(n-1)--}$	$A_{(n-1)--}$	$A_{(n-1)\lambda m}$	y_{n-1}
N	$A_{n\lambda1}$	$A_{n\lambda2}$	$A_{n\lambda3}$	$A_{n\lambda4}$	A_{n--}	A_{n--}	A_{n--}	$A_{n\lambda m}$	y_n

To perform PCR, the data set is transformed and represented in a new orthogonal coordinate system to remove colinearity among the data set (Figure 1.16).[63] The first principal component (PC1) is drawn through the data set in the direction of the maximum variance in the data. The second principal component (PC2) is then drawn through the data set in the direction of the next maximum variance in the data set, and the third principal component (PC3) is drawn in the next maximum variance in the data set and so on, such that PC1, PC2, and PC3 are all orthogonal to each other. PC1, PC2, and PC3 now represent a set of variance-scaled eigenvectors that provide a new orthogonal coordinate system for representation of the data. In mathematical terms,[62] the individual principal component of an n-component data set is calculated by:

$$PCi = P_{11}X_1 + P_{21}X_2 + P_{31}X_3 + \ldots + P_{n1}X_n \qquad 1.14$$

where PCi is principal component i, P_{ij} are the coefficients of the linear combination called loading, and X are the variables, i.e. the steady-state fluorescence emission intensity data in Chapters 3 through 5. Each principal component is a linear combination of the n-vectors that make up the original variable space. The magnitude of loading is used to evaluate the importance of PCi to that data point, and the coordinates of the data in the new coordinate system are referred to as scores (see Figure 1.17). In most cases, fewer PCs are needed to explain the majority of variance in the data. As illustrated in Figure 1.18, higher PCs generally contain no useful information and can be regarded as associated with "noise" in the data set.[63] It should also be apparent that elimination of higher PCs reduces the dimensionality of the data set, therefore fewer PCs are desired as the optimal number of factors (eigenvectors) to be used in regression analysis. For all calibration data sets in Chapters 3 through 5, the optimal number of factors was three or less.
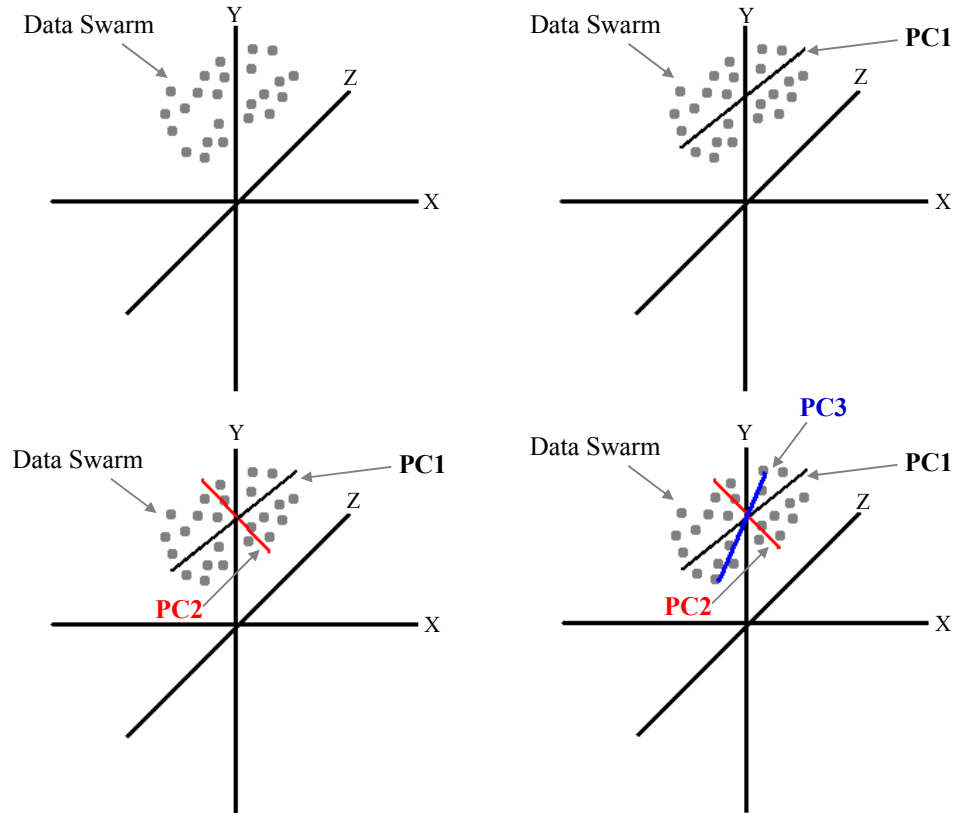
Figure 1.16 Example of a (A) data swarm with colinearity plotted in an xyz coordinate system with (B) PC1; (C) PC1 orthogonal to PC2; (C) PC1, PC2, and PC3 all orthogonal to each other. (Modified from reference 63)
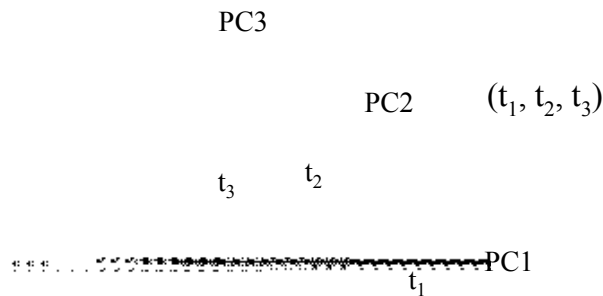
Figure 1.17 Scores plot of data point on new coordinate system. (Modified from reference 63)
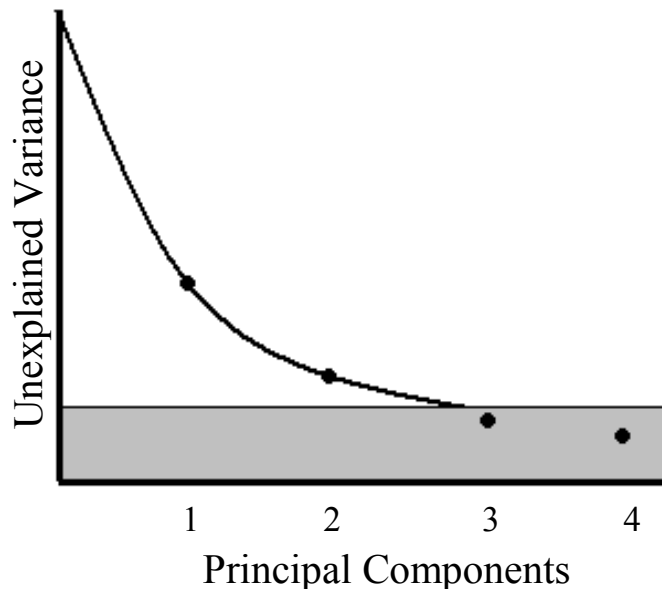
Figure 1.18   Plot of unexplained variance versus principal components. (Modified from reference 63)

Multiple regression in the form of PLS-1 is very effective because it is based upon successive extraction of linear combinations of the predictors.[63] Thus, PLS-1 accounts for factors that explain both response and predictor variation by reducing sample response prediction error. Linear functions of the predictors explain as much variation in each response as possible, as well as accounts for variation in the predictors. Unlike PCR, PLS-1 regression methods include the dependent variable in the data compression.

PLS-1 regression is generally used when there are fewer observations than predictor variables. This regression technique has been widely used for correlating small spectral changes with known compositional changes, and the methods are well established in analytical chemistry.[32,53,68-70] All multiple regression modeling involves a two-phase process. In stage one, or the calibration phase, spectra of a training set of known composition (i.e. the enantiomeric composition of the analyte in Chapters 3 through 5) are collected over a given wavelength range. Then a regression model is developed to correlate the changes in the fluorescence emission

spectral data with the known compositions of the training set samples. In the second stage, or validation phase, the regression model developed in the calibration phase is validated with a new, independently prepared test- or validation-set of samples of known enantiomeric composition. In the validation phase, the spectra of the validation samples are taken over the same wavelength range that was used to prepare the model in the calibration phase. The enantiomeric compositions of the validation samples are then predicted from the spectral data using the model developed in the calibration phase. The performance of the model in predicting future samples is evaluated by how well the predicted enantiomeric compositions compare with their actual values.

1.5 Scope of Dissertation

The goal of the research described in this dissertation is to improve chiral analysis by use of multiple regression modeling techniques in chromatographic and spectroscopic methods. In addition, more universal chiral selectors for enantiomeric composition prediction of a variety of analytes by guest-host complexation and steady-state fluorescence measurements are explored.

A multiple analysis in the form of MLR is used to optimize separation parameters and predict the migration behavior, resolution and resolution per unit time of achiral and chiral compounds using MEKC in Chapter 2. Separations of achiral and chiral analytes were performed by use of an achiral molecular micelle, poly(sodium N-undecylenic sulfate), and chiral molecular micelles, poly(sodium N-undecanoyl-L-leucylvalinate) or poly(sodium N-undecanoyl-L-isoleucylvalinate) at various operating temperatures, applied voltages, pH, and molecular micelle concentrations in the background electrolyte. The separation parameters were subsequently used as input variables for MLR models validated with independent samples. The root-mean-square percent relative error ($RMS\%RE$) is used as a figure of merit for characterizing

the performance of the models of migration time, resolution and resolution per unit time. The predicted migration time, resolution, and resolution per unit time of the chiral as well as the achiral analytes compare favorably with the experimental response values, indicating the versatility and wide applicability of this technique in MEKC.

In the remaining chapters, steady-state fluorescence spectroscopy is employed to investigate the use of chiral molecular micelles as chiral selectors in chiral analysis by multiple regression modeling of spectral data. In the research described in Chapter 3, PLS-1 is used to correlate changes in the fluorescence spectral data of 1,1'-bi-2-naphthol (BOH), 1,1'-binaphthyl-2,2'-diamine (BNA), or 2,2,2-trifluoroanthrylethanol (TFA) in the presence of poly(sodium N-undecanoyl-L-leucylvalinate), poly(sodium N-undecanoyl-L-leucinate) or poly(sodium N-undecanoyl-L-valinate) as the enantiomeric composition of the chiral analytes was varied. In the research described in Chapter 4, novel fluorescent chiral molecular micelles (FCMMs) are synthesized, characterized, and employed as chiral selectors for enantiomeric recognition of non-fluorescent chiral molecules using steady state fluorescence spectroscopy. PLS-1 is used to correlate changes in the fluorescence emission spectra of poly(sodium N-undecanoyl-L-tryptophanate) due to varying enantiomeric compositions of glucose, tartaric acid, and serine for a set of calibration samples. In an effort to develop a universal chiral selector, poly(sodium N-undecanoyl-L-phenylalaninate), is employed for enantiomeric recognition and the determination of enantiomeric composition for four fluorescent and four non-fluorescent chiral molecules using steady-state fluorescence spectroscopy described in Chapter 5. PLS-1 of the calibration samples containing the FCMM, poly(sodium N-undecanoyl-L-phenylalaninate), in the presence of BNA, TFA, propranolol, naproxen, chloromethyl menthyl ether, citramalic acid, tartaric acid, and limonene were obtained in buffer systems as well as methanol/water mixtures. The validation of

the calibration models yielded low *RMS%RE* values ranging from 1.57 to 6.10% (Chapter 3), 2.04 to 4.06% (Chapter 4), and 1.77 to 15.80% (Chapter 5). The methanol/water mixtures significantly reduced the error for the predictions with hydrophobic molecules: 1.26 to 7.95% (25:75 methanol/water), and 1.21 to 4.28% (75:25 methanol/water). In addition, in terms of *RMS%RE*, the ability of the models to accurately predict the enantiomeric composition of future samples was found to be dependent on the chiral analyte, molecular micelle used, concentration of chiral selector, and the pH of the buffer medium.

1.6 References

[1]   Hecht, E. *Optics* 4th ed., Addison-Wesley: Boston, 2002.

[2]   Pasteur, L. *Ann. Chim. Phys*. 1848, *24*, 442-446.

[3]   Kreuzfeld, H. J.; Hateley, M. J. *Enantiomer* 1999, *4*, 491-496.

[4]   http://web99.arc.nasa.gov/~astrochm/aachiral.html (accessed on July 24, 2007).

[5]   Buxton, S.; Roberts, S. *Organic Stereochemistry* Longman, Singapore, 1996.

[6]   Cahn, R. S.; Ingold, C. K.; Prelog, V. *Exper*. 1956, *15*, 81-124.

[7]   Jamali, F.; Mehvar, R.; Pasutto, F. M. *J. Pharm. Sci*. 1989, *78*, 695-715.

[8]   Aboul-Enein, H. Y.; Wainer, I. W. *The Impact of Stereochemistry on Drug Development and Use*; John Wiley: New York, 1997.

[9]   Caldwell, J. *J. Chromatogr. A*. 1996, *719*, 3-13.

[10]   Hacksell, U.; Ahlenius, S. *Trends Biotechnol*. 1993, *11*, 73-74.

[11]   Witte, D. *et al. Pharm. World Sci*. 1993, *15*, 10-16.

[12]   Jacques, J., Ed. *The Molecule and Its Double*, McGraw-Hill, New York, 1993.

[13]   Crossley, R., Ed. *Chirality and the Biological Activity of Drugs*, CRC Press, New York, 1995.

[14]   Camilleri, P. *Capillary Electrophoresis – Theory and Practice*, CRC Press, Boca Raton, 1993.

[15]   U.S. Food and Drug Administration; *Development of New Stereoisomeric Drugs* [policy statement] 1992, *22*, 249.

[16]   Rouhi A. M. *Chem. Eng. News* 2002, *80*, 43-53.

[17]   Rouhi, A. M. *Chem. Eng. News* 2003, *81*, 45-55.

[18]   Easson, E. H.; Stedman, E. *J. Biochem.* 1933, *27*, 1257-1260.

[19]   Davankov, V. A. *Chirality* 1997, *9*, 99-102.

[20]   Landers, J. P., Ed. *Handbook of Capillary Electrophoresis*, 2nd ed. CRC Press, Boca Raton, 1997.

[21]   Hjerten, S. *Chromatogr. Rev.* 1967, *9*, 122.

[22]   Mikkers, F. E. P. *et al. J. Chromatogr.* 1979, *11*, 169.

[23]   Jorgenson, J. W.; Lukacs, K. D. *Anal. Chem.* 1981, *53*, 1298-1302.

[24]   Heiger, D. *High Performance Capillary Electrophoresis: An Introduction*, Agilent Technologies, Germany, 2000.

[25]   Terabe, S. T. *et al. Anal. Chem.* 1984, *56*, 111-113.

[26]   Terabe, S. T.; Otsuka, K.; Ando, T. *Anal. Chem.* 1985, *57*, 834-841.

[27]   Du-Nouy, P. L. *Gen. Physiol.* 1919, *1*, 521-524.

[28]   Lakowicz, J. R. *Principles of Fluorescence Spectroscopy* 2nd ed. Kluwer Academic/Plenum Publishers, New York, 1999.

[29]   Schulman, S. G. Ed. *Molecular Luminescence Spectroscopy: Methods and Applications Part 3*, Wiley, New York, 1993.

[30]   Pu, L. *Chem. Rev.* 2004, *104*, 1687-1716.

[31]   Fakayode, S. O. *et al. Analyst* 2005, *130*, 233-241.

[32]   Tran, C. D; Oliveira, D. *Anal. Biochem.* 2006, *356*, 51-58.

[33]   Finn, M. G. *Chirality* 2002, *14*, 534-540.

[34]   Lightner, D. A.; Gurst, J. E. *Organic Conformational Analysis and Stereochemistry from Circular Dichroism Spectroscopy* Wiley-VCH, New York, 2000.

[35]   Tran, C. D.; Dotlich, M. J. *J. Chem. Ed.* 1995, *72*, 71-73.

[36]   Nokihara, K.; Gerhardt, J. *Chirality* 2001, *13*, 431-434.

[37]   Rothchild, R. *Enantiomer* 2000, *5*, 457-471.

[38]   Yao, Z.-P. *et al. Anal. Chem.* 2000, *72*, 5394-5401.

[39]   Hara, S.; Dobashi, A. *Chem. Abstr.* 1993, *118*, Pat. 04149205.

[40]   Wren, S.; Rowe, R. *J. Chromatogr.* 1992, *603*, 235.

[41]   Wang, J.; Warner, I. *Anal. Chem.* 1994, *66*, 3773-3776.

[42]   Edward, S.; Shamsi, S. *J. Chromatogr. A* 2000, *903*, 227-236.

[43]   Xu, Y.; McCarroll, M. *J. Phys. Chem. B* 2005, *109*, 8144-8152.

[44]   Otsuka, K.; Terabe, S. *J. Chromatogr. A* 2000, *875*, 163-178.

[45]   Rizvi, S. *et al. Anal. Chem.* 2007, *79*, 879-898.

[46]   Harrell, C. W. *Langmuir* 2003, *19*, 10684-10691.

[47]   Szejtli, J.; Osa, T. *Comprehensive Supramolecular Chemistry: Cyclodextrins* Pergamon, Oxford, 1996.

[48]   Szejtli, J. *Pure Appl. Chem.* 2004, *76*, 1825-1845.

[49]   Easton, C. J.; Lincoln, S. F. *Modified Cyclodextrins* Imperial College Press, London, 1999.

[50]   Corradini, R. *et al. J. Incl. Phenom. Macrocycl. Chem.* 2007, *57*, 625-630.

[51]   Ye, J. C.; Chen, G. S.; Zeng, S. *J. Chromatogr. B* 2006, *834*, 289-294.

[52]   Denola, N. L. *et al. Electrophoresis* 2006, *27*, 2367-2375.

[53]   Fakayode, S. O.; Busch, M. A.; Busch, K. W. *Talanta* 2006, *68*, 1574-1583.

[54]   Gong, Y. H. *et al. J. Heterocyclic Chem.* 2001, *38*, 1317-1321.

[55]   Ha, P. T. T.; Hoogmartens, J.; Van Schepdael, A. *J. Pharma. Biomed. Anal.* 2006, *41*, 1-11.

[56]   Tanaka, Y.; Otsuka, K.; Terabe, S. *J. Chromatogr. A* 2000, *875*, 323-330.

[57]   Liang, Y. J. *et al. Int. J. Mass Spec.* 1999, *187*, 977-988.

[58]   Moghimi, A. *J. Mol. Struc.* 2005, *752*, 68-77.

[59]   Armstrong, D. W.; Rundlett, K. L.; Chen, J. R. *Chirality* 1994, *6*, 496-509.

[60]   Zheng, J.; Shamsi, S. A. *Electrophoresis* 2006, *27*, 2139-2151.

[61]   Otto, M. *Chemometrics: Statistics and Computer Application in Analytical Chemistry* Wiley-VCH, Weinheim, 1999.

[62]   Harris, R. J. *A Primer of Multivariate Statistics 3rd ed.* Lawrence Erlbaum Associates, Mahway, 2001.

[63]   Esbensen, K. H. *Multivariage Data Analysis – In Practice: An Introduction to Multivariate Data Analysis and Experimental Design 5th ed.* CAMO Process AS, Norway, 2002.

[64]   Otto, M. *Chemometrics: Statistics and Computer Application in Analytical Chemistry*, Wiley-VCH, Weinheim, 1999.

[65]   Adams, M. J. *Chemometrics in Analytical Spectroscopy* Royal Society of Chemistry, Cambridge, 1995.

[66]   Beebe, K. R.; Pell, R. J.; Seasholtz, M. B. *Chemometrics A Practical Guide* John Wiley, New York, 1998.

[67]   Brereton, R. G. *Chemometrics Data Analysis for the Laboratory and Chemical Plant* Wiley, Chichester, 2003.

[68]   Tran, C. D.; Grishko, V. I; Oliveira, D. *Anal. Chem.* 2003, *75*, 6455-6462.

[69]   Tran, C. D.; Oliveira, D.; Grishko, V. I. *Anal. Biochem.* 2004, *325*, 206-214.

[70]   Fakayode, S. O. *et al. J. Fluoresc.* 2006, *16*, 59-67.

CHAPTER 2

USE OF MULTIPLE ANALYSES FOR OPTIMIZATION OF SEPARATION PARAMETERS AND PREDICTION OF MIGRATION TIME AND RESOLUTION IN MICELLAR ELECTROKINETIC CHROMATOGRAPHY

2.1 Introduction

Resolution of enantiomeric compounds into individual optical isomers continues to be one of the most challenging separation problems in chemistry. Isolation of the individual isomers of a chiral drug is an important problem because the pharmacokinetic characteristics of the individual enantiomers may be different[1]. These differences may result in physiological problems; therefore, there are many ongoing efforts to improve chiral separations.

Micellar electrokinetic chromatography (MEKC) is a widely used separation mode of capillary electrophoresis originally developed for the high resolution of neutral analytes.[2] Separation of neutral analytes is accomplished by use of surfactants that act as a pseudostationary phase in the running buffer. However, the use and application of MEKC is no longer limited to separation of neutral molecules and has been successfully employed over the years for separation of diverse charged compounds as well as chiral molecules of pharmaceutical interest by various research groups.[3-9]

Conventional micelles or monomeric surfactants have been widely used for the separation of analytes in MEKC because they are relatively simple to use, easy to prepare, commercially available, inexpensive and afford high reproducibility of analyte separation. Molecular micelles have also been employed for MEKC because they have no critical micelle concentration (CMC), allowing a wider range of concentration to be used during separation studies.[10] Additionally, the covalent bonds between molecular micelle aggregates eliminates the

dynamic equilibrium that occurs between the surfactant monomers and the micelle. Hence, molecular micelles have enhanced stabilities, rigidities, and controllable sizes.[11,12]

In MEKC, the separation, resolution, and migration behavior of the analytes are influenced by parameters such as the molecular micelle concentration in the background electrolyte (BGE), applied voltage, pH, and operating temperature. The traditional optimization of separation parameters in chromatography is laborious, time consuming and often performed by trial and error. Thus, optimization of separation parameters for baseline resolution and short migration times has been the subject of many studies.

Recently, the use of various chemometric experimental designs for optimization of separation parameters of analytes in MEKC involving full or fractional factorial design, Plackett-Burman design, central composite design, Box Benken design, and artificial neural networks have been employed.[13-24] A general application of chemometric experimental designs for capillary electrophoresis optimization methods has also been described.[25,26] The Plackett-Burman design is a technique typically used for screening purposes before the optimization of parameters using a central composite or Box Benken design to reduce the number of required experiments. The use of full factorial design for optimization requires more experiments. In the previous experimental design optimization studies, monomeric sodium dodecyl sulfate or monomeric chiral surfactant was used in the running buffer for the separations. In addition, most previous studies were used to investigate either a small number of samples or a small experimental design was used to optimize the migration time of the analyte. In this chapter, experimental design and multiple analysis for optimization of separation parameters involving the use of chiral molecular micelles in MEKC for the prediction of migration time, enantiomeric resolution and resolution per unit time of chiral molecules of pharmaceutical and environmental interest is reported.

The multiple analysis for optimization of separation parameters for the prediction of migration time, resolution, as well as the resolution per unit time of chiral binaphthyl derivatives, (±)-1,1`-bi-2-naphthyl-2,2`-dihydrogen phosphate (BNP) and (±)-1,1`-bi-2-naphthol (BOH) is achieved by use of a chiral molecular micelle poly(sodium *N*-undecanoyl-L-leucylvalinate) (poly-L-SULV). Binaphthyl derivatives are atropisomers because they possess a chiral plane of symmetry instead of an asymmetric carbon. The separation of the enantiomers was performed at various separation parameters using a full factorial experimental design. In addition, the same experimental procedure was used to optimize the separation parameters of six other chiral analytes with stereogenic carbon centers (benzoin, hydrobenzoin, coumachlor, warfarin, lorazepam, and temazepam) by use of the chiral molecular micelle poly(sodium *N*-undecanoyl-L-isoleucylvalinate) (poly-L-SUILV). To demonstrate the robustness of the technique, the same experimental approach was used for the separation of four achiral compounds (4-chlorophenol, pentachlorophenol, clonazepam and diazepam) using an achiral molecular micelle, poly(sodium *N*-undecylenic sulfate) (poly-SUS).

2.2 Methods

2.2.1 Materials

Pentachlorophenol (PCL), 4-chlorophenol (CPL), clonazepam (CZP), diazepam (DZP) and racemates of the chiral compounds (±)-1,1`-bi-2-naphthyl-2,2`-dihydrogen phosphate (BNP), (±)-1,1`-bi-2-naphthol (BOH), 2-hydroxy-2-phenylacetophenone (benzoin), 1,2-diphenyl-1,2-ethanediol (hydrobenzoin), (±)-3-(*a*-acetonyl-*p*-chlorobenzyl)-4-hydroxycoumarin (coumachlor), 4-hydroxy-3-(3-oxo-1-phenylbutyl)coumarin (warfarin), 7-chloro-5-(2-chlorophenyl)-1,3-dihydro-3-hydroxy-2H-1,4-benzodiazepin-2-one (lorazepam), and temazepam were purchased from Sigma (St. Louis, MO, USA). *N*-Hydroxysuccinimide, undecylenic acid,

sodium bicarbonate, dicyclohexylcarbodiimide were purchased from Fluka (Milwaukee, WI, USA). Undecylenyl alcohol, sodium borate, monobasic sodium phosphate, dibasic sodium phosphate, chlorosulfonic acid, pyridine, sodium hydrogen carbonate, tris(hydroxymethyl)aminomethane (TRIS), sodium hydroxide (NaOH), hydrochloric acid (HCl), ethyl acetate, methanol, tetrahydrofuran (THF), and the dipeptide (L,L) isoleucyl-valinate were obtained from Sigma-Aldrich (Milwaukee, WI, USA). The dipeptide (L,L) leucyl-valinate was purchased from Bachem Bioscience Inc (King of Prussia, PA, USA). The purity of all analytes and reagents was 98% or higher and used as received. The molecular structures of the analytes investigated are illustrated in Figure 2.1.

| BNP | BOH | Warfarin (War) | Coumachlor (Coum) |

| Hydrobenzoin (HB) | Benzoin (Benz) | Temazepam (TZP) | Lorazepam (LZP) |

| 4-chlorophenol (CPL) | Pentachlorophenol (PCL) | Clonazepam (CZP) | Diazepam (DZP) |
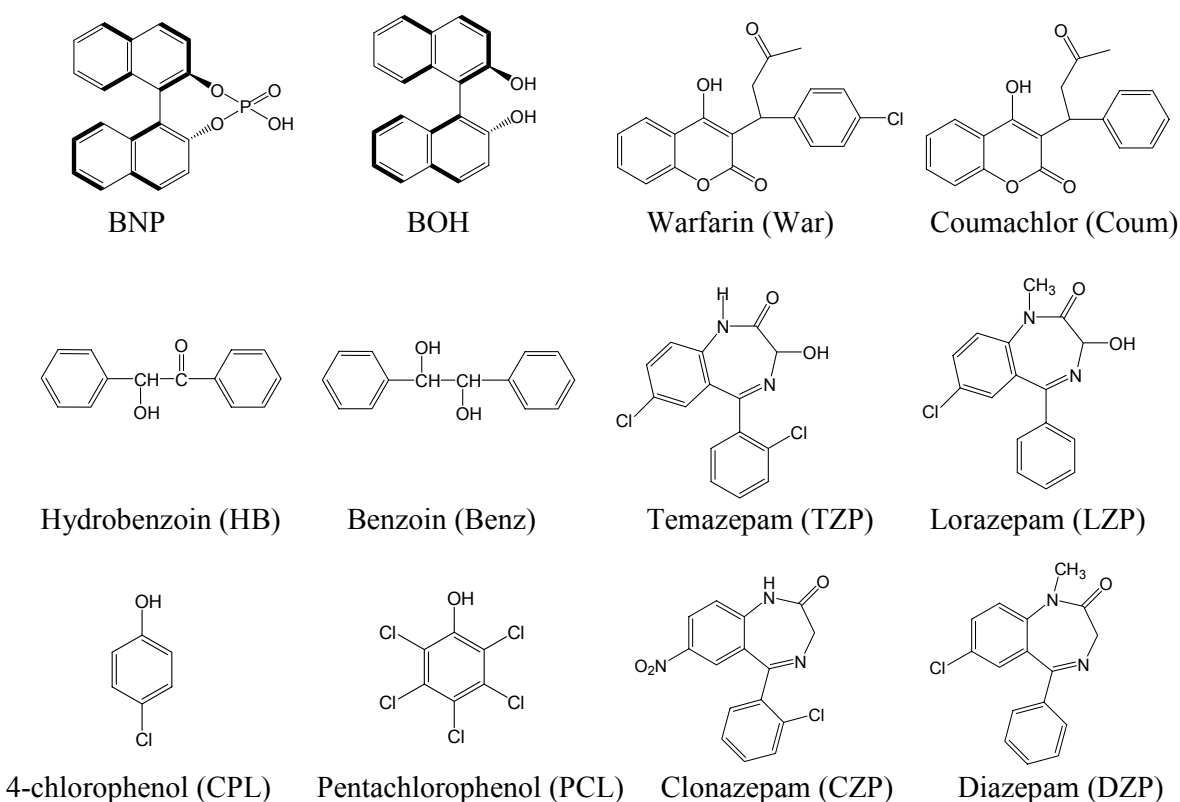
Figure 2.1   Molecular structure of the analytes.

2.2.2 Instrumentation

MEKC separations were performed on a Hewlett-Packard 3D CE instrument (Model G1600AX) from Agilent (Palo Alto, CA, USA). The CE instrument was equipped with a UV diode array detector, with UV detection at 254 nm, and ChemStation software for the processing and evaluating the experimental results. The analytes were pressure injected at 30 mbar for 3 s. A fused silica capillary column (Polymicro Technologies, Phoenix, AZ, USA) of total length of 58 cm and effective length of 50 cm was conditioned by flushing the column with 1 M NaOH for one hour, 0.1 M NaOH for 30 min, and water for 15 min. In between each run, the column was flushed with 0.1 M NaOH for 2 min followed by buffer for 2 min. The pressure was maintained at 900-920 mbar during the column flushing steps.

2.2.3 Syntheses of Molecular Micelles

Sodium undecylenic sulfate (SUS) monomer was synthesized using Bergstrom's procedure[27] with modifications described by Shamsi *et al*.[28] Scheme 2.1 shows the synthesis of poly(sodium undecylenic sulfate). Chlorosulfonic acid (7.5 mL) was added dropwise to ω-undecenyl alcohol (16.5 mL) and pyridine (75 mL) in a round-bottom flask. The reactants were refluxed for three hours followed by the addition of 600 mL of deionized water containing sodium carbonate (4 g) and sodium hydroxide (80 g). The reaction was allowed to stir for 16 hours and the resulting solution was extracted using n-butanol. The SUS monomers were isolated following the evaporation of the n-butanol and pyridine using a rotary evaporator and a vacuum desiccator. Recrystallization of the product was performed with hot isopropanol. The solution was cooled to room temperature and refrigerated overnight. The crystals were rinsed with cold isopropanol and water then dried by lyophilization.
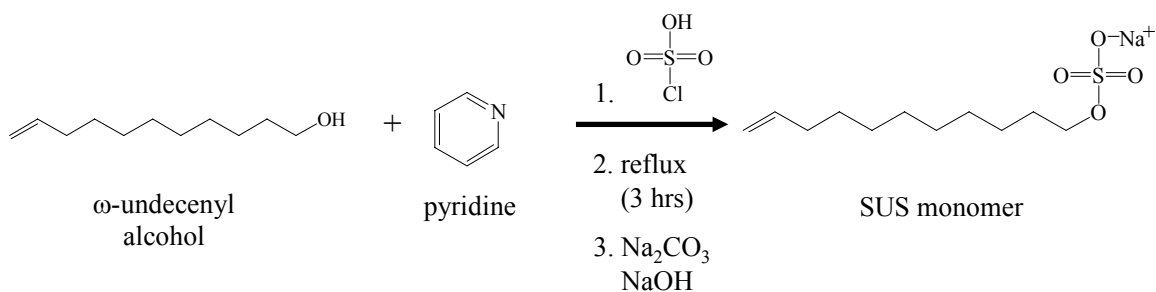
Scheme 2.1   Synthesis of SUS monomer.

The chiral molecular micelles, poly-L-SULV and poly-L-SUILV, were synthesized according to the procedure described by Wang and Warner[29] (Scheme 2.2). Undecylenic acid (45 g), dicyclohexylcarbodiimide (DCC), and *N*-Hydroxysuccinimide (NHS) were added to anhydrous ethyl acetate in a round bottom flask and allowed to stir for 16 hours. The NHS ester of undecylenic acid was isolated by filtering the white solid by-product, dicyclohexylurea, from the solution and evaporating the ethyl acetate using rotary evaporation. Purification was achieved by recrystallization of the ester in hot isopropanol. The refrigerated ester solution was washed with cold isopropanol and water then dried using a lyophilizer. The surfactant monomer was synthesized by reacting the ester with sodium bicarbonate, THF, water and the amino acid dipetide (leucine valine or isoleucine valine). THF was evaporated and the surfactant monomer was precipitated with dilute HCl. An equimolar amount of sodium bicarbonate was reacted with the dried monomer in order to form the sodium salt of SULV and SUILV monomer.
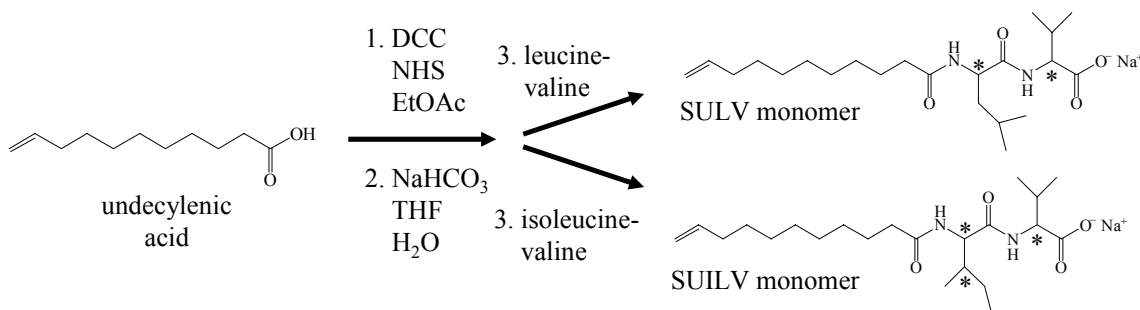
Scheme 2.2   Syntheses of SULV and SUILV monomers.

Polymerization of the resulting sodium salts of SUS, SULV, and SUILV was achieved by exposing a 100 mM aqueous solution to ^{60}Co γ-rays (0.7 krad/hr) for seven days. H^{1}NMR was used to monitor complete polymerization by the disappearance of the vinyl protons (6 – 5 ppm).

2.2.4 Buffer and Analyte Preparation

The BGE for the separation of 4-cholorophenol, pentachlorophenol, clonazepam and diazepam was 25 mM dibasic phosphate and 25 mM borate while racemic BNP, BOH, temazepam and lorazepam analytes were separated using 100 mM TRIS and 10 mM sodium borate. The separation of coumachlor, warfarin, hydrobenzoin and benzoin was performed using 50 mM phosphate (25 mM dibasic and 25 mM monobasic). The buffer pH was adjusted by adding either 0.1 M NaOH or 0.1M HCl. The BGE solutions were filtered through a 0.45-μm nylon syringe filter (Nalgene, Rochester, NY, USA) prior to the addition of molecular micelle. Varying molecular micelle concentrations were added to the BGE for separation of the analytes. Addition of the molecular micelle was followed by ultrasonication for 15 min to ensure proper degassing of the solutions. Poly-SUS was used for the separation of achiral chlorophenol (4-chlorophenol and pentachlorophenol) and achiral benzodiazepine (clonazepam and diazepam) analytes and poly-L-SULV was used for the separation of BNP and BOH. Poly-L-SUILV was used for the separation of other chiral analytes. All analytes, BNP and BOH (0.1 mg/ mL), hydrobenzoin and benzoin (0.5 mg/mL), and temazepam, lorazepam, coumachlor, warfarin, 4-chlorophenol, pentachlorophenol, clonazepam and diazepam (0.2 mg/mL), were prepared in methanol.

2.2.5 Data Analysis

Multivariate data analysis was performed using The Unscrambler, (CAMO, Inc., Corvallis, OR, version 9.1) chemometric software system.

2.2.6 Experimental Design Procedure and Multiple Analysis

The influence of four separation parameters: molecular micelle concentration, applied voltage, pH and operating temperature on migration behavior and resolution of analytes was investigated by performing the separations at various experimental conditions using a full factorial design. The design method employed for optimization usually depends upon the available time and resources. Plackett-Burman design is typically used for screening purposes while other design techniques such as central composite and Box Benken design are used for the optimization with a fewer number of experiments. Full factorial design requires more experiments; however, both the main effect of the design variables on the response as well as the interaction between the variables can be investigated. In this study, a full factorial design was used for the optimization of separation parameters to investigate the main effects of the variables on the migration behavior and resolution response as well as the interaction between the variables. In addition, this design technique was used in order to determine the best and global optimum separation conditions of various analytes which might be missed using fewer experiments.

The separations of the binaphthyl derivative enantiomers and chlorophenols were performed at four applied voltage levels (15, 20, 25 and 30 kV), three levels of operating temperatures (15, 20 and 25 °C), three levels of BGE pH (9.0, 9.5 and 10.0), and three levels of BGE molecular micelle concentration (0.5, 0.75 and 1.0 %). The small pH range (9-10) was chosen for the design because enantiomeric baseline resolution of BOH and BNP could only be obtained in this pH range. In addition, pH is not linearly related to migration time or resolution of analytes. A total of 108 experiments (4×3×3×3) were performed for the separation of BNP and BOH at the designed separation conditions. Analyses were performed in triplicate at each

experimental design condition. The results of the separations were reproducible with low percentage standard deviation ranging between 0.1 and 5% obtained for the migration times of the analytes. The average results are reported and used in the data analysis.

For each analyte, the result of the separation at various separation conditions was randomly divided into two data sets. The first data set was used as the training set for MLR calibration while the second data set was used for the validation and prediction of the migration time, resolution and resolution per unit time responses. Experimental data where separation of analytes could be achieved were not used for the calibration or the validation.

Multilinear regression modeling (MLR) was used to investigate the main effects of the separation parameters on the migration behavior and resolution of the analytes.

2.3 Results and Discussion

2.3.1 Study with Chiral Analytes

The separation of analytes at various molecular micelle concentrations, applied voltages, pH and operating temperatures had a marked effect on the migration behavior as well as the resolution of analytes. A typical electropherogram for the separation of enantiomers of BNP and BOH under different separation conditions is illustrated in Figure 2.2. In general, shorter migration times of BNP and BOH are obtained at high pH, high temperature, high voltage, and low molecular micelle concentration in BGE. Figure 2.2A illustrates the influence of molecular micelle concentration on the migration time of the analyte. For all experimental runs, the migration time of the analyte increased with increasing molecular micelle concentration in BGE. This is because the analyte interacts more strongly with the molecular micelle resulting in longer migration times for higher poly-L-SULV concentrations. The effect of applied voltage on the migration time of BNP and BOH is illustrated in Figure 2.2B. As expected, the migration times

of the analytes decrease with increasing applied voltage. Higher applied voltages resulted in a faster electroosmotic flow, which ultimately caused shorter migration times for the analytes. Figure 2.2C illustrates the effect of running buffer pH on analyte migration time, where migration time decreased with an increase in pH. Increasing the pH of the buffer solution caused an increase in anionic character of both the anionic BNP (pKa ~9) and partially anionic BOH (pKa = 9.5). As a result, the binding of each analyte with the anionic poly-L-SULV decreased, ultimately resulting in a shorter migration times for the enantiomers of both analytes at the higher pH. Increasing the operating temperature resulted in a shorter migration time for chlorophenols. Generally, separations at higher temperatures also resulted in shorter migration times for BNP and BOH (Figure 2.2D). However, increase in migration times at higher temperatures was observed in some cases for BNP and BOH, depending on the prevailing condition of other separation parameters. In contrast with the migration times obtained for BNP and BOH, better enantiomeric resolutions were generally obtained at low pH, high molecular micelle concentration, low temperature, and low voltage.

Enantiomeric resolution is a result of differences in strength of the interaction between enantiomers and the chiral molecular micelle or chiral selector. The ultimate goal of chiral separation is to obtain baseline resolution of the analytes. The optimization of separation parameters for the prediction of migration time and resolution of analytes is very important in analytical separation. However, optimization of separation parameters to predict the resolution per unit time (R_s/t) i.e. how much resolution can be achieved in a short migration time, particularly if the value of R_s/t reaches a maximum at a given point of the experimental multidimensional space, is probably the most interesting. The ultimate goal of chiral separation is to obtain baseline resolution of the analytes at reasonable migration times. Therefore,

resolution per unit time is a powerful parameter that can be used to evaluate the best design separation condition(s) where better resolution can be obtained at short migration time of analytes. For that reason, I also optimize the separation parameters for the prediction of resolution per unit time to establish the best separation working condition of the analytes.
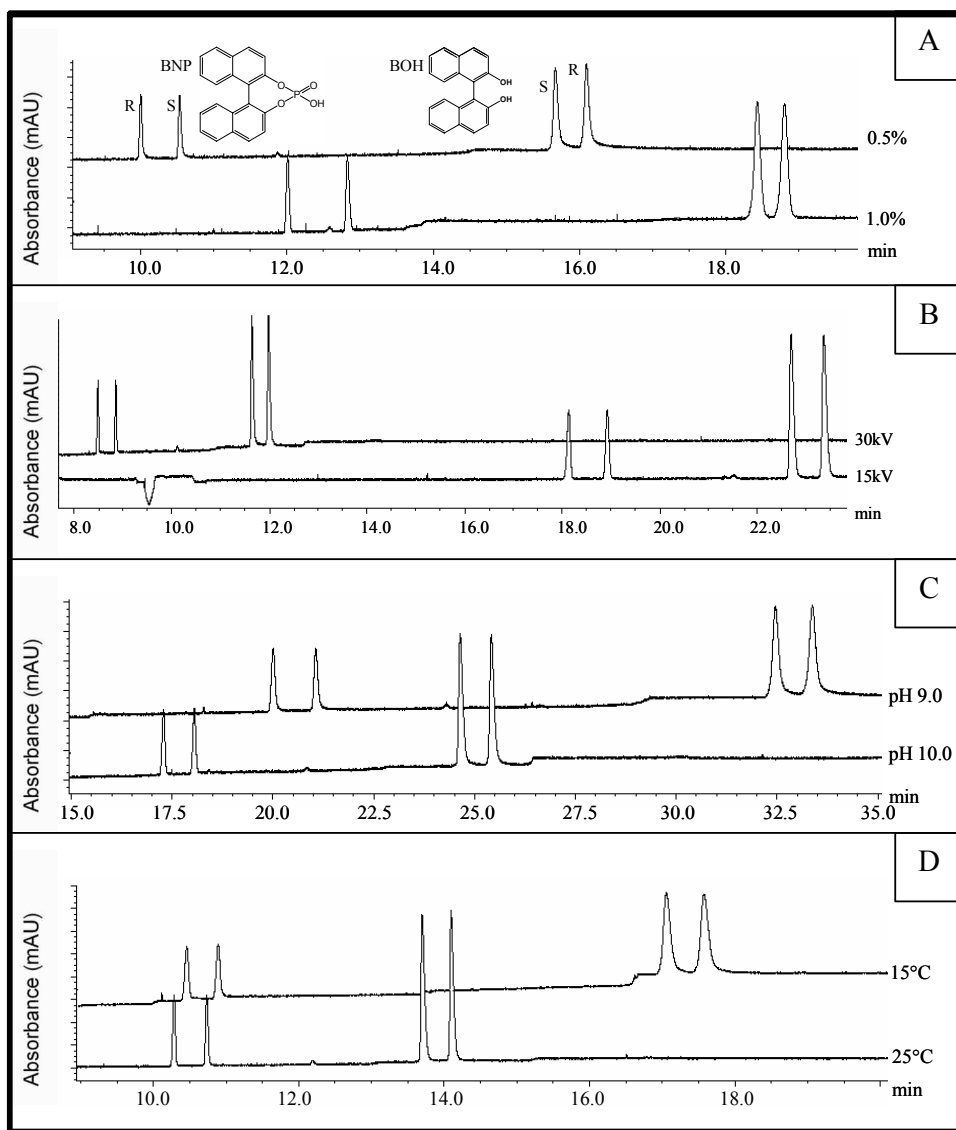
Figure 2.2 Typical electropherograms for the separation of BNP and BOH at various separation parameters. MEKC conditions: 100 mM Tris/10 mM borate buffer, 0.2 mg/mL BNP and BOH, pressure injection: 30 mbar for 3 s, UV detection at 254 nm. (A) 0.5% or 1.0% w/v poly-L-SULV, 15°C, pH 9.0, +30 kV applied voltage, (B) +30 kV or +15 kV applied voltage, 0.5% w/v poly- L –SULV, 15°C, pH 10.0. (C) pH 9.0 or pH 10.0, +15 kV applied voltage, 0.5% w/v poly- L –SULV, 20°C. (D) 25°C or 15°C, pH 10.0, +25 kV applied voltage, 0.5% w/v poly- L-SULV.

When the *x*-variables are reasonably uncorrelated and the number of *x*-variables is much less than the number of samples (experimental runs in this study), MLR is the chemometric method of choice for the investigation of the main effects of the *x*-variables on the *y*-response in that MLR parameter estimates are directly chemically interpretable. There was little correlation between the separation parameters for BNP, BOH and other chiral analytes (see Table 2.1) and the number of the *x*-variables in this study (four), is far less than the number of experimental runs.

Table 2.1   Correlation coefficients among the design variables. * pH was constant, [conc] is the molecular micelle concentration.

	BNP	BOH	HB	BENZ	WAR	COUM	TZP	LZP
Voltage α temp	-0.013	-0.013	-0.011	-0.019	-0.230	-0.164	-0.330	-0.330
Voltage α pH	-0.010	-0.010	-0.153	-0.024	*	-0.040	0.095	-0.059
pH α [conc]	-0.018	-0.018	-0.101	-0.010	*	-0.110	-0.158	-0.212
Voltage α [conc]	0.001	0.001	0.150	0.023	0.056	-0.148	0.235	-0.031
Temp α [conc]	-0.046	-0.046	0.062	0.030	0.287	-0.009	0.257	-0.107

Modeling of the separation systems was performed as a two-stage process. In the first (calibration) phase, a MLR model is developed from the training data set containing the separation parameters, migration times, resolutions and resolution per unit times of the analytes using full cross validation. The data sets used for the calibration of BNP and BOH are illustrated in Table 2.2. The data sets for the calibration of the remaining chiral analytes (benzoin and hydrobenzoin, coumachlor and warfarin, lorazepam and temazepam) are found in Appendix I A-F. The use of statistical experimental design and multiple analysis for simultaneous optimization of separation parameters is advantageous over the traditional optimization of one separation

50

parameter or factor at a time in that simultaneous optimization of separation parameters will result in a more general or global optimum separation working conditions. In contrast, only local optimum separation conditions can be achieved with the traditional optimization of one factor at a time. In general, low values of R_s/t are obtained for the separation of BNP and BOH under most of the experimental design separation conditions, reaching the optimum value at the best separation conditions where better resolutions were achieved at short migration times of the analytes. The same general trend of R_s/t was obtained for the separation of other analytes. The summary of the best separation working condition(s) of the analytes based on their R_s/t values are listed in Table 2.3.

Table 2.2   Orthogonal array data set for MLR regression modeling for BNP and BOH.

Expt	Voltage (kV)	Temp (°C)	pH	poly-L-SULV (%w/v)	Ave. Migration Time (t) (min)		Resolution (Rs)		(Rs/t) (per min)	
					BNP	BOH	BNP	BOH	BNP	BOH
1	20	15	9.0	1.00	18.649	27.050	7.49	2.43	0.40	0.09
2	30	20	9.5	0.50	8.738	13.212	1.37	1.60	0.16	0.12
3	30	25	10.0	0.75	11.076	19.125	3.50	1.01	0.32	0.05
4	20	15	10.0	1.00	18.086	24.378	4.87	1.46	0.27	0.06
5	30	15	9.5	0.50	8.883	12.199	2.00	0.94	0.23	0.08
6	15	25	9.5	0.50	17.825	27.647	1.25	1.69	0.07	0.06
7	20	15	10.0	0.50	13.208	16.861	5.00	3.59	0.38	0.21
8	30	15	10.0	0.50	8.668	11.810	5.10	3.30	0.59	0.28
9	25	20	10.0	1.00	13.979	20.222	5.63	1.66	0.40	0.08
10	20	25	9.0	1.00	19.472	35.292	2.74	1.21	0.14	0.03
11	30	20	9.5	1.00	10.320	14.879	4.83	1.36	0.47	0.09
12	20	20	9.0	1.00	18.759	29.057	7.02	1.61	0.37	0.06
13	20	15	9.5	0.75	14.937	19.427	2.60	1.25	0.17	0.06
14	30	20	9.5	0.75	9.627	14.460	3.29	1.21	0.34	0.08
15	15	20	10.0	0.50	17.698	25.057	4.25	3.02	0.24	0.12
16	30	25	9.5	0.50	8.577	13.833	1.14	1.48	0.13	0.11
17	30	15	9.5	0.75	9.799	13.525	3.12	1.27	0.32	0.09
18	15	20	10.0	0.75	21.104	31.594	4.24	1.95	0.20	0.06
19	15	15	9.5	0.50	17.950	23.500	2.61	1.06	0.15	0.05
20	20	15	10.0	0.75	14.742	18.672	5.85	3.38	0.40	0.18
21	15	20	9.0	1.00	25.267	39.622	6.22	1.69	0.25	0.04
22	25	20	9.0	1.00	15.023	23.424	6.94	1.49	0.46	0.06
23	30	15	9.5	1.00	10.412	14.054	5.61	1.59	0.54	0.11
24	20	20	10.0	0.50	13.096	18.729	4.62	2.96	0.35	0.16
25	25	20	9.5	1.00	12.653	18.039	4.91	1.47	0.39	0.08

Table 2.2 continued

26	20	15	9.5	0.50	13.490	17.841	2.33	0.94	0.17	0.05
27	25	15	9.0	1.00	14.950	22.109	7.59	2.05	0.51	0.09
28	25	25	9.0	0.75	10.513	14.522	3.05	1.18	0.29	0.08
29	15	20	9.5	1.00	21.137	29.094	4.94	1.55	0.23	0.05
30	15	25	10.0	0.50	18.388	29.336	3.75	2.84	0.20	0.10
31	15	25	9.0	0.50	20.937	36.300	4.03	2.46	0.19	0.07
32	20	20	9.5	0.50	13.319	18.616	1.61	0.95	0.12	0.05
33	20	20	10.0	0.75	14.828	21.250	4.69	2.11	0.32	0.10
34	30	15	10.0	0.75	9.823	13.514	4.87	2.65	0.50	0.20
35	15	15	9.0	1.00	24.411	35.164	7.52	2.13	0.31	0.06
36	15	15	10.0	0.75	19.432	23.926	5.00	3.06	0.26	0.13
37	25	25	10.0	0.75	12.964	21.640	3.97	1.29	0.31	0.06
38	25	20	9.0	0.50	12.286	19.963	4.87	2.52	0.40	0.13
39	25	20	9.0	0.75	11.904	17.590	5.02	1.47	0.42	0.08
40	15	15	9.5	1.00	21.418	27.334	4.74	1.65	0.22	0.06
41	25	20	10.0	0.50	10.605	15.626	4.36	2.88	0.41	0.18
42	25	20	9.5	0.75	11.727	17.269	3.48	1.24	0.30	0.07
43	15	20	10.0	1.00	23.458	32.821	6.01	1.89	0.26	0.06
44	30	20	10.0	1.00	11.738	17.568	5.23	1.48	0.45	0.08
45	30	25	9.5	0.75	9.427	14.789	2.53	1.13	0.27	0.08
46	20	20	9.0	0.75	15.241	22.633	6.04	1.84	0.40	0.08
47	25	15	9.5	1.00	12.565	16.469	5.67	1.67	0.45	0.10
48	15	15	10.0	0.50	18.570	23.067	4.41	3.11	0.24	0.13
49	30	20	10.0	0.75	10.235	15.960	4.45	1.76	0.43	0.11
50	15	25	9.0	0.75	18.766	27.003	4.22	1.59	0.22	0.06
51	20	25	9.0	0.75	13.570	19.152	3.80	1.27	0.28	0.07
52	25	25	10.0	0.50	10.677	17.317	3.39	2.28	0.32	0.13
53	20	15	9.0	0.50	15.418	23.080	6.24	2.80	0.40	0.12
54	30	20	10.0	0.50	8.963	13.857	4.19	2.47	0.47	0.18
55	30	25	9.5	1.00	10.382	15.767	3.26	1.09	0.31	0.07
56	25	20	10.0	0.75	12.053	17.837	4.61	2.01	0.38	0.11
57	20	25	10.0	0.50	13.499	21.513	3.55	2.38	0.26	0.11
58	25	25	9.5	1.00	12.684	19.080	3.93	1.19	0.31	0.06
69	25	15	10.0	0.50	10.526	13.907	4.93	3.49	0.48	0.25
60	15	20	9.0	0.75	20.842	31.075	5.08	2.08	0.24	0.07
61	25	15	10.0	1.00	13.307	17.292	6.40	2.42	0.48	0.14
62	20	25	9.5	0.50	13.418	21.307	1.23	1.44	0.09	0.07
63	20	25	10.0	0.75	17.258	32.214	3.91	1.59	0.23	0.05
64	15	20	9.5	0.75	19.983	29.031	3.32	1.15	0.17	0.04
65	30	20	9.0	0.75	9.807	14.464	4.13	1.49	0.42	0.10
66	25	25	9.0	1.00	15.327	29.432	2.94	1.09	0.19	0.04
67	20	20	9.5	0.75	14.682	21.084	3.24	1.17	0.22	0.06
68	25	15	9.0	0.75	13.058	19.074	7.71	2.48	0.59	0.13
69	30	15	9.0	1.00	12.433	18.634	7.37	1.77	0.59	0.09
70	25	15	9.5	0.50	10.808	14.619	2.16	0.85	0.20	0.06
71	30	15	9.0	0.50	10.294	15.913	6.22	2.89	0.60	0.18
72	30	25	9.0	0.50	10.588	18.531	3.31	1.59	0.30	0.09
73	15	15	9.5	0.75	19.793	25.460	2.28	1.65	0.12	0.06

Table 2.2 continued

Table 2.3 The best design separation working conditions of analytes.

Analyte	Voltage (kV)	Temp (°C)	pH	Molecular Micelle (%w/v)	Ave. Mig. Time (t) (min)	Resolution (Rs)	Rs/t per (min)
BNP	30	15	9.0	1.00	12.433	7.37	0.59
	30	15	9.0	0.50	10.296	6.22	0.60
	25	15	9.0	0.75	13.058	7.71	0.59
BOH	30	15	10.0	0.50	11.810	3.30	0.28
	30	15	10.0	0.75	13.514	2.65	0.20
	25	15	10.0	0.50	13.907	3.49	0.25
Benzoin	30	15	7.2	0.75	7.048	1.35	0.19
	30	20	7.2	1.00	6.531	1.29	0.20
	30	20	7.2	0.75	5.892	1.29	0.21
	20	15	7.2	1.00	14.564	1.66	0.11
	15	15	7.2	1.00	21.424	1.52	0.07
Hydrobenzoin	30	15	7.2	0.75	6.217	1.04	0.17
	30	25	7.2	1.00	5.156	0.77	0.15
	25	25	7.2	1.00	6.663	1.06	0.16
	15	20	7.5	1.00	16.370	0.92	0.06
Coumachlor	30	20	7.5	1.00	8.596	1.35	0.16
	25	20	7.5	1.00	11.619	1.70	0.15
	25	15	7.5	0.75	12.225	1.69	0.14
Warfarin	30	15	7.5	1.00	8.608	0.76	0.09
	25	20	7.5	1.00	10.224	0.96	0.09
	25	15	7.5	1.00	12.533	0.83	0.07
	15	15	7.5	1.00	22.140	1.04	0.05
Lorazepam	30	25	9.0	0.75	13.521	0.95	0.07
	30	20	9.0	0.75	15.770	0.98	0.06
	30	20	9.0	1.00	17.546	0.94	0.05
Temazepam	30	15	9.0	0.75	13.253	0.72	0.05
	25	15	9.0	0.75	18.514	0.87	0.05
	25	15	8.0	1.00	19.940	0.98	0.05
	20	15	9.0	1.00	32.552	1.09	0.03
CPL & PCL	30	25	10.0	0.75	6.620	49.23	7.44
	25	20	9.5	1.00	11.660	51.24	4.39
	25	25	9.5	1.00	10.079	59.58	5.91
CZP & DZP	30	15	9.0	0.50	12.194	8.64	0.71
	30	15	8.5	0.50	15.078	18.45	1.22
	30	15	9.0	0.75	18.565	17.62	0.95

The plot of the regression coefficients of the design variables for the migration time, resolution and resolution per unit time of BNP, BOH and other chiral analytes investigated from the MLR analysis are illustrated in Figure 2.3. High regression coefficients were obtained between the design variables and the migration times, resolution and resolution per unit time response for BNP, BOH and other analytes (migration time, $R^2 = 0.9542$-0.9860; resolution, $R^2 = 0.8016$-0.9738; resolution per unit time, $R^2 = 0.7579$-0.9712). In addition, the residual errors of calibration and validation models were also generally small. Statistical methods involving analysis of variance and surface response plots (Figure 2.4) were further used to evaluate the overall significance of the models and to determine the influence, contribution, and significance of the design variables on each response. All the models were highly significant ($p < 0.005$ at 95 % confidence), indicating they were good enough for future response predictions. Although the four separation parameters do influence the migration time, enantiomeric resolution as well as the resolution per unit time, it is apparent from Figure 2.3 that the influence and contribution of the separation parameters were analyte dependent.

In the second (validation) phase, the second data set was used to predict the migration time, resolution and resolution per unit time using the MLR model developed in the calibration phase. The real test of any regression model is its capability to accurately predict the migration time and resolution of the analyte in future independent experimental runs. The actual experimental migration times, the calculated experimental resolutions and experimental resolution per unit times as well as the predicted migration times, resolution and resolution per unit times obtained for the separation of BNP and BOH at various separation conditions in the validation study are tabulated in Table 2.4 and Table 2.5, respectively.

54
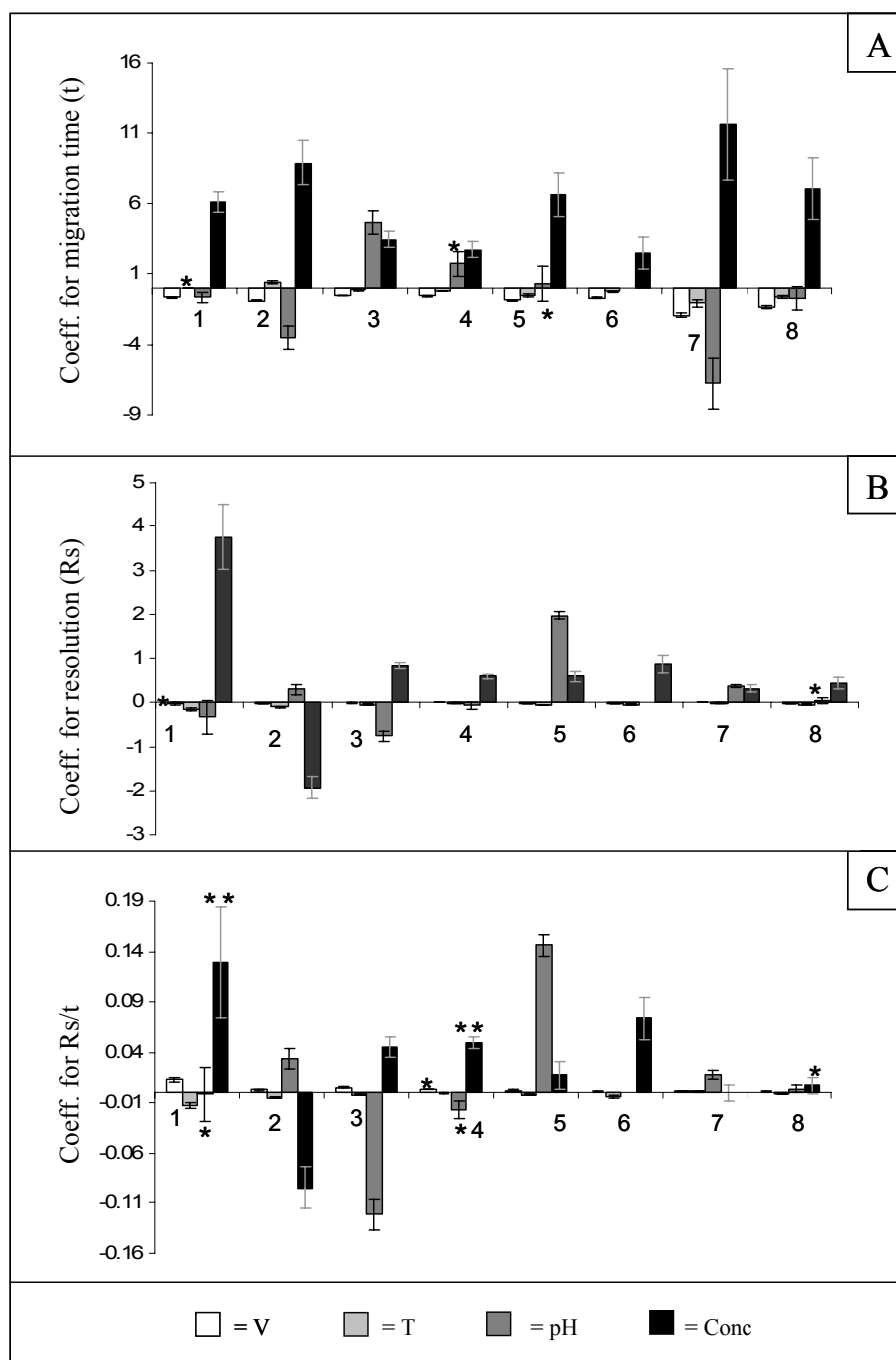
Figure 2.3 The plot of scaled and centered regression coefficients from MLR model for responses of the analytes. (A)   average migration time; (B) enantiomeric resolution; (C) resolution per unit time. 1. BNP; 2. BOH; 3. Benz; 4. HB; 5. Coum; 6. War; 7. LZP; 8. TZP. Insignificant coefficients are marked with *, coefficients marked ** are at the edge of being significant while unmarked coefficients are highly significant (95% of confidence).
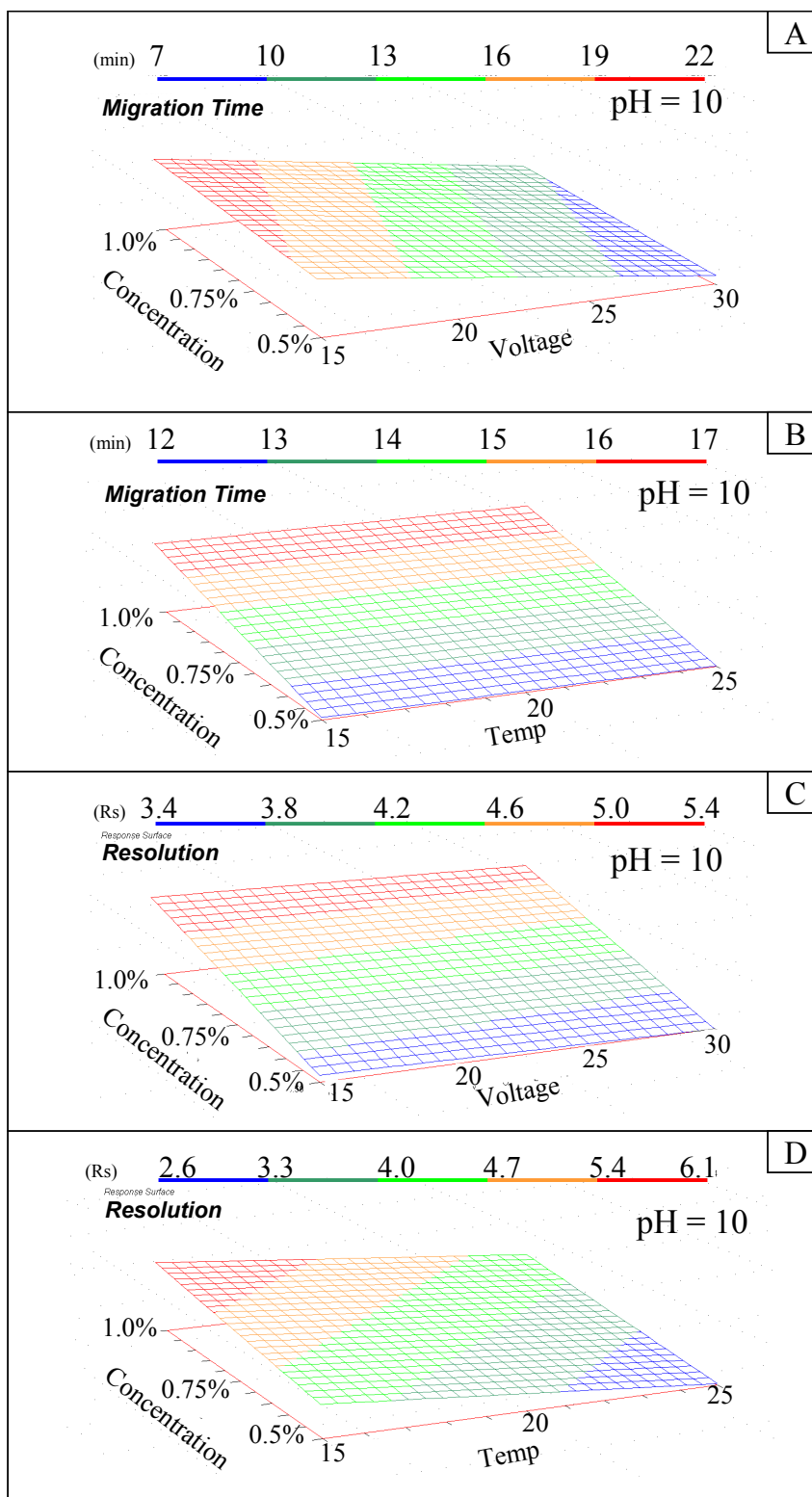
Figure 2.4 Surface response plots for BNP. Effect of (A) concentration and voltage on migration time, (B) concentration and temperature on migration time, (C) concentration and voltage on resolution, and (D) concentration and temperature on resolution.

Table 2.4 Experimental and predicted migration time, resolution, and resolution per unit time from validation of BNP.

Exp	Voltage (kV)	Temp (°C)	pH	poly-L-SULV (%w/v)	Ave. MT (t) (min)		Resolution (Rs)		(Rs/t) (per min)	
					Exp	Pred	Pred	Exp	Pred	Pred
1	20	20	10.0	1.00	11.066	10.768	6.36	5.79	0.57	0.54
2	25	25	10.0	1.00	17.468	17.536	5.78	5.16	0.33	0.29
3	25	25	9.5	0.75	16.141	14.066	4.20	4.27	0.26	0.30
4	30	25	9.0	0.75	11.488	12.866	2.71	3.49	0.24	0.27
5	20	25	10.0	1.00	8.440	9.847	2.94	3.57	0.35	0.36
6	25	15	9.0	0.50	19.649	17.479	4.63	4.35	0.24	0.25
7	15	25	9.5	1.00	12.357	11.780	5.79	4.33	0.47	0.37
8	30	20	9.0	1.00	21.285	21.285	4.13	4.61	0.19	0.22
9	20	15	9.5	1.00	12.620	11.500	6.04	5.32	0.48	0.46
10	15	15	9.0	0.75	15.980	17.987	5.63	6.13	0.35	0.34
11	15	25	9.5	0.75	21.755	20.199	6.34	5.45	0.29	0.27
12	25	15	10.0	0.75	19.931	19.691	2.92	3.67	0.15	0.19
13	25	25	9.0	0.50	11.866	12.587	5.29	4.94	0.45	0.39
14	20	25	9.5	0.75	12.547	11.665	3.82	2.72	0.30	0.23
15	30	15	9.0	0.75	14.991	16.278	2.94	3.58	0.20	0.22
16	20	20	9.0	0.50	10.786	9.961	6.39	5.19	0.59	0.52
17	30	25	10.0	0.50	15.341	15.135	5.10	3.61	0.33	0.24
18	20	25	9.0	0.50	6.556	7.466	2.05	2.30	0.31	0.31
19	15	20	9.0	0.50	15.594	15.078	4.01	2.81	0.26	0.19
20	20	25	9.5	1.00	20.562	18.548	4.65	3.70	0.23	0.20
21	20	15	9.0	0.75	15.939	17.872	3.85	4.52	0.24	0.25
22	20	20	10.0	1.00	16.451	16.786	6.94	5.36	0.42	0.32
RMS%RE					8.78		18.99		15.76	

The root mean-square percent relative error (*RMS%RE*) is a useful figure of merit for quantitatively expressing the predictive utility of the models for migration time and resolution:

$$RMS\%RE = \sqrt{\frac{\sum(\%RE_i)^2}{n}} \; ; \; \%RE_i = \frac{100 \times (\hat{y}_i - y_i)}{y_i} \qquad 2.1$$

where y_i is the experimentally observed result for the ith validation sample, $\hat{y}_i$ is the predicted result, and n is the number of validation samples in the set. The prediction capability of the model for the migration times of *R*- and *S*-enantiomers of the analytes is almost the same, therefore the average migration time (t) of *R*- and *S*-enantiomers of the analytes is predicted. In

addition, the average migration time was used to calculate the resolution per unit time of the analytes. The *RMS%RE* obtained for the predicted average migration times of BNP enantiomers was 8.8 %, with the *RMS%RE* of 19.0% for the predicted resolution of BNP enantiomers. In the validation study for BOH, the *RMS%RE* for the predicted average migration time for BOH enantiomers was 12.3%, with *RMS%RE* of 16.5% for the predicted resolution of BOH. In terms of *RMS%RE*, the models predicted the migration times of the analytes slightly better than the enantiomeric resolutions.

Table 2.5   Experimental and predicted migration time, resolution and resolution per unit time from validation of BOH.

Exp	Voltage (kV)	Temp (°C)	pH	poly-L-SULV (%w/v)	Ave. MT (t) (min)		Resolution (Rs)		(Rs/t) (per min)	
					Exp	Pred	Exp	Pred	Exp	Pred
1	30	25	9.0	1.00	23.403	20.093	0.81	0.79	0.03	0.04
2	30	15	10.0	1.00	14.876	14.001	2.07	1.86	0.14	0.13
3	30	20	9.0	0.50	17.020	13.616	2.20	1.74	0.13	0.13
4	20	20	10.0	1.00	24.965	25.205	1.78	1.79	0.07	0.07
5	25	25	10.0	1.00	27.607	22.369	1.22	1.32	0.04	0.06
6	20	25	10.0	1.00	31.009	27.046	1.21	1.45	0.04	0.05
7	25	15	9.0	0.50	18.741	16.452	2.84	2.21	0.15	0.13
8	15	25	9.5	1.00	31.278	32.924	1.41	1.39	0.05	0.04
9	30	20	9.0	1.00	20.119	18.252	1.23	1.12	0.06	0.06
10	20	15	9.5	1.00	20.698	24.564	1.74	1.93	0.08	0.08
11	15	15	9.0	0.75	31.332	28.124	2.37	2.17	0.08	0.08
12	25	15	10.0	0.75	15.784	16.369	2.72	2.30	0.17	0.14
13	25	25	9.0	0.50	21.912	20.135	1.74	1.54	0.08	0.08
14	20	20	9.5	1.00	21.983	26.405	1.60	1.59	0.07	0.06
15	20	25	9.5	0.75	24.246	25.929	1.19	1.56	0.05	0.06
16	30	15	9.0	0.75	16.011	14.093	1.91	1.77	0.12	0.13
17	25	20	9.5	0.50	15.795	17.093	1.63	2.07	0.10	0.12
18	20	20	9.0	0.50	24.775	22.970	3.18	2.01	0.13	0.09
19	20	25	9.0	0.50	26.975	24.811	2.04	1.67	0.08	0.07
20	15	20	9.0	0.50	32.944	27.647	2.50	2.14	0.08	0.08
21	20	25	9.5	1.00	23.769	28.247	1.35	1.25	0.06	0.04
22	20	15	9.0	0.75	23.926	23.447	2.52	2.03	0.11	0.09
RMS%RE					12.34		16.49		20.46	

To investigate the versatility of MLR modeling of MEKC separation parameters, the same experimental procedure was used with six other chiral analytes (benzoin, hydrobenzoin, coumachlor, warfarin, lorazepam, and temazepam) of different molecular structures complexities, and compound class (Figure 2.1). A different molecular micelle, poly-L-SUILV, was used for these chiral separations. It must be emphasized that the baseline separations and enantiomeric resolutions of these analytes are very challenging; hence, separation parameter optimization of these compound classes is very difficult. In fact, the separation of warfarin can only be achieved at pH 7.5; therefore, the pH was kept constant. The separations of benzoin, hydrobenzoin, coumachlor, lorazepam, and temazepam were performed at two pH levels each: benzoin and hydrobenzoin at pH 7.2 and 7.5, coumachlor at pH 7.0 and 7.5, lorazepam and temazepam at pH 8.0 and pH 9.0. As previously described for the separation of BNP and BOH, the separation of other chiral analytes at various design separation conditions were divided into two data sets. The first data set was used as a training set for MLR calibration while the second data set was used for the prediction of the average migration time, the resolution as well as the resolution per unit time of the analytes.

Figure 2.5 illustrates the summary of the validation results obtained for the average migration time, resolution and resolution per unit time of the analytes when independently validated. The actual experimental migration times, the calculated experimental resolutions and experimental resolution per unit times as well as the predicted migration times, resolution and resolution per unit times obtained for the separation of the remaining chiral analytes (benzoin and hydrobenzoin, coumachlor and warfarin, lorazepam and temazepam) at various separation conditions in the validation study are listed in Appendix II (A-F). Although the prediction capability of the model for each analyte differs slightly, the predicted migration times,

59

enantiomeric resolutions and resolution per unit times compare favorably with the experimentally observed migration times, resolutions and resolution per unit times.
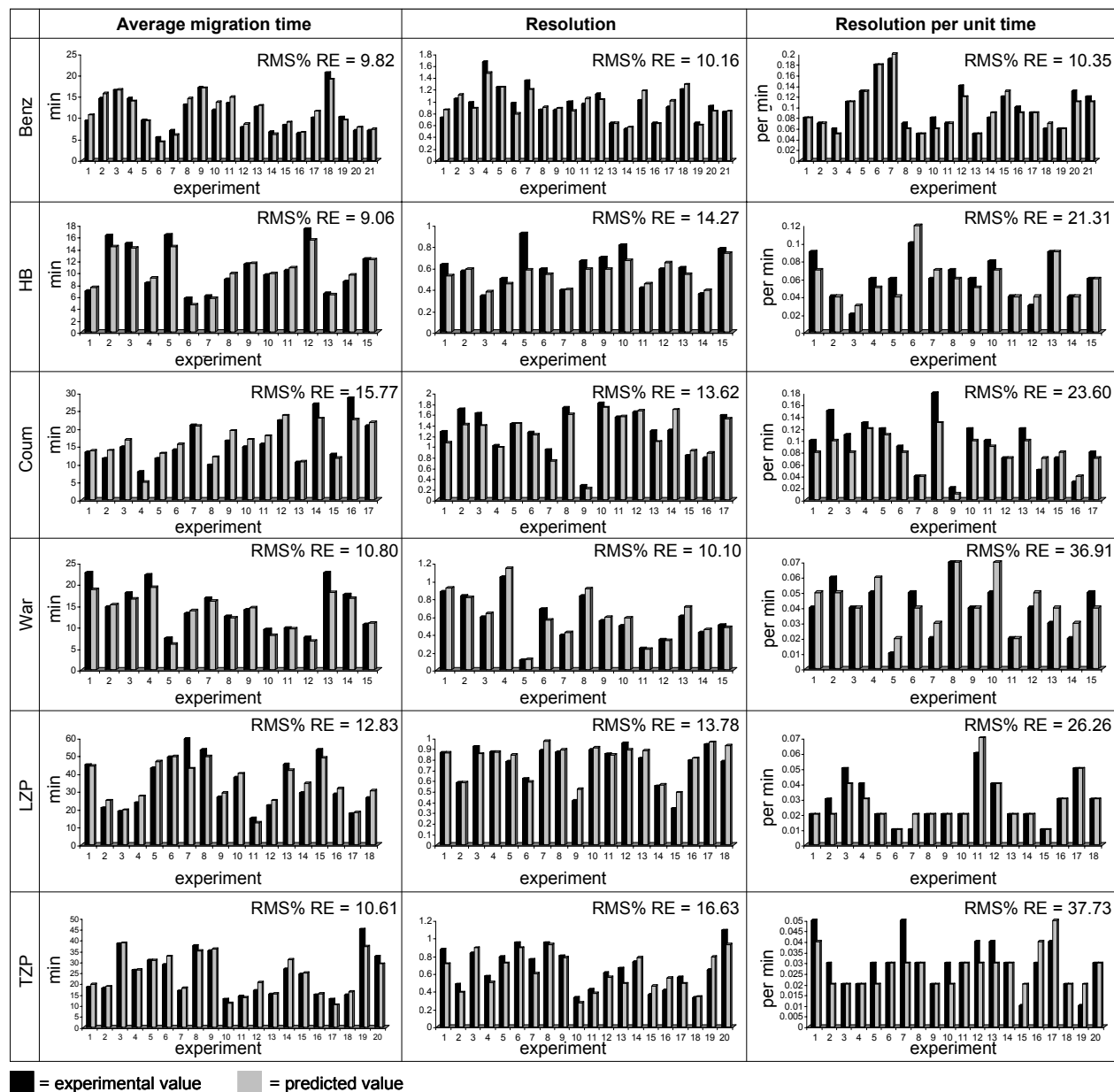
Figure 2.5 Results of MLR validation study for other chiral analytes.

2.3.2 Study with Achiral Analytes

To demonstrate the general utility of the technique in MEKC, the same experimental procedure was used to model the separation parameters and predict the migration times of achiral chlorophenols (4-chlorophenol and pentachlorophenol) and achiral benzodiazepines (clonazepam and diazepam). The achiral analytes were separated under similar experimental procedures described for BNP and BOH; however, an achiral, molecular micelle, poly-SUS, was used. The calibration data sets of the achiral analytes are found in Appendix I G-H. The results obtained for the 4-chlorophenol, pentachlorophenol, clonazepam and diazepam when the models were independently validated are illustrated in Figure 2.6. The actual experimental migration times, the calculated experimental resolutions and experimental resolution per unit times as well as the predicted migration times, resolution and resolution per unit times obtained for the separation of the achiral benzodiazepines (clonazepam and diazepam) and achiral phenols (4-chlorophenol and pentachlorophenol) at various separation conditions in the validation study are listed in Appendix II (G and H). Once again, the predicted migration time, resolution and resolution per unit time obtained for the four achiral analytes compare well with the experimental values.
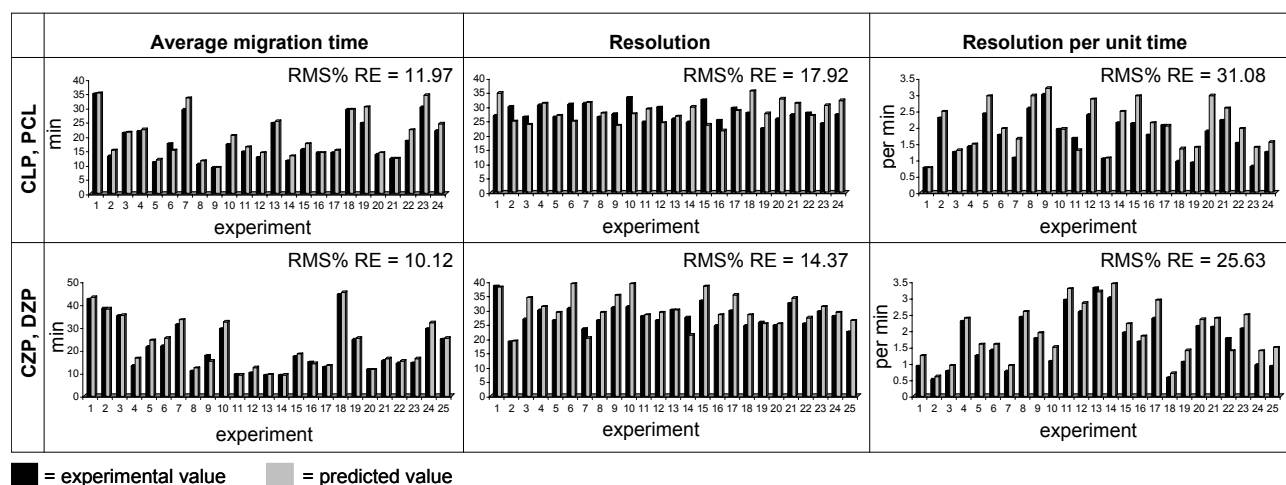
Figure 2.6   Results of MLR validation study for achiral analytes.

2.3.3 Comparative Analysis Using PLS-1 and PCR Analysis

The prediction capability of a MLR model can be limited if there is colinearity among the independent variables. Principal component regression (PCR) and partial-least-square (PLS-1) regression are the modern multiple regression techniques usually employed to remove colinearity among the independent variables.[32,33,35] In contrast with MLR where the y-matrix and x-matrix data set are directly regressed, modern PCR and PLS-1 regression avoid colinearity between the independent variables by representing the data set in a new orthogonal coordinate system. In the case of PCR, the independent data set is first decomposed using a principal component analysis. PLS-1 regression is particularly useful in that both the independent and dependent data set are simultaneous decomposed, hence, the response prediction error is minimized. In a statistical term, PLS-1 attempts to maximize the covariance between the y- and x-data set. The use of PCR and PLS-1 regression modeling for MEKC separation optimization has been previously demonstrated.[20,37]

To further test the quality of the MLR models and their predictive capability, PCR and PLS-1 regression were used to model the training data set of the analytes for subsequent prediction of migration times, resolutions and resolution per unit times using the validation data set of the respective analyte. The summary of the prediction of average migration time, resolution and resolution per unit time from the validation study of various analytes using MLR, PLS-1 and PCR are illustrated in Figure 2.7. In terms of *RMS%RE*, there was no significant difference in the prediction ability of MLR, PCR and PLS-1 models for migration times, resolutions and resolution per unit time of most analytes. However, slightly better prediction of resolution and resolution per unit time for HB and TZP are obtained using PCR and PLS-1 regression. Similar predictive power of MLR, PLS-1 and PCR models is expected since there

was little or no correlation between the design orthogonal variables for the analytes investigated (see Table 2.1). However, in the case where the design variables are highly correlated, PLS-1 regression or PCR remains the best choice of modeling.
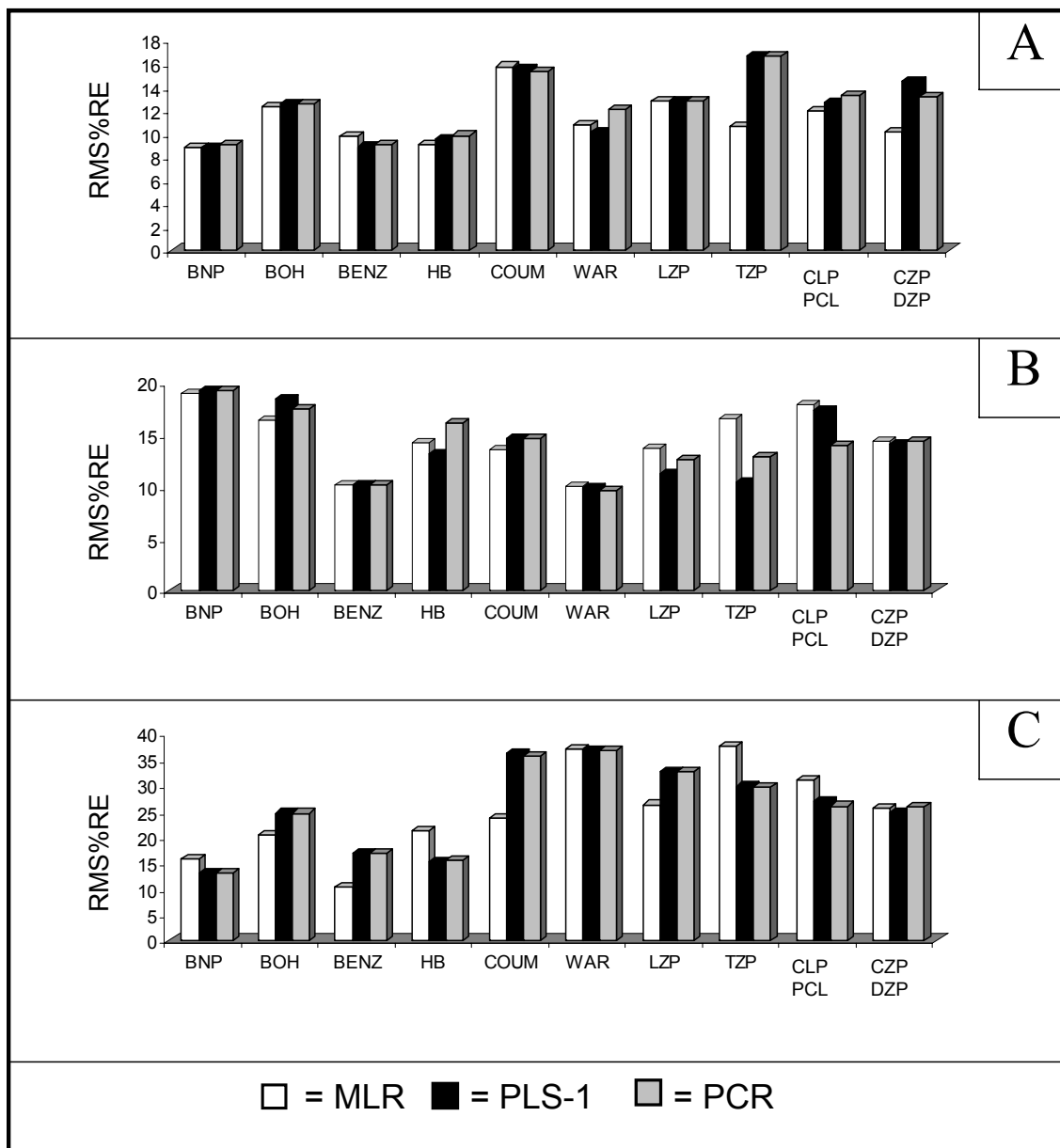
Figure 2.7 Overall *RMS%RE* obtained from validation study of all analytes using MLR, PCR and PLS-1: (A) average migration time, (B) resolution, (C) resolution per unit time.

2.4 Conclusions

It is well established that the separation of analytes in MEKC is a function of separation parameters such as molecular micelle concentration in the BGE, applied voltage, pH buffer, and operating temperature. These separation parameters were optimized by experimental design and multiple regression analysis to predict the migration times, the resolutions and resolution per unit times of the analytes. These predicted values compared favorably with the experimental migration times and resolutions of the analytes. This approach has proven to be versatile because the separation parameters of analytes with a chiral plane of symmetry, chiral molecules with stereogenic centers, as well as achiral molecules were optimized. In addition, the use of multiple analysis modeling of separation parameters to predict migration time and resolution of analytes is advantageous over the traditional labor intensive and trial and error method for the optimization of separation parameters.

2.5 References

[1]   Jamali, F.; Mehvar, R.; Pasutto, F. M. *J. Pharm. Sci.* 1989, *78*, 695-715.

[2]   Terabe, S.; Otsuka, K.; Ichikawa, K.; Tsuchiya, A.; Ando, T. *Anal. Chem.* 1984, *56*, 111-113.

[3]   Nishi, H.; Tsumagari, N. *Anal. Chem.* 1989, *61*, 2434-2439.

[4]   Chiari, M.; Nesi, M.; Ottolina, G.; Righetti, P. G. *J. Chromatogr. A* 1994, *680*, 571-577.

[5]   Doshi, A.; Ono, T.; Hara, S.; Yamaguchi, J. *Anal. Chem.* 1989, *61*, 1984-1986.

[6]   Otsuka, K.; Terabe, S. *J. Chromatogr.* 1990, *515*, 221-226.

[7]   Nishi, H.; Fukuyama, T.; Matsuo, M.; Terabe, S. *Anal. Chim. Acta* 1990, *236*, 281-286.

[8]   Wang, J.; Warner, I. *J. Chromatogr. A* 1995, *711*, 297-304.

[9]   Agnew-Heard, K. A; Pena, M. S; Shamsi, S. A.; Warner, I. M. *Anal. Chem.* 1997, *69*, 958-964.

[10]   Shamsi, S. A.; Palmer, C. P.; Warner, I. M. *Anal. Chem.* 2001, *73*, 140A-149A.

[11]   Haynes III, J.; Warner, I. M.; Shamsi, S. A. *Rev. Anal. Chem.* 1999, *18*, 317-382.

[12]   Billiot, F. H.; Billiot, E. J; Warner, I .M. *J. Chromatogr. A* 2001, *922*, 329-338.

[13]   Vindevogel, J.; Sandra, P. *Anal. Chem.* 1991, *63*, 1530-1536.

[14]   Burns, S. T.; Khaledi, M. G. *Anal. Chem.* 2004, *76*, 5451-5458.

[15]   Havel, J.; Breadmore, M.; Macka, M.; Haddad, P. R. *J. Chromatogr. A* 1999, *850*, 345-353.

[16]   Jalali-Heravi, M.; Kyani, A. *J. Chem. Inf. Comput. Sci.* 2004, *44*, 1328-1335.

[17]   Wan, H.; Ohman, M.; Blomberg, L. G. *J. Chromatogr. A* 2001, *916*, 255-263.

[18]   Zhang, Y.; Li, H.; Havel, J. *Talanta* 2005, *65*, 853-860.

[19]   Detroyer, A.; Heyden, Y. V.; Cambre, I.; Massart, D. L *J. Chromatogr. A* 2003, *986,* 227-238.

[20]   Thorsteinsdottir, M.; Westerlund, D.; Andersson, G.; Kaufmann, P. *J. Chromatogr. A* 1998, *809*, 191-201.

[21]   Harang, V.; Eriksson, J.; Sanger-van de Griend, C. E.; Jacobsson, S. P.; Westerlund, D. *Electrophoresis* 2004, *25,* 80-93.

[22]   Mikaeli, S.; Thorsen, G.; Karlberg, B. *J. Chromatogr. A* 2001, *907,* 267-277.

[23]   Frias-Garcia, S. ; Sanchez, M. J. ; Rodriguez-Delgado, M. A. *Electrophoresis* 2004, *25,* 1042-1050.

[24]   Altria, K. D.; Howells, J. S. *J. Chromatogr. A* 1995, *696*, 341-348.

[25]   Altria, K. D.; Clark, B. J.; Filbey, S. D.; Kelly, M. A.; Rudd, D. R. *Electrophoresis* 1995, *16*, 2143-2148.

[26]   Sentellas, S. ; Saurina, J. *J. Sep. Sci.* 2003, *26*, 875-885.

[27]   Bergstrom, S. *Physiol. Chem.* 1936, *238*, 163-168.

[28]   Shamsi, S.A.; Akbay, C.; Warner, I. M. *Anal. Chem.* 1998, *70*, 3078-3083.

[29]   Wang, J.; Warner, I. M. *Anal. Chem.* 1994, *66*, 3773-3776.

[30]   Otto, M. *Chemometrics: Statistics and Computer Application in Analytical Chemistry*, Wiley-VCH, Weinheim, 1999.

[31]   Burns, D. A.; Ciurczak, E. W. (Eds.), *Handbook of Near-Infrared Analysis*, second ed., Marcel Dekker, New York, 2001.

[32]   Martens, H.; Naes, T. *Multivariate Calibration,* John Wiley, New York, 1989.

[33]   Adams, M. J. *Chemometrics in Analytical Spectroscopy*, Royal Society of Chemistry, Cambridge, 1995.

[34]   Malinowski, E. R. *Factor Analysis in Chemistry*, John Wiley, New York, 1991.

[35]   Beebe, K. R.; Pell, R. J.; Seasholtz, M. B. *Chemometrics A Practical Guide*, John Wiley, New York, 1998.

[36]   Brereton, R. G. *Chemometrics Data Analysis for the Laboratory and Chemical Plant*, Wiley, Chichester, 2003.

[37]   Gallego, J. M.;Arroyo, J. P. *J. Sep. Sci.* 2003, *26*, 947-952.

CHAPTER 3

THE USE OF POLY(SODIUM *N*-UNDECANOYL-L-LEUCYLVALINATE), POLY(SODIUM *N*-UNDECANOYL-L-LEUCINATE), AND POLY(SODIUM *N*-UNDECANOYL-L-VALINATE) MOLECULAR MICELLES AS CHIRAL SELECTORS FOR DETERMINATION OF ENANTIOMERIC COMPOSITION OF SAMPLES BY MULTIVARIATE REGRESSION MODELING OF FLUORESCENCE SPECTRAL DATA

3.1 Introduction

Chiral analysis continues to be a topic of keen interest in the pharmaceutical industry because of differences in pharmacological and physiological properties of enantiomers. While one enantiomer of a chiral drug may have therapeutic effects, the other enantiomer may be ineffective or toxic, leading to serious health problems for humans.[1-3] These potentially harmful effects of different enantiomers have prompted serious health concerns from government and regulatory agencies. This is particularly true for drugs that were initially approved as racemates, but are now being submitted for approval by the pharmaceutical industry as single-enantiomer drugs. Because of these concerns, the pharmaceutical industry is required to document the pharmacological and physiological properties of all single-enantiomer drugs.

Chiral analysis is often performed by use of chromatography or capillary electrophoresis,[4-8] and nuclear magnetic resonance (NMR) using chiral solvents.[9] Chiral stationary phases used in chromatographic separations frequently employ chiral cavitands that involve the formation of transient non-covalent guest-host complexes between the guest analyte and a selector. Several chiral cavitands such as cyclodextrins,[10-12] protein antibiotics[13,14] and crown ethers[15,16] have been widely used for chiral discrimination and for enantio-differentiation of chiral molecules. Chiroptical methods such as polarimetry, optical rotary dispersion, circular dichroism, and vibrational circular dichroism have also been used for chiral analysis.[4,17,18]

While most of these techniques are unquestionably effective, some of the current analytical techniques of chiral analyses have several major drawbacks. For example, chromatography and capillary electrophoresis are slow and not particularly attractive for high-throughput- or rapid screening of chiral compounds. Moreover, in the case of chiral chromatography, chiral columns are frequently expensive and can have relatively short lifetimes. Chiroptical methods, such as the polarimetric method of chiral analysis, require a relatively large sample size and the measured optical rotation by the polarimeter can be solvent dependent. In addition, the sensitivity of some techniques like circular dichroism is relatively low, while techniques like NMR and mass-spectrometric methods are very expensive in terms of instrumentation. A relatively inexpensive spectroscopic method, like fluorescence spectroscopy, is therefore highly desirable in the pharmaceutical industry today, where accurate and rapid screening of chiral molecules is of considerable interest as the marketing of drugs switches from racemic mixtures to single-enantiomer formulations.

Busch and co-workers recently reported a new rapid, accurate, and robust method for determining the enantiomeric composition of chiral molecules that combines ordinary ultraviolet/visible absorption- or fluorescence spectroscopy, cyclodextrin guest-host chemistry, and multivariate regression modeling.[19-23] In these studies, chiral analysis by the regression modeling of spectral data was shown to be a reliable method for determining the enantiomeric composition of chiral samples using ordinary spectroscopic methods. Tran and co-workers used a similar approach with near-infrared spectroscopy for determination of the enantiomeric composition of molecules of pharmaceutical interest.[24,25]

Poor solubility of native CDs as well as highly hydrophobic guests are major problems encountered in previous studies, and different strategies, such as the use of modified CDs[21] or the

use of an achiral monomeric sodium dodecyl sulfate surfactant in combination with organic solvents[20] have been employed in an attempt to ameliorate these problems.

In this chapter, the use of three chiral molecular micelles as chiral selectors for the determination of the enantiomeric composition of three chiral molecules (Figure 3.1) using steady-state fluorescence spectroscopy and multivariate regression modeling of the spectral data is reported. The three chiral surfactants used were poly(sodium *N*-undecanoyl-L-leucylvalinate) [poly-L-SULV], poly(sodium *N*-undecanoyl-L-leucinate) [poly-L-SUL] and poly(sodium *N*-undecanoyl-L-valinate) [poly-L-SUV]. The two chiral binaphthyl analyte molecules [1,1'-bi-2-naphthol (BOH) and 1,1'-binaphthyl-2,2'-diamine (BNA), see Figure 3.1], as well as a chiral anthracene derivative, 2,2,2-trifluoroanthrylethanol (TFA), were selected for their fluorescence properties. BOH and BNA, although they do not possess typical chiral centers, are, nevertheless, chiral because they have axial chirality. Both compounds are stable to racemization.

Molecular micellar agents, also known as surfactants, are amphiphilic in nature, containing an apolar long-chain hydrocarbon tail and polar head groups. Chiral surfactants may function as nearly ideal chiral selectors for analytes such as the binaphthyl and anthracene derivatives used in this study by providing a chiral micellar environment for the highly hydrophobic analytes. Both chiral monomeric and molecular micelles have been used as selectors for chiral discrimination.[26-31] However, the use of molecular micelles is desirable because they are more stable and more rigid than monomeric surfactants. In addition, because molecular micelles have controllable sizes and have no critical micelle concentration, the use of molecular micelles eliminates the dynamic equilibrium between the micelles and the monomer. Compared to other chiral selectors such as cyclodextrins, crown ethers or protein antibiotics, molecular micelles are relatively more soluble in aqueous and organic solvents. Additionally, the

polar head group as well as the number of stereogenic centers in the molecular micelles can easily be controlled and modified. Molecular micelles, therefore, have potentially wider applications and can be used for chiral analytes of various molecular size and polarity.

Poly-L-SULV, a negatively charged dipetide molecular micelles with two chiral centers, has a low aggregation number and is highly soluble in water. Furthermore, poly-L-SULV has good chiral discriminating capability and has been used successfully for the chiral separation of various analytes with different molecular structures in micellar electrokinetic chromatography (MEKC).[32] In addition, the chiral recognition ability of poly- L-SULV, using fluorescence anisotropy, has been demonstrated.[33] Poly-L-SUL and poly-L-SUV are single amino-acid-based molecular micelles, each with one chiral center, that have been used for enantiomeric separation of several analytes in MEKC.[31]

3.2 Methods

3.2.1 Materials

Enantiomerically pure (*R*)-1,1'-bi-2-naphthol (*R*-BOH), (*S*)-1,1'-bi-2-naphthol (*S*-BOH), (*R*)-1,1'-binaphthyl-2,2'-diamine (*R*-BNA), (*S*)-1,1'-binaphthyl-2,2'-diamine (*S* -BNA), (*R*)-2,2,2,-trifluoroanthrylethanol (*R*-TFA), and (*S*)-2,2,2,-trifluoroanthrylethanol (*S* -TFA), sodium borate, and tris(hydroxymethyl)aminomethane (TRIS) were purchased from Aldrich Chemical Company (Milwaukee, WI) and used as received. The methanol used in the study (ACS certified) was also obtained from Aldrich. Doubly-deionized water, used throughout in the study, was obtained from a PURELAB Ultra Genetic water polishing system (US Filter).

3.2.2 Instrumentation

The fluorescence emission of each sample was recorded using a spectrofluorometer (SPEX Fluorolog-3) equipped with double excitation and emission monochromators. A 400W

Xe arc-lamp was used for excitation and a thermoelectrically cooled Hamamatsu R-928 photomultiplier tube, operating in the photon-counting mode, was used for detection. All data were collected using a 0.4 cm path length quartz cuvet.

3.2.3 Syntheses of Molecular Micelles

The synthesis and polymerization of poly-L-SULV was described in Chapter 2. The monomers L-SUL and L-SUV followed the same synthetic procedure as described for L-SULV. The leucine-valine dipetide was replaced with either leucine or valine to yield the final monomers L-SUL or L-SUV, respectively.

3.2.4 Sample Preparation

A solution containing 1.5 % w/v of molecular micelles was made by dissolving 1.500 g of poly-L-SULV in 100 mL of doubly-deionized water or in a solution containing 100 mM Tris and 10 mM borate buffer at pH 10.0. Stock solutions of each enantiomer were made by weighing appropriate amounts of each enantiomer and dissolving them in methanol. From the stock solution, appropriate concentrations (1×10^{-4} or 5×10^{-6} M) of the enantiomer solutions were made by transferring appropriate aliquots of the stock solution to a dry volumetric flask. After transfer, the methanol was then gently evaporated under a stream of ultra-high-purity nitrogen gas. The solution was then made up to the mark with 1.5 % molecular micelles solution and sonicated for at least 20 min to ensure complete dissolution of analyte. Following dissolution, the samples were allowed to equilibrate for 15 min.

Training-set samples and calibration-set samples were made for each chiral analyte so that for a given experiment, all solutions contained a fixed molecular micelle concentration and a fixed concentration of chiral analyte. The enantiomeric composition of the calibration samples

was varied from 0.1 to 0.9 mol fraction. The samples were allowed to equilibrate for at least 30 min before the fluorescence emission spectra of the samples were recorded.

3.2.5 Data Analysis

The mean-centered spectral data were subjected to multivariate regression analysis using commercial chemometric software (The Unscrambler version 9.1; CAMO, Inc., Corvalis, OR). Partial-least-square-regression models (PLS-1) were developed from the spectral data using full-cross validation. The regression models were validated with new independently-prepared sets of validation samples.

3.3 Results and Discussion

3.3.1 Study with Poly-L-SULV

The fluorescent chiral analytes and molecular micelles used for this study are illustrated in Figure 3.1. Figure 3.2A illustrates fluorescence emission spectra (λ_{ex} = 380 nm) of 1×10^{-4} M (*R)*- and (*S)*-BOH enantiomers in 1.5 % w/v poly-L-SULV. Although the concentrations of both enantiomers are the same, they have notably different emission spectra in the presence of poly-L-SULV. The differences in the spectra of the enantiomers illustrated in Figure 3.2A can be attributed to different noncovalent enantiomeric interactions within the micellar environment of the chiral molecular micelles. Such differences in enantiomeric interactions with the chiral poly-L-SULV surfactant will ultimately produce diastereomeric effects that influence the spectra. As expected, there was no apparent difference in the spectra of the two enantiomers in the presence of achiral poly-(sodium *N*-undecylenic sulphate) surfactant.

Figure 3.2B illustrates the fluorescence emission spectra obtained for a set of eight solutions containing a fixed BOH analyte concentration (1×10^{-4} M) of various enantiomeric composition in the presence of chiral poly-L-SULV surfactant. The samples have maximum

emission at 445 nm. Although the BOH concentration was fixed, the fluorescence emission intensity of the spectra varied with the enantiomeric composition of the BOH samples. Samples containing different ratios of the (*R*)- and (*S*)-enantiomers will produce different diastereomeric effects, resulting in spectra that vary with enantiomeric composition.
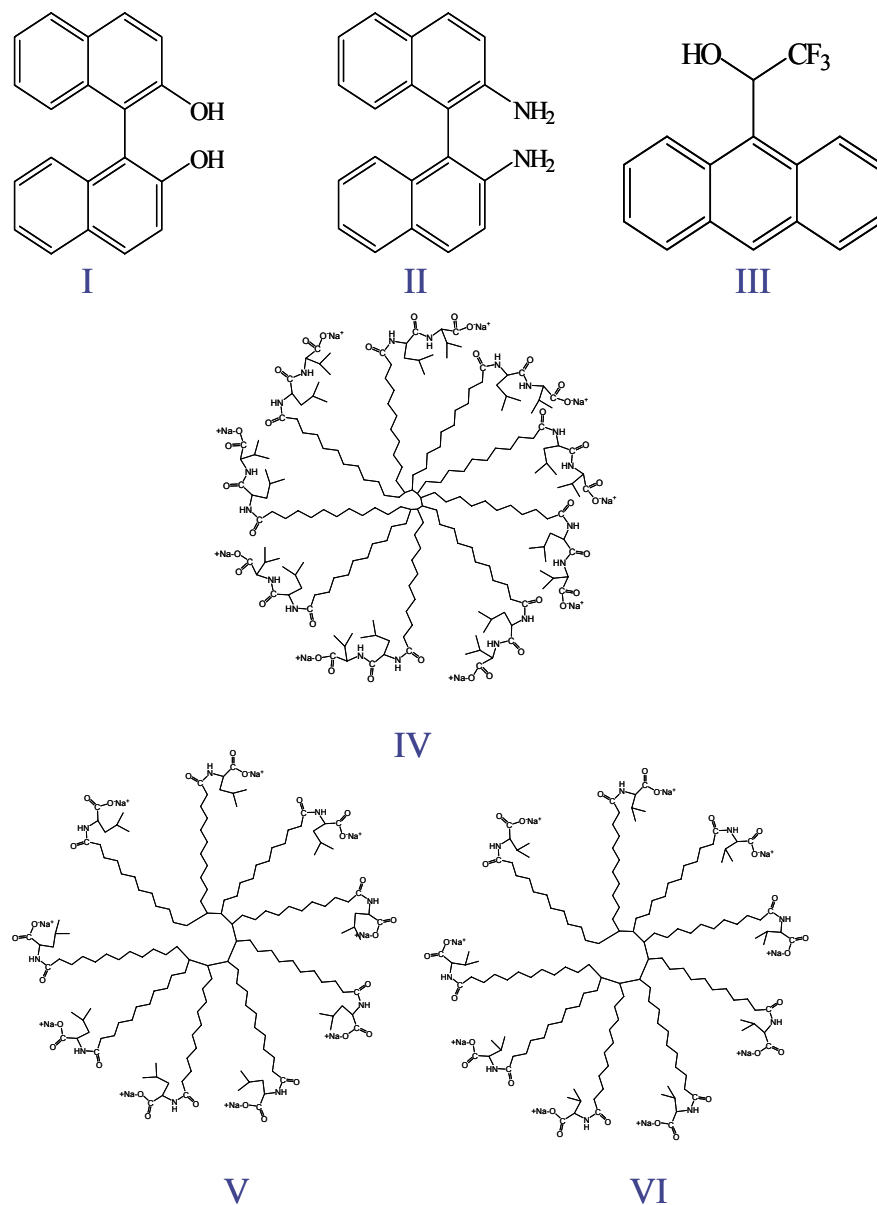
Figure 3.1 Molecular structures of: (**I**) BOH; (**II**) BNA; (**III**) TFA; (**IV**) poly-L-SULV (**V**) poly-L-SUL; (**VI**) poly-L-SUV.
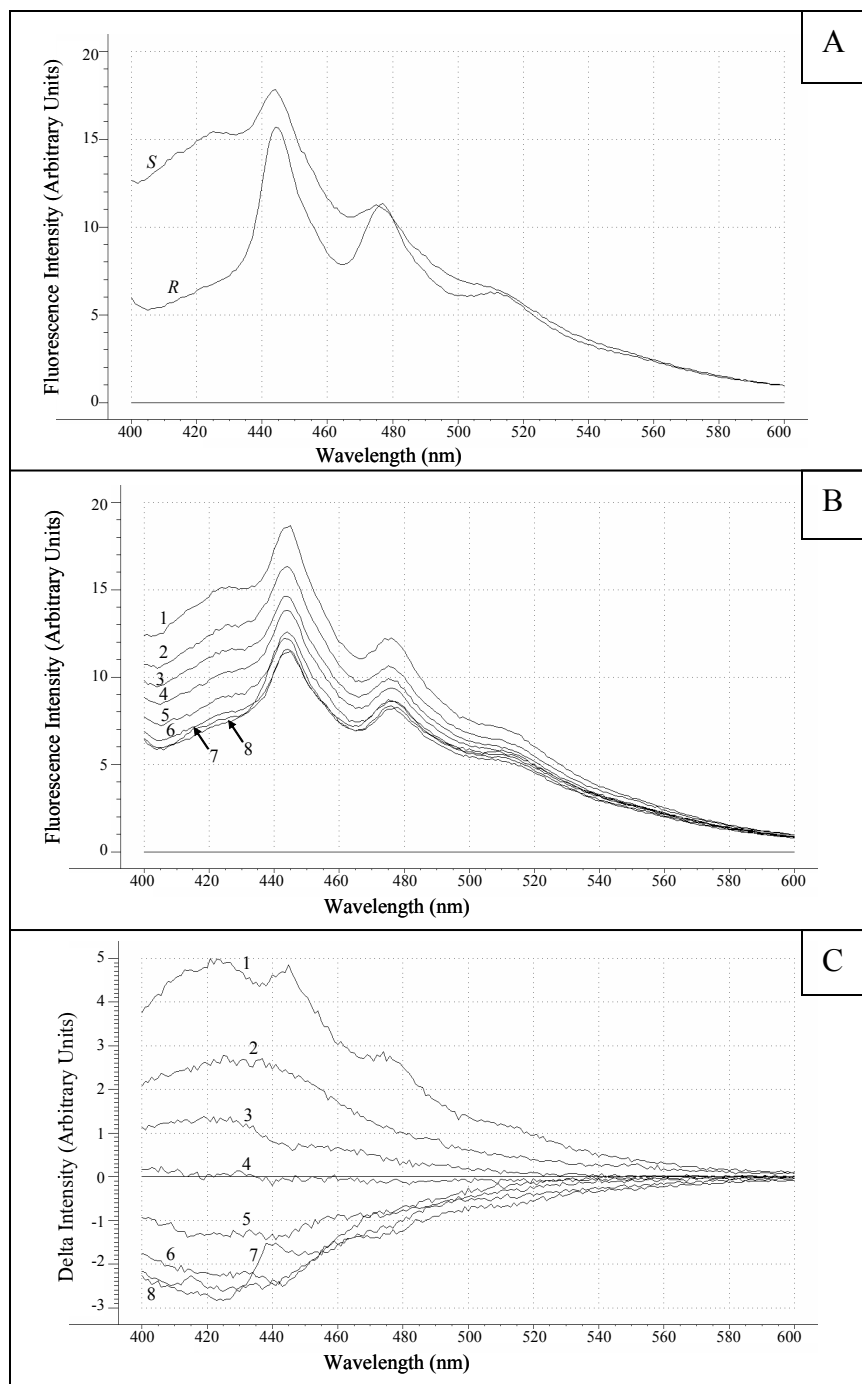
Figure 3.2 (A). Fluorescence emission spectra ($\lambda_{ex} = 380$ nm) of 1×10^{-4} M BOH enantiomers in the presence of 1.5 % w/v poly-L-SULV; (B) Fluorescence emission spectra of solutions containing 1.5 % w/v poly-L-SULV and 1×10^{-4} M BOH of various enantiomeric compositions. Mol fraction of (*R*)-BOH: (1) 0.1; (2) 0.3; (3) 0.4; (4) 0.6; (5) 0.7; (6) 0.8; (7) 0.9; (8) 0.95. (C). Mean-centered spectral plot of solutions containing 1.5 % w/v poly-L-SULV and 1×10^{-4} M BOH of various enantiomeric compositions. Mol fraction of (*R*)-BOH: (1) 0.1; (2) 0.3; (3) 0.4; (4) 0.6; (5) 0.7; (6) 0.8; (7) 0.9; (8) 0.95.

74

Better insight into the spectral variations that occur with different enantiomeric compositions can be gained from a plot of the mean-centered spectra (Figure 3.2C). The mean-centered plot was obtained by averaging the spectra of the eight solutions and then subtracting this average spectrum from the spectrum of each individual sample on a wavelength-by-wavelength basis. Figure 3.2C is interesting because the spectra of samples containing enantiomeric mol fractions of (R)-BOH less than 0.5 are above the origin of the graph while those containing mol fractions of (R)-BOH greater than 0.5 are below.

Fluorescence emission spectra (λ_{ex} = 365 nm) of 1 × 10^{-4} M (R)- and (S)-BNA in the presence of poly-L-SULV are illustrated in Figure 3.3A. As observed for BOH, the (R)- and (S)-BNA enantiomers have different spectra in the presence of poly-L-SULV. With this analyte, the two enantiomers have the same general spectral profile, but the fluorescent intensities observed for the two enantiomers are different. In addition, while the (S)-BOH isomer produced the most fluorescence intensity in the study with poly-L-SULV (Figure 3.2A), the opposite was observed for BNA in the presence of poly-L-SULV.

Figure 3.3B illustrates the fluorescence emission spectra of the eight solutions containing 1 × 10^{-4} M of BNA with varying enantiomeric composition in the presence of poly-L-SULV. The samples have a maximum fluorescence emission at 412 nm. Once again, a variation of emission spectral intensity with enantiomeric composition of BNA analyte is observed. The mean-centered spectral plot for the BNA samples is illustrated in Figure 3.3C. In contrast to the mean-centered spectral plot obtained for the BOH samples, samples containing enantiomeric compositions of (R)-BNA less than 0.5 mol fraction are below the origin, while those containing less than 0.5 mole fraction of (R)-BNA are above.
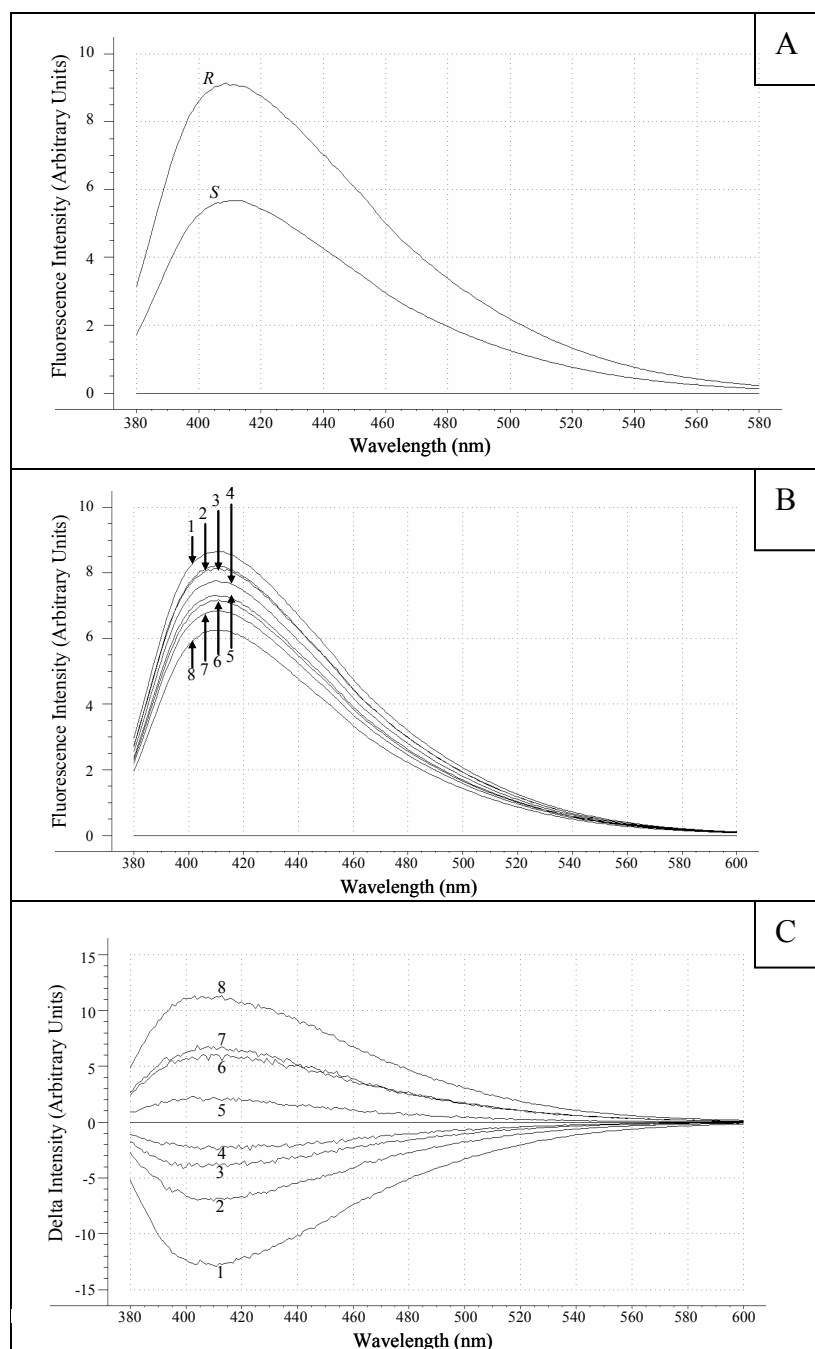
Figure 3.3 (A). Fluorescence emission spectra (λ_{ex} = 365 nm) of 1×10^{-4} M BNA enantiomers in the presence of 1.5 % w/v poly-L-SULV; (B) Fluorescence emission spectra of solutions containing 1.5 % w/v poly- L –SULV and 1×10^{-4} M BNA of various enantiomeric compositions. Mol fraction of (*R*)-BNA: (1) 0.115; (2) 0.350; (3) 0.450; (4) 0.500; (5) 0.650; (6) 0.750; (7) 0.820; (8) 0.980. (C). Mean-centered spectral plot of solutions containing 1.5 % w/v poly-L-SULV and 1×10^{-4} M BNA of various enantiomeric compositions. Mol fraction of (*R*)-BNA: (1) 0.115; (2) 0.350; (3) 0.450; (4) 0.500; (5) 0.650; (6) 0.750; (7) 0.820; (8) 0.980.

76
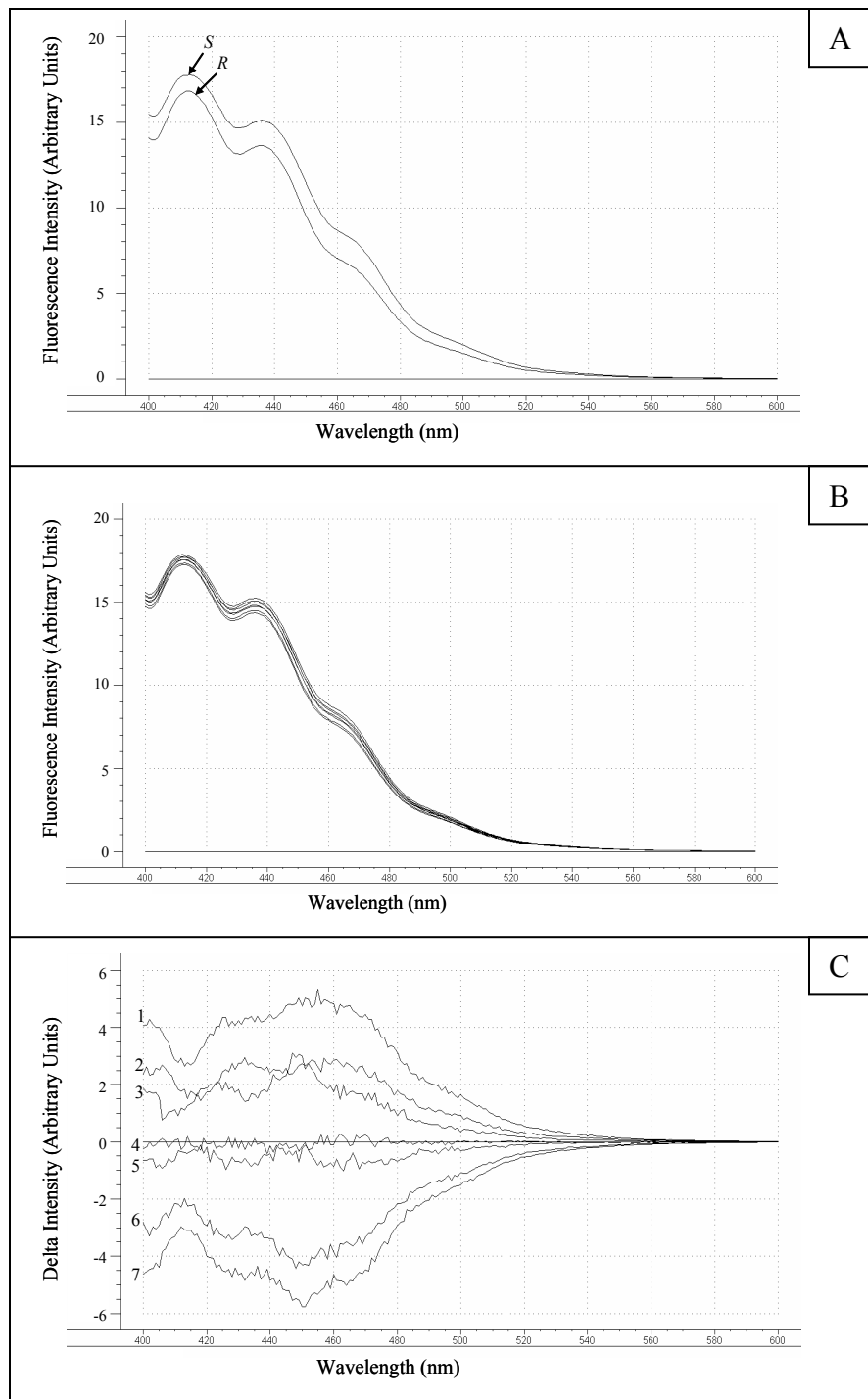
Figure 3.4 (A). Fluorescence emission spectra (λ_{ex} = 380 nm) of 1×10^{-4} M TFA enantiomers in the presence of 1.5 % w/v poly-L-SULV; (B) Fluorescence emission spectra of solutions containing 1.5 % w/v poly-L–SULV and 1×10^{-4} M TFA of various enantiomeric compositions. Spectra too close to label individually. (C). Mean-centered spectral plot of solutions containing 1.5 % w/v poly-L-SULV and 1×10^{-4} M TFA of various enantiomeric compositions. Mol fraction of (*R*)-BNA: (1) 0.20; (2) 0.35; (3) 0.40; (4) 0.55; (5) 0.60; (6) 0.80; (7) 0.90.

Figure 3.4A illustrates the fluorescence emission spectra of (*R*)- and (*S*)-TFA enantiomers in the presence of poly-L-SULV ($\lambda_{ex} = 380$ nm). In this case, only a slight change in emission intensity is observed for the two enantiomers. The emission spectra of seven solutions containing a fixed concentration of TFA analyte (1×10^{-4} M) of various enantiomeric compositions in the presence of poly-L-SULV is illustrated in Figure 3.4B. The maximum fluorescence emission for the TFA samples was at 414 nm. Again, the spectra of the various TFA samples depend upon the enantiomeric composition of the samples. Compared to the variations observed in the emission spectra of BOH and BNA (Figures 3.2B and 3.3B), changes in the emission intensity observed with the TFA samples are somewhat smaller. As with BOH, the mean-centered emission spectra of samples containing mol fractions of (*R*)-TFA less than 0.5 are above the origin of the graph, while those containing more than 0.5 mol fraction of (*R*)-TFA are below.

Multivariate regression methods have been widely used for correlating small spectral changes with known compositional changes, and the methods are well established in analytical chemistry.[34-37] Multivariate regression modeling is a two-phase process. In stage one, or the calibration phase, spectra of a training set of known composition (i.e. the enantiomeric composition of the analyte in this study) are collected over a given wavelength range. Then a regression model is developed to correlate the changes in the fluorescence emission spectral data with the known compositions of the training-set samples. In the second stage, or validation phase, the regression model developed in the calibration phase is validated with a new, independently prepared test- or validation-set of samples of known enantiomeric composition. It must be stressed that while the analyte concentration in the validation- and calibration-sample sets must be the same (i.e., 1×10^{-4} M in this study), the two sets must contain samples with

78

different enantiomeric compositions. In the validation phase, the spectra of the validation samples are taken over the same wavelength range that was used to prepare the model in the calibration phase. The enantiomeric compositions of the validation samples are then predicted from the spectral data using the model developed in the calibration phase. The performance of the model in predicting future samples is evaluated by how well the predicted enantiomeric compositions compare with their actual values.

The regression coefficient, the slope, and the offset obtained from the PLS-1 regression modeling of the BOH samples in the presence of poly-L-SULV are listed in Table 3.1 A perfect model would have a regression coefficient of 1, a slope of 1, and an offset of 0. As expected, better regressions of the spectral data with the enantiomeric composition of the analytes were obtained in the wavelength regions that showed the most variation in the spectral data obtained with the training set of samples. While the regression parameters for the different models look quite good, the real test of any regression model is its ability to correctly predict the composition of unknown samples. To test the prediction ability, the models were validated with sets of independently prepared validation samples of known enantiomeric composition. For this purpose, new sets of sample solutions containing 1×10^{-4} M of each analyte were prepared in 1.5 % w/v poly-L-SULV, having different enantiomeric compositions from those used to prepare the regression models. The spectra of these samples were then recorded over the same wavelength region as used to develop the regression models. The results of the validation study for each guest are listed in Tables 3.2. The ability of the model to correctly predict enantiomeric composition of the validation samples was evaluated by use of the root-mean-square percent relative error (*RMS%RE*). A detailed equation for the calculation of the *RMS%RE* is found in Chapter 2.

Table 3.1   Figures of merit obtained from multivariate regression analysis of calibration samples for *R*-enantiomers of BOH, BNA, and TFA.

Analyte	Regression coefficient	Slope	Offset
BOH	0.9986	0.9972	1.69×10^{-3}
BNA	0.9979	0.9959	2.37×10^{-3}
TFA	0.9989	0.9979	1.15×10^{-3}

Table 3.2   Actual and predicted mol fraction of (*R*)-BOH, (*R*)-BNA, (*R*)-TFA containing 1×10^{-4} M of each analyte in 1.5% w/v poly-L-SULV.

BOH			BNA			TFA		
Actual	Predicted	%RE	Actual	Predicted	%RE	Actual	Predicted	%RE
0.233	0.290	2.47	0.125	0.131	4.80	0.101	0.093	-2.47
0.318	0.320	0.63	0.347	0.337	-2.88	0.265	0.278	4.91
0.465	0.444	-4.52	0.465	0.439	-5.59	0.310	0.315	1.61
0.501	0.487	-2.79	0.511	0.493	-3.52	0.400	0.376	-6.00
0.628	0.637	1.43	0.634	0.647	2.05	0.531	0.555	-5.80
0.792	0.763	-3.66	0.792	0.787	-0.63	0.603	0.568	4.52
0.846	0.876	3.55	0.846	0.807	-4.61	0.798	0.831	4.13
0.957	0.978	2.19	0.978	1.027	5.01	0.955	0.932	-2.41
0.978	1.008	3.07	0.995	0.974	-2.11	0.985	0.998	1.32
0.989	0.982	-0.71	---	---	---	0.995	1.080	8.54
RMS%RE		**2.78**			**3.81**			**5.21**

In the study with BOH, the *RMS%RE* for the ten validation samples was 2.78 %. For the validation study with BNA, the *RMS%RE* was 3.81 %, and for the validation study with TFA,

the *RMS%RE* was 5.21 %. While the results of the validation studies for the three analytes are quite good, they do depend somewhat on the analyte. In terms of *RMS%RE*, the validation result obtained for BOH was slightly better than those obtained for BNA and TFA.   The analyte dependence of the *RMS%RE* observed in this study will ultimately depend on the extent of the interaction between the chiral analyte and the chiral selector. In this study, for example, BOH and TFA are partially anionic whereas BNA is neutral. Analyte differences such as this will ultimately influence the interactions with the negatively charged poly-L-SULV, resulting in models with different predictive capabilities.

The ability of the model to accurately predict the enantiomeric composition of the validation samples depends on the extent of the spectral variation obtained with the test set of samples in the calibration phase. For example, comparing the spectral data in Figures 3.2B, 3.3B, and 3.4B for the calibration sets, the spectral variation with BOH and BNA in the presence of poly-L-SULV is much greater than that observed with the TFA samples.

The spectral differences observed with the calibration samples as the enantiomeric composition of the samples is varied will ultimately depend on the diastereomeric interactions that occur between the analyte and the chiral selector. While the exact details of these diastereomeric interactions are not known at this time, factors like hydrophobicity of the analyte, solubility of the analyte in the chiral poly-L-SULV micellar environment, the possibility of multiple analyte/surfactant interactions, polarity, charge, and size of the analyte may all play a role in producing subtle spectral variations that depend upon the enantiomeric composition of the analyte.

In the case of BOH and TFA, the hydrophilic hydroxyl groups can form hydrogen bonds with the carbonyl groups of poly-L-SULV. In the case of BNA, strong electrostatic interactions

can also occur between the amine groups on BNA and the carbonyl groups of the poly-L-SULV molecular micelle. Unlike TFA, which has only one hydroxyl group, the two hydroxyl groups of BOH and two amine groups of BNA can simultaneously interact with the two carbonyl groups of poly-L-SULV, which may result in stronger diastereomeric interactions (because two sites are involved) for BOH and BNA.

3.3.2 Comparative Study of Single Amino Acid and Dipeptide Based Molecular Micelles

The dipeptide poly-L-SULV molecular micelle used in the previous study has two chiral centers associated with the dipeptide composed of valine and leucine. To study the influence of the molecular micelle on the diastereomeric micellar interactions with the analyte, two single-amino-based molecular micelles (poly-L-SUL and poly-L-SUV) were selected. By contrast with poly- L-SULV, the two single-amino-based molecular micelles poly-L-SUL and poly-L-SUV each have only one chiral center associated with the single amino acids on the respective molecular micelles.

In the studies with the single-amino-acid-based molecular micelles, the sample preparation and multivariate regression modeling were performed as described in the study with poly-L-SULV. In these studies, spectral variations were observed with test sets of BOH, BNA, and TFA of varying enantiomeric composition for samples containing poly-L-SUL. By contrast, no notable spectral variations were observed with test sets of BOH and BNA when poly-L-SUV was used as chiral selector. As a result, it was not surprising that no reasonable model could be developed from the spectral data obtained with BOH and BNA in the presence of poly-L-SUV. Similar poor enantiomeric resolution was observed for BOH and BNA in MEKC studies[31] when poly-L-SUV was used as a chiral selector. By contrast, when poly-L-SUV was used as a chiral

selector with TFA, reasonable spectral variations were observed for samples with various enantiomeric compositions.

Figure 3.5 illustrates a bar graph that compares the *RMS%RE* values obtained for the regression models for BOH, BNA, and TFA in the presence of single-amino acid poly-L-SUL and dipetide poly-L-SULV. In all cases, better predictions of the enantiomeric composition of samples were obtained when dipetide poly-L-SULV was used as a chiral selector. While the two molecular micelles have slightly different hydrophobicities and molecular sizes, the major difference in the prediction ability of the regression models made with poly-L-SULV may be due to the fact that poly-L-SULV has two chiral centers. It is expected that better chiral discrimination would result with a chiral selector that could simultaneously interact at two chiral centers with a chiral analyte.
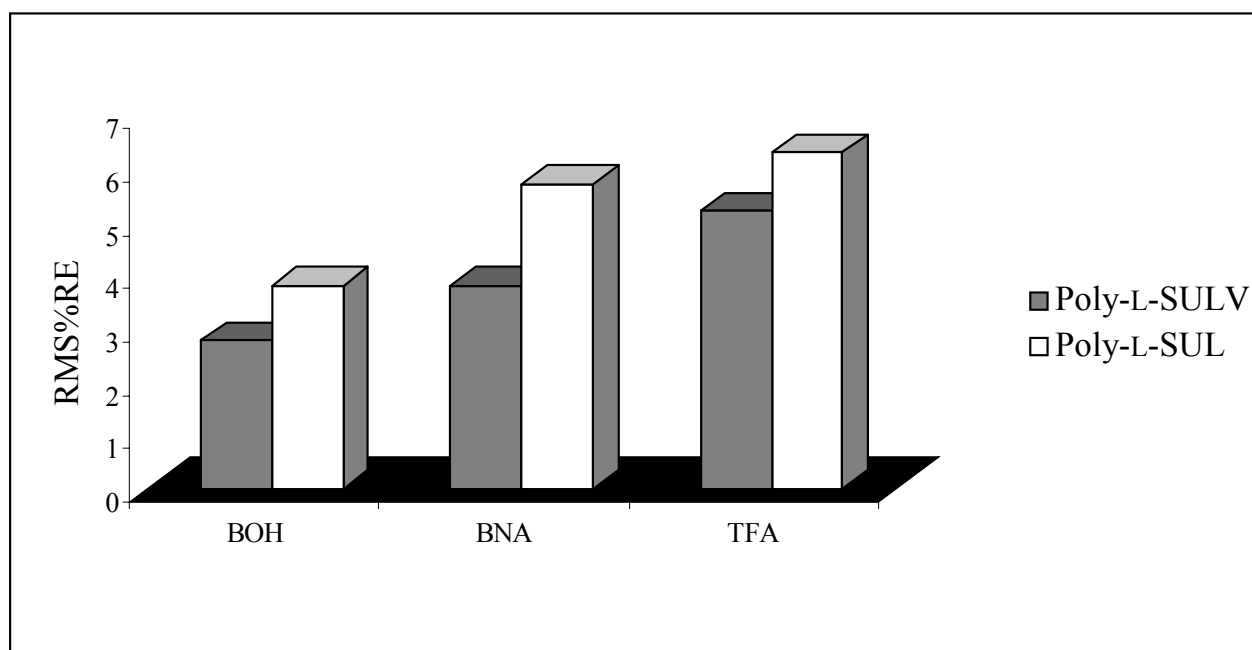
Figure 3.5   *RMS%RE* for BOH, BNA, and TFA using poly-L-SULV and poly-L-SUL.

3.3.3 Guest-Host Complexation in Tris/Borate Buffer Medium

To study the influence of the solvent medium on the chiral discrimination with molecular micelles, a series of experiments was performed in Tris/borate buffered solutions. It is known, for example, that in MEKC, the buffer medium and pH can play a prominent role in the chiral discrimination capability of molecular micelles. Once again, sample preparation and multivariate regression modeling were performed as described previously for studies using poly-L-SULV. However, in this study, the molecular micelle chiral selectors were prepared in a 100 mM Tris and 10 mM borate buffer solution at pH 10.0. This buffer medium was chosen for the study because Tris/borate buffer at pH 10.0 has been previously shown to be the optimum buffer condition for the separation of BOH and BNA in MEKC.[32]

Figure 3.6 illustrates the summary of the *RMS%RE* values obtained from the validation studies when buffered and unbuffered solutions of the molecular micelle were used as chiral selectors. As shown in the figure, in all cases better predictions were obtained when Tris/borate buffered solutions were used. In agreement with the results of the comparative study of poly-L-SULV and poly-L-SUL for BOH and BNA in ordinary aqueous solution, better predictions were obtained for BOH and BNA when poly-L-SULV was used as a chiral selector in a Tris/borate buffered solution (Figure 3.6C). Figure 3.6D illustrates the results of the validation study conducted for TFA when poly-L-SUV was used as a chiral selector in both aqueous and Tris/borate buffered solutions. As with the results obtained for BOH and BNA, better results were obtained for TFA in the buffered solutions. The better regression models obtained in the buffered solutions may be attributed to differences in the charge of the analytes in the buffered solutions.
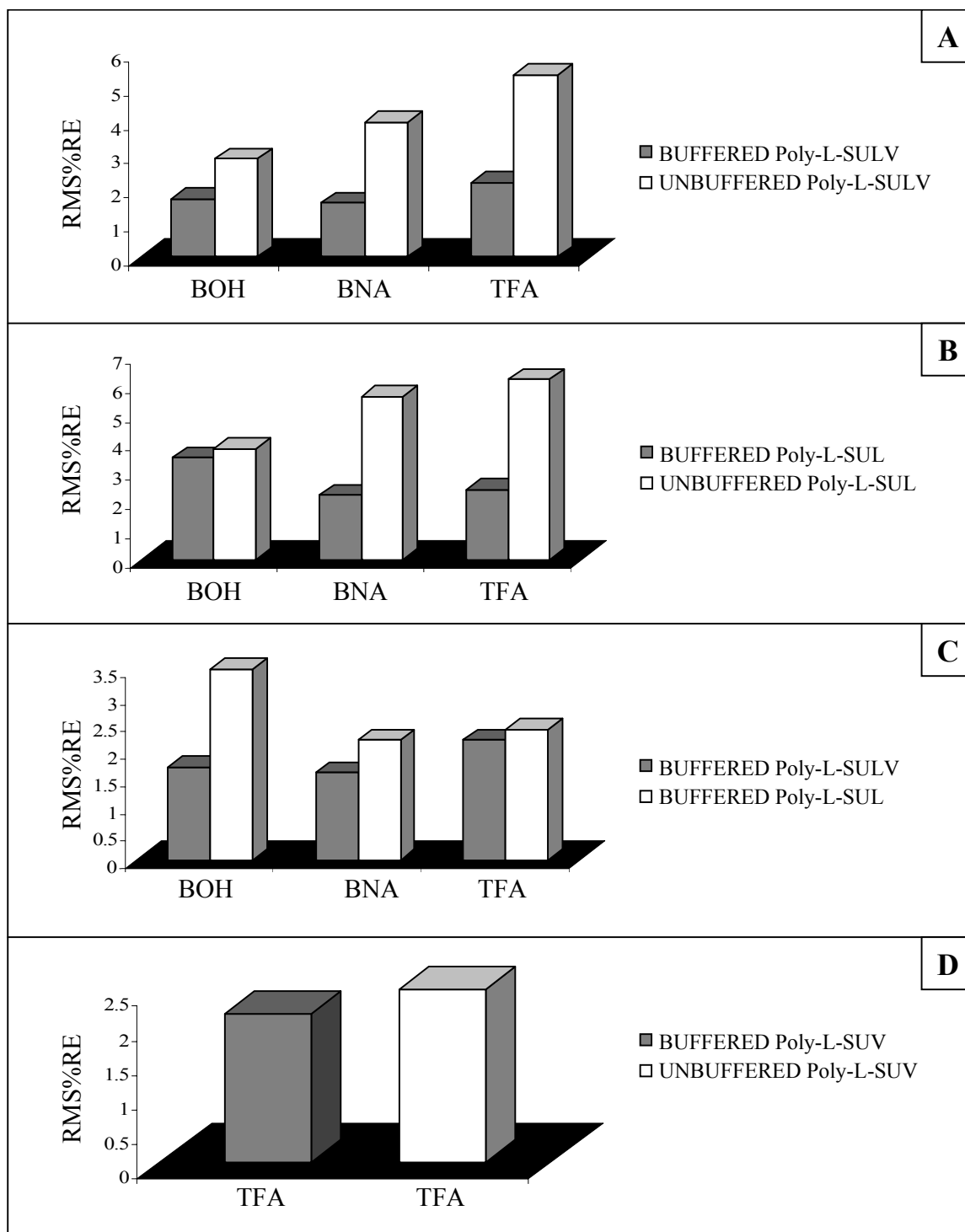
Figure 3.6   *RMS%RE* for BOH, BNA, and TFA with various molecular micelles in buffered and unbuffered solutions using (A) poly-L-SULV, (B) poly-L-SUL, (C) poly-L-SULV and poly-L-SUL, and (D) poly-L-SUV.

3.3.4 Effect of Molecular Micelle-to-Analyte Ratio

To determine the effect of molecular micelle concentration on the results obtained by regression modeling, a series of experiments was performed with BNA and TFA where the chiral analyte concentration was reduced to 5×10^{-6} M while keeping the concentration of poly-L-SULV constant at 1.5 % w/v as in the previous studies. This was possible because of the high sensitivity afforded by using fluorescence spectroscopy with the highly fluorescent polynuclear aromatic chiral analytes. Once again, the sample preparation and multivariate regression modeling were performed as described previously. By lowering the chiral analyte concentration while keeping the concentration of the molecular micelle constant at 1.5 w/v %, the ratio of the surfactant concentration to the chiral analyte concentration is increased. In other words, there is more poly-L-SULV per mol of chiral analyte.

Figure 3.7 illustrates the predicted versus actual plots obtained from the regression models prepared with BNA and TFA. Validation studies conducted with these models for BNA and TFA gave *RMS%RE* values of 2.1 % and 2.3 %, respectively. Compared with the previous studies where higher analyte concentrations were used (1×10^{-4} M), the regression models made with lower chiral analyte concentrations (5×10^{-6} M) actually had better prediction capabilities (lower *RMS%RE* values). This result might be attributed to having a higher surfactant-to-analyte ratio, particularly if more surfactant leads to more micellar interactions with the analyte. In Chapter 2 of this dissertation, better selectivity and enantiomeric discrimination of chiral analytes were reported in MEKC at high molecular micelle concentration in the BGE.[38]

Admittedly, further study of the diastereomeric micellar interactions is needed to fully understand how chiral molecular micelles serve as chiral selectors. The use of fluorescence anisotropy and fluorescence lifetime studies to investigate these micellar interactions might give

additional information and a clearer understanding of their nature. Potentially, with further development, this technique may be useful for the rapid- and high-throughput screening of hundreds of potential drug candidates by the pharmaceutical industry and for routine analysis of racemates, pure enantiomers, and any intermediates in the manufacturing process. In addition, this technique is expected to be useful for the determination of enantiomeric composition of chiral pesticides and herbicides in the environment.
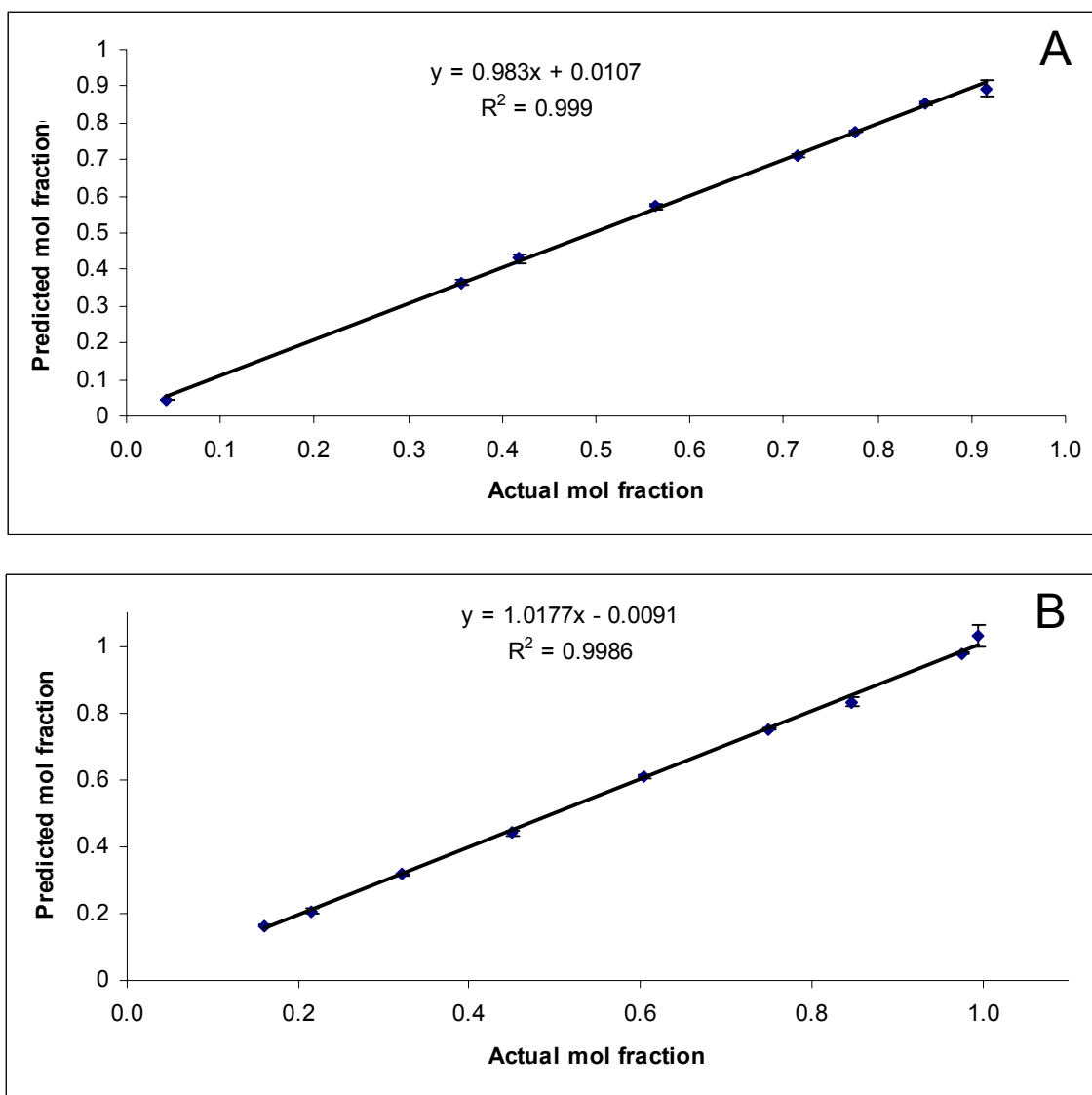
Figure 3.7 Predicted mol fraction composition versus actual known composition for 5×10^{-6} M of R-enantiomer in 1.5% w/v poly-L-SULV chiral selector. (A) R-BNA, (B) R-TFA.

3.4. Conclusions

Chemometric modeling by PLS-1 regression analysis of steady-state fluorescence spectral data obtained for chiral analytes in the presence of chiral molecular micelles has been shown to produce regression models with good predictive abilities. The ability of the model to correctly predict the enantiomeric composition of unknown samples was found to depend upon the chiral analyte being analyzed, the chiral molecular micelle used, and the solvent medium used. Generally, better predictions were obtained when the dipetide molecular micelle, poly-L-SULV, was used as a chiral selector and when the samples were prepared in Tris/borate buffered solutions. Better predictions were also obtained when the concentration ratio of molecular micelle to chiral analyte was increased. Compared with chiral selectors like cyclodextrin, the use of chiral molecular micelles facilitated easy solubility of highly hydrophobic analytes that would not have been possible with cyclodextrin alone.

3. 5 References

[1]   Buxton, S.; Roberts, S., *Organic Stereochemistry*, Longman, Singapore, 1996.

[2]   F. Jamali, R. Mehvar, F. M. Pasutto *J. Pharm. Sci.* 1989, *78*, 695-715.

[3]   Caldwell, J. *J. Chromatogr. A*. 1996, *719,* 3-13.

[4]   Schreier, P.; Bernreuther, A.; Huffer, M. *Analysis of Chiral Organic Molecules*, Walter de Gruyter, New York, 1995.

[5]   Aboul-Enein, H. Y.; Ali, I. *Chiral Separations by Liquid Chromatography and Related Technologies*, Marcel Dekker, New York 2005.

[6]   Zief, M.; Crane, L. *Chromatographic Chiral Separations*, Marcel Dekker, New York, 1998.

[7]   Subramanian, G. *Chiral Separation Techniques: A Practical Approach*, Wiley-VCH, Weinheim, 2001.

[8]   Schmid, M.; Laffranchini, M.; Gubitz, G. *Electrophoresis*, 1999, *20,* 2458-2461.

[9]   Liu, X.; Ilankumaran, P.; Guzei, I.; Verkade J. *J. Org. Chem*. 2000, *65*, 701- 706.

[10]   Szejili, J.; Osa, T. Eds. *Supramolecular Chemistry—Cylcodextrins*, Volume 3, Oxford, Pergamon. 1996.

[11]   Easton, C.; Lincoln, S. *Modified Cyclodextrins*, Imperial College Press, London, 1999.

[12]   Wang, J.; Warner, I. *J. Chromatogr. A*. 1995, *711,* 297-304.

[13]   Maichel, B.; Potocek, B; Gas, B.; Chiari, M.; Kenndler, E. *Electophoresis* 1998, *19*, 2124-2128.

[14]   Desiderio, C.; Fanali, S. *J. Chromatogr. A*. 1998, *807*, 37-56.

[15]   Pascoe, R.; Peterson, A.; Foley, J. *Electrophoresis* 2000, *21*, 2033-2042.

[16]   Hyun, M.; Jin, J.; Lee, W. *J. Chromatogr. A*. 1998, *822*, 155-161.

[17]   Finn, M. *Chirality* 2000, *14*, 534-540.

[18]   Lightner, D.; Gurst, J. *Organic Conformation Analysis and Stereochemistry from Circular Dichroism Spectroscopy*, Wiley-CVH, New York, 2000.

[19]   Fakayode, S.; Busch, M.; Bellert, D.; Busch, K. *Analyst* 2005, *130*, 233-241.

[20]   Fakayode, S.; Busch, M.; Busch, K. *Talanta* 2006, *68*, 1574-1583.

[21]   Fakayode, S.; Swamidoss, I.; M. A. Busch, K. W. Busch *Talanta* 2005, *65*, 838-845.

[22]   Busch, K.; Swamidoss, I.; Fakayode, S.; Busch, M. *Anal. Chim. Acta*, 2004, *525*, 53-62.

[23]   Busch, K.; Swamidoss, I.; Fakayode, S.; Busch, M. *J. Am. Chem. Soc*. 2003, *125*, 1690-1691.

[24]   Tran, C.; Grishko, V.; Oliveira D. *Anal. Chem*. 2003, *75*, 6455-6462.

[25]   Tran, C.; Oliveira, D.; Grishko, V. *Anal.Biochem*. 2004, *325*, 206-214.

[26]   Edward, S.; Shamsi S. *J. Chromatogr. A*. 2000, *903*, 227-236.

[27]   Wang, J.; Warner, I. *J. Chromatogr. A*. 1995, *711*, 297-304.

[28]   Agnew-Heard, K.; Pena, M.; Shamsi, S.; Warner, I. *Anal. Chem*. 1997, *69*, 958-964.

[29]   Yarabe, H.; Shamsi, S.; Warner, I. *Anal. Chem*. 1999, *71*, 3992-3999.

[30]   Shamsi, S.; Warner, I. *Electrophoresis* 1997, *18*, 853-872.

[31]   Billiot, H.; Billiot, E.; Warner, I. *J. Chromatogr. A*. 2001, *922*, 329-338.

[32]   Shamsi, S.; Valle, B.; Billiot, F.; Warner, I. *Anal. Chem*. 2003, *75*, 379-387.

[33]   McCarroll, M.; Billiot, F.; Warner, I. *J. Am. Chem. Soc*. 2001, *123*, 3173-3174.

[34]   Malinowski, E. *Factor Analysis in Chemistry*, John Wiley, New York, 1991.

[35]   Adams, M. *Chemometrics in Analytical Spectroscopy*, Royal Society of Chemistry, Cambridge, 1995.

[36]   Martens, H.; Naes, T. *Multivariate Calibration*, John Wiley, New York, 1989.

[37]   Beebe, K.; Pell, R.; Seasholtz, M. *Chemometrics A Practical Guide*, John Wiley, New York, 1998.

CHAPTER 4

DETERMINATION OF ENANTIOMERIC COMPOSITIONS OF ANALYTES USING NOVEL FLUORESCENT CHIRAL MOLECULAR MICELLES AND STEADY-STATE FLUORESCENCE

4.1 Introduction

The number of chiral chemicals used in the pharmaceutical industry as starting materials, intermediates, and prescribed drugs, continues to increase each year. As a result of the differing biological activity of individual enantiomers, rapid chiral analysis of these chemicals continues to be extremely important in the pharmaceutical industry.[1-3] Considerable differences in the toxicological, pharmacological, or pharmacokinetic properties of individual enantiomers also highlight the importance of assessing the stereochemical purity of a compound in the cosmetic and fragrance industries and environmental analysis. In an effort to eliminate potential toxic side effects, most approved new chiral chemicals are marketed worldwide as single-enantiomer drugs rather than as racemates.[4] Thus, as a consequence of policies of the United States Food and Drug Administration, accurate determination of enantiomeric composition and purity is necessary for production of drugs containing only the therapeutically active enantiomers, which requires sensitive and accurate analytical techniques.[5]

Chiral analysis has previously been achieved by use of various chiral selectors such as cyclodextrins (CDs),[6-10] antibiotics,[11-14] and crown ethers.[15-18] However, despite good chiral recognition ability, these chiral selectors have several limitations resulting from low solubility, high cost, and difficult synthetic procedures. Several recent advances have been made in an attempt to address some of these problems. For example, the use of modified or substituted CDs, rather than native CDs, has led to improved guest selectivity.[6] Another often encountered problem is the limited solubility of large hydrophobic chiral molecules. However, this problem

can be alleviated by use of surfactants that form micelles with apolar pockets and a polar surface. Use of these micelles enhances the solubilization and interaction of highly hydrophobic molecules.

Molecular micelles, also known as polymeric surfactants, have been used in numerous analytical approaches such as chiral discriminators for the analysis of chiral molecules of different molecular size and polarity.[19-25] In Chapter 3 of this dissertation, the utility of molecular micelles as chiral selectors for determining the enantiomeric composition of three highly hydrophobic fluorescent chiral molecules using steady-state fluorescence spectroscopy and multivariate regression analysis of spectral changes in chiral guest-host complexes was demonstrated. In this study, differences in analyte fluorescence emission were observed due to the formation of diastereomeric complexes between the chiral molecular micelle and chiral analyte. These observed spectral differences correlated well with enantiomeric composition because of the stability of guest-host complexes formed between the enantiomers and the chiral selector. This analytical approach offered several advantages for chiral analyses, including rapidity and accuracy, high sensitivity, and low sample consumption.

Although the chiral selector employed in the previous chapter of this dissertation was non-fluorescent, a more useful approach using fluorescent chiral selectors would be attractive for the analysis of non-fluorescent chiral analytes. In addition, the limitation of statistical analysis of differences in fluorescence spectra due to the requirement that chiral analytes be fluorescent would be eliminated. A significant number of chiral molecules do not fluoresce; therefore, fluorescent sensors with diverse molecular structures have been applied in chiral analysis.[26] Chiral fluorescent sensors, i.e. fluorescent chiral molecular micelles (FCMMs), should allow the enantioselective recognition of chiral molecules which may or may not contain a fluorophore.

Therefore, the use of FCMMs for the analysis of non-fluorescent chiral compounds of pharmaceutical and biological interest is explored.

In this chapter, the synthesis, characterization, and chiral selectivity of novel amino acid based FCMMs are reported. By varying the chiral head group of the molecular micelle, we were able to design FCMMs capable of discriminating non-fluorescent chiral analytes. The use of the fluorescent amino acids tryptophan, tyrosine, and phenylalanine, enabled the analysis of a wider variety of chiral analytes using spectroscopic techniques. The syntheses of six FCMMs, the L- and D-enantiomers of poly(sodium *N*-undecanoyl tryptophanate) [poly-SUW], poly(sodium *N*-undecanoyl tyrosinate) [poly-SUY], and poly(sodium *N*-undecanoyl phenylalaninate) [poly-SUF], was accomplished using a two step process from the corresponding amino acid and undecylenic acid. Characterization of FCMMs was performed using ^{1}H and ^{13}C nuclear magnetic resonance (NMR) spectroscopy, mass spectrometry (MS), circular dichroism (CD), and surface tension measurements. Fluorescence spectroscopy, including fluorescence quantum yield, lifetime, and steady-state fluorescence emission, as well as UV/vis absorption were used for the evaluation of FCMMs spectral properties. Finally, the chiral recognition ability of selected FCMMs with non-fluorescent chiral molecules (glucose, tartaric acid, and serine) as well as the determination of enantiomeric composition was evaluated using steady-state fluorescence spectroscopy and multivariate regression analysis.

4.2 Methods

4.2.1 Materials

N-Hydroxysuccinimide, undecylenic acid, sodium bicarbonate, and dicyclohexylcarbodiimide were purchased from Fluka (Milwaukee, WI). Undecylenyl alcohol, monobasic sodium phosphate, dibasic sodium phosphate, sodium hydroxide, hydrochloric acid,

ethyl acetate, and tetrahydrofuran were obtained from Sigma-Aldrich (Milwaukee, WI). Enantiomerically pure serine, tartaric acid, glucose, and α-pinene were also purchased from Sigma-Aldrich (Milwaukee, WI). The amino acids, D-tryptophan, L-tryptophan, D-tyrosine, L-tyrosine, D-phenylalanine, and L-phenylalanine were purchased from Bachem Bioscience Inc. (King of Prussia, PA). All chemicals were used as received. The purity of all analytes and reagents was 99% or higher.

4.2.2 Instrumentation

^{1}H and ^{13}C NMR spectra were acquired in d_6-DMSO on a Bruker ARX-300 spectrometer (Bruker BiosSpin, Billerica, MA). Chemical shift (δ) values are reported in ppm. Coupling constants are reported in Hz. CD was performed using a Jasco J-710 spectropolarimeter (Jasco Inc., Easton, MD) and recorded at room temperature. Absorbance measurements were performed on a Shimadzu UV-3101PC UV-Vis-near-IR scanning spectrometer (Shimadzu, Columbia, MD) using a 1 cm^2 quartz cuvette. Steady-state fluorescence spectra and lifetime measurements were acquired using a SPEX Fluorolog-3 (model FL3-22TAU3; Jobin Yvon, Edison, NJ) equipped with double excitation and emission monochromators (slit widths, 2 nm), a 400 W Xe-arc lamp, and a Hamamatsu R-928 photomultiplier tube. A 0.4 cm path length quartz fluorescence cuvet was used for fluorescence emission data collection. Absorption and fluorescence emission were collected at room temperature and the blank was subtracted from each spectrum.

4.2.3 Syntheses of Molecular Micelles

The monomers of FCMMs were synthesized with minor changes according to the previously reported procedure.[27] Scheme 4.1 shows the two step synthesis from the corresponding amino acid and undecylenic acid. A more detailed synthetic procedure of the synthesis scheme can be found in Chapter 2 of this dissertation. The monomers SUW, SUY, and

94

SUF followed the same synthetic procedure as described for L-SULV. The leucine-valine dipetide was replaced with either tryptophan, tyrosine, or phenylalanine to yield the final monomers L-SUW, D-SUW, L-SUY, D-SUY, L-SUF, and D-SUF, respectively. ^{1}H-NMR and ^{13}C-NMR spectra of L-SUW, L-SUY, and L-SUF can be found in Appendix III.
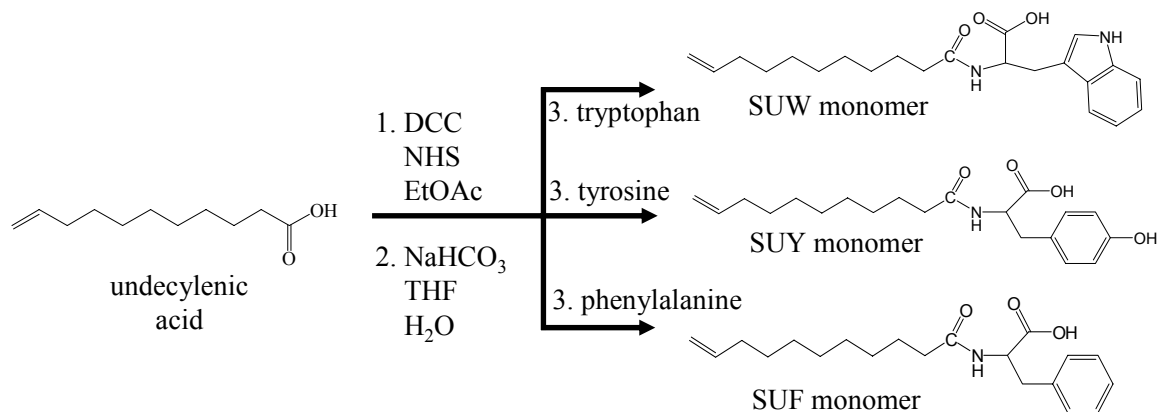
Scheme 4.1 Syntheses of SUW, SUY, and SUF monomers.

Characterization of Undecanoyl-L-Tryptophan. m.p.: 126-129°C, yield: 72%. CMC: 6.9 mM. ^{1}H-NMR (300 MHz, DMSO-d_6) δ (ppm): 1.20-1.42 (m, 12H), 2.01 (bs, 4H), 3.01 (dd, J = 14.40, 6.28 Hz, 1H), 3.25 (dd, J = 14.47, 4.66 Hz, 1H), 4.21 (d, J = 5.52 Hz, 1H), 6.91 (t, J = 7.12 Hz, 1H), 7.00 (t, J = 7.04 Hz, 1H), 7.08 (s, 1H), 7.25 (d, J = 7.4 Hz, 1H), 7.29 (d, J = 8.0 Hz, 1H), 7.50 (d, J = 7.71 Hz, 1H), 10.85 (bs, 1H). ^{13}C-NMR (62.5 MHz, DMSO-d_6) δ (ppm): 26.1, 28.5, 29.1, 29.4, 29.6, 29.7, 34.0, 36.6, 55.9, 111.8, 112.5, 115.4, 118.5, 119.4, 121.0, 124.0, 129.1, 136.7, 139.7, 171.1, 175.8.

Characterization of Undecanoyl-L-Tyrosine. m.p.: 179-182°C, yield: 61%. CMC: 3.4 mM. ^{1}H-NMR (300 MHz, DMSO-d_6) δ (ppm): 1.24-1.42 (m, 12H), 2.03 (bs), 2.79 (dd, J = 6.07, 2.79 Hz, 1H), 2.96 (dd, J = 4.24, 2.96 Hz, 1H), 4.05 (d, J = 5.57 Hz, 1H), 4.95 (d, J = 10.35 Hz,

1H), 5.01 (d, $J = 18.09$ Hz, 1H), 5.81 (ddt, $J = 16.87, 10.08, 6.80$ Hz, 1H), 6.59 (d, $J = 7.85$ Hz, 2H), 6.91 (d, $J = 7.94$ Hz, 2H), 7.12 (d, $J = 7.06$ Hz, 1H), 9.72 (bs, 1H). ^{13}C-NMR (62.5 MHz, DMSO-d$_6$) δ (ppm): 26.0, 26.2, 29.1, 29.4, 29.5, 29.6, 29.7, 34.0, 36.6, 37.6, 56.2, 115.4, 129.9, 131.0, 139.6, 156.4, 171.7, 175.1.

Characterization of Undecanoyl-L-Phenylalanine. m.p.: 109-112°C, yield: 86%. CMC: 8.0 mM. ^{1}H-NMR (300 MHz, DMSO-d$_6$) δ (ppm): 1.18-1.31 (m, 12H), 1.98 (d, $J = 5.37$ Hz, 4H), 4.91 (d, $J = 10.82$ Hz, 1H), 4.96 (d, $J = 17.35$ Hz, 1H), 7.13 (s, 5H), 7.30 (d, $J = 7.05$, 1H). ^{13}C-NMR (62.5 MHz, DMSO-d6) δ (ppm): 26.2, 29.1, 29.3, 29.5, 29.6, 29.7, 29.8, 34.0, 36.5, 38.6, 56.1, 115.4, 126.2, 128.3, 130.2, 139.6, 140.4, 171.9, 175.6.

CMC Determination. Surface tension measurements were collected in pure water for the determination of CMC values of each FCMM using a Sigma 703 Digital Tensiometer (Monroe, CT). Polymerization of FCMMs at five times the CMC was achieved by γ-irradiation using a ^{60}Co source (model 484 R, from J. O. Shepherd, San Fernando, CA) of 0.7 krad/h for 168 h (total dose, 118 krad). ^{1}H-NMR was performed to verify complete polymerization of the products by the loss of the vinyl proton signals at 6.0 – 5.0 ppm.

4.2.4 Sample Preparation

All FCMM samples for CD, steady-state fluorescence spectroscopy and UV absorption studies were prepared in 50 mM dibasic sodium phosphate buffer. The buffer was filtered through a 0.45-μm nylon syringe filter (Nalgene, Rochester, NY) and the pH was adjusted using an ORION model 410A pH meter (Pulse Instruments, Van Nuys, CA) to pH 7 with 0.1 M NaOH prior to the addition of FCMM. Calibration and validation samples for steady-state fluorescence measurements containing FCMM chiral selector and varying analyte enantiomeric composition

were prepared from stock solutions (1×10^{-4} M) dissolved in buffer. Final concentrations were made by transferring appropriate volumes of FCMM and analyte to dry volumetric flasks and diluting with buffer solution. All solutions were sonicated 15 min to ensure proper dissolution and were allowed to equilibrate for 30 minutes.

4.2.5 Data Analysis

The Unscrambler, (CAMO, Inc., Corvallis, OR, version 9.1) chemometric software system was used for multivariate regression analysis of all fluorescence emission spectra. PLS-1 calibration models were developed using full-cross validation. The regression models were validated using an independent set of validation samples with different mole fractions from calibration samples.

4.3   Results and Discussion

4.3.1   Circular Dichroism Measurements

The optical configuration of D-SUW, L-SUW, D-SUY, L-SUY, D-SUF, and L-SUF monomers was confirmed by CD measurements performed with a 1.0-cm path-length cell. D-SUW had a positive band with a maximum at ~232 nm. Optical configuration was confirmed from the L-SUW spectra showing a similar negative CD band at the same wavelength. Similar trends were observed for D-SUY and L-SUY (wavelength maximum ~231 nm) and D-SUF and L-SUF (wavelength maximum ~220 nm) allowing for the unambiguous determination of opposite configuration of each chiral monomer. Following polymerization, CD measurements were repeated for each FCMM. Figure 4.1A-C illustrates the structures for poly-L-SUW, poly-L-SUY, and poly-L-SUF. The CD bands of FCMMs showed the same wavelength maxima and ellipticity as corresponding monomers, confirming the retention of L and D configurations of poly-SUW (Figure 4.2A), poly-SUY (Figure 4.2B), and poly-SUF (Figure 4.2C).

poly-L-SUW poly-L-SUY poly-L-SUF

glucose tartaric acid serine α-pinene

Figure 4.1 Molecular structures of FCMMs and chiral analytes.

Figure 4.2 CD spectra of (A) poly-D-SUW and poly-L-SUW; (B) poly-D-SUY and poly-L-SUY; (C) poly-D-SUF and poly-L-SUF.

4.3.2 FCMM Spectroscopic Characteristics

Both configurations of poly-SUW (2.0×10^{-5} M), poly-SUY (7.0×10^{-5} M), and poly-SUF (2.6×10^{-4} M) showed maximum absorption at 280 nm, 276 nm, and 259 nm, respectively. The corresponding monomers for both configurations had the same absorption maxima as the polymerized molecular micelles. Molar absorptivity (ε) values calculated at the absorbance maximum are listed in Table 4.1. Poly-SUW had the strongest absorption as compared to the other FCMMs. The observed molar absorptivities of FCMMs followed similar trends as for known absorptivity values for the corresponding free amino acids.[28] Phenylalanine has the weakest fluorescence and the simplest structure as compared to tyrosine, which has an added hydroxyl group, and tryptophan having an added indole ring. As expected, these structural variations resulted in a significant difference in fluorescence emission spectra for the FCMMs. Fluorescence emission spectra were collected for each FCMM, using an excitation wavelength (λ_{ex}) close to the maximum absorption wavelength. Poly-SUW ($\lambda_{ex} = 280$), poly-SUY ($\lambda_{ex} = 280$), and poly-SUF ($\lambda_{ex} = 260$) had a maximum fluorescence emission at 370 nm, 320 nm, and 305 nm, respectively.

Table 4.1   Photophysical characteristics of FCMMs.

FCMM	Absorption Characteristics		Fluorescence Characteristics		Fluorescence Lifetimes		
	λ_{max} (nm)	ε (L mol^{-1} cm^{-1})	λ_{ex}, λ_{em} (nm)	Φ	τ_1 (ns)	τ_2 (ns)	τ_3 (ns)
Poly-SUW	280	4237	280, 370	0.08	1.9 (41%)	5.4 (59%)	–
Poly-SUY	276	1060	280, 320	0.04	3.1 (90%)	0.9 (10%)	–
Poly-SUF	259	321	260, 305	0.11	14.7 (20%)	4.1 (46%)	1.0 (34%)

Fluorescence quantum yields for the FCMMs were determined by Williams' comparative method.[29] A series of dilute solutions of poly-L-SUW (2.0×10^{-6} M - 2.0×10^{-5} M), poly-L-SUY (2.5×10^{-5} M - 7.0×10^{-5} M), and poly-L-SUF (1.4×10^{-4} M - 2.6×10^{-4} M) were prepared in 50 mM phosphate buffered at pH 7. Tryptophan in water was used as the fluorescence standard ($\Phi = 0.12$, pH 7)[28] for poly-L-SUW and poly-L-SUY. All solutions, including the standard, were excited at 280 nm. In the case of poly-L-SUF, phenylalanine in water was used as the fluorescence standard ($\Phi = 0.022$, pH 7),[28] and each were excited at 260 nm. Both UV-vis absorption and fluorescence spectra were recorded for five solutions where the FCMM concentration was varied such that the absorbance remained below 0.05. The following equation[29] was used to calculate the quantum yield of each FCMM:

$$\Phi_x = \Phi_{st} \, (Grad_x \, / \, Grad_{st}) \, (\eta_x^2 \, / \, \eta_{st}^2) \qquad\qquad 4.1$$

where Φ is the fluorescence quantum yield, $Grad$ is the gradient from the plot of integrated fluorescence intensity vs. absorbance, η is solvent refractive index (water = 1.33),[29] and subscripts st and x refer to the standard and unknown, respectively. The calculated quantum yields for poly-L-SUW, poly-L-SUY, and poly-L-SUF were 0.08, 0.04, and 0.11, respectively (Table 4.1). Poly-L-SUW and poly-L-SUY had a lower quantum yield than the pure amino acid. However, the fluorescence quantum yield of poly-L-SUF was five times higher than phenylalanine, indicating that the FCMM is a more sensitive fluorophore.

The fluorescence lifetimes of poly-L-SUW, poly-L-SUY, and poly-L-SUF were measured in 50 mM dibasic sodium phosphate (pH 7). A 320 nm long-pass filter was used to optically isolate the signals for each FCMM. Thirty logarithmically spaced frequencies were collected over a frequency range of 10 to 100 MHz using five averages and a 99 s integration time. Frequency-domain measurements were collected for all FCMMs versus *p*-terphenyl which has a

lifetime of 1.17 ns. Frequency-domain phase and modulation decay profiles were analyzed using the Globals software package developed at the Laboratory for Fluorescence Dynamics (University of Illinois at Urbana-Champaign). Enantiomerically pure tryptophan, tyrosine, and phenylalanine have been reported to have single lifetime values of 2.6 ns, 3.6 ns, and 6.4 ns, respectively.[28] In contrast, each FCMM had more than one significant lifetime component as listed in Table 4.1. Generally, it is expected that the fluorescence quantum yields and lifetimes of the FCMMs are likely to be different from the corresponding amino acid standard due to polymerization, aggregation, structure, cavity size, dynamic equilibrium, and hydrophobicity. Also, multiple fluorophores brought into close proximity because of polymerization have been reported to have increased quantum yields and different fluorescence lifetimes as compared to the corresponding monomer.[30,31]

4.3.3 Chiral Recognition

Steady-state fluorescence spectroscopy was used to investigate the chiral recognition ability of the FCMMs with non-fluorescent chiral analytes. The analytes glucose, tartaric acid, and serine were selected due to the differences in structure and non-fluorescent properties. Glucose is a carbohydrate used as a source of energy by the human body and is critical in the production of proteins. Tartaric acid is a known antioxidant, food additive, and an intermediate in chiral molecule synthesis. Serine is an amino acid commonly found in proteins.

The fluorescence emission spectra of 5.0×10^{-6} M D- and L- forms of glucose, tartaric acid, and serine in the presence of 3.0×10^{-5} M FCMM are illustrated in Figure 4.3A, 4.3B, and 4.3C, respectively. Chiral recognition can be confirmed by observing a difference in fluorescence emission intensity of each FCMM in the presence of D- and L-enantiomers of the analyte. This spectral difference is due to the formation of diastereomeric complexes between

enantiomer and FCMM chiral selector. Several factors, such as analyte size, solubility, and shape, as well as hydrophobicity and hydrogen-bonding capability affect the magnitude of interactions between analyte and chiral selector. In addition, the obtained results indicated that such interactions were analyte and chiral selector dependent, which determined the extent of spectral variation. The concentration of FCMMs was held constant; however, it is clear that poly-L-SUW had the largest spectral difference in the presence of each analyte (Figure 4.3I-A1, B1, C1). The emission intensity of poly-L-SUW in the presence of D-glucose and D-serine was higher than the emission intensity of poly-L-SUW in the presence of L-glucose and L-serine. The opposite trend was observed for the emission of poly-L-SUW in the presence of D- and L- tartaric acid. There was no apparent variation in the fluorescence emission spectra of the D- and L-enantiomers of any analyte in the presence of poly-L-SUY (Figure 4.3II-A1, B1, C1) and only a slight difference was observed in the presence of poly-L-SUF (Figure 4.3III-A1, B1, C1).

The variations in fluorescence emission spectra illustrated in Figure 4.3I can be attributed to the diastereomeric complex formed between chiral selector and each analyte enantiomer. The enantiomeric interactions are different and analyte/chiral selector dependent ultimately leading to differences in the spectra. Figure 4.3I (A2, B2, C2) illustrates the mean-centered spectra plots for each enantiomer in the presence of FCMMs. In general, the mean-centered spectra plot provides better insight into the spectral variations and chiral recognition ability of each FCMM. The plots were obtained by subtracting the spectrum of D- and L- form in the presence of FCMM from the D- and L- mean spectra at each wavelength. The poor chiral recognition ability of poly-L-SUY and poly-L-SUF is further confirmed by the noisy centered lines close to the origin of the mean-centered spectra plots.
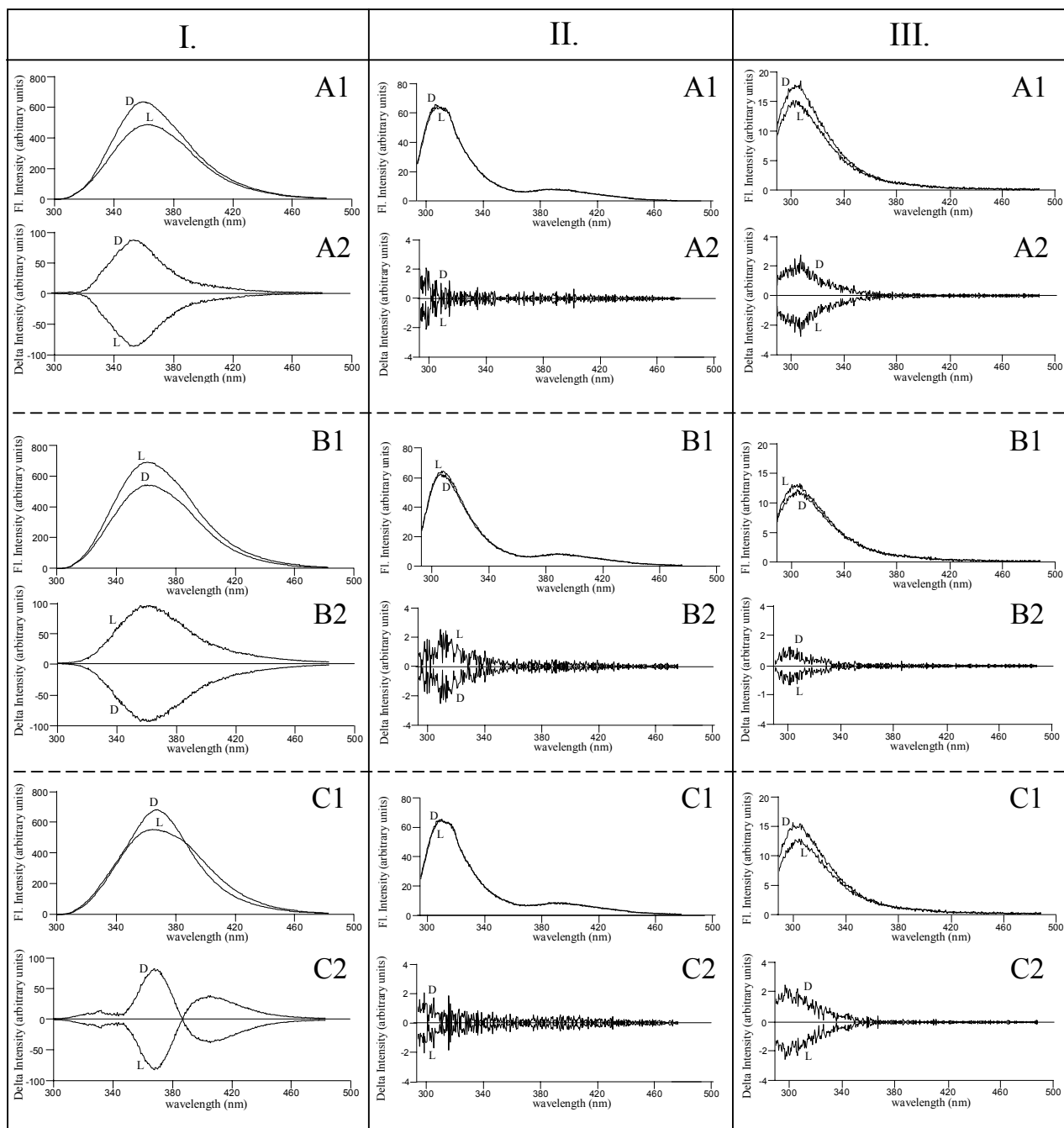
Figure 4.3 Fluorescence emission spectra (1) and mean-centered spectral plots (2) of 3.0×10^{-5} M (I) poly-L-SUW [$\lambda_{ex} = 280$ nm]; (II) poly-L-SUY [$\lambda_{ex} = 280$ nm]; (III) poly-L-SUF [$\lambda_{ex} = 260$ nm] in the presence of 5.0×10^{-6} M enantiomers of (A) Glucose; (B) Tartaric acid; (C) Serine.

The hydrogen-bonding interactions between poly-L-SUW and the multiple hydroxyl groups of glucose, tartaric acid and serine were likely stronger than the hydrogen-bonding interactions with poly-L-SUY and poly-L-SUF. This suggests that poly-L-SUY and poly-L-SUF do not have hydrogen-bonding driven complexations. As a result, chiral recognition studies were performed with a hydrophobic molecule, α-pinene, in order to determine if hydrophobic interactions were possible with poly-L-SUY and poly-L-SUF. Pinene is a terpene, which plays an important role in the fragrance and pharmaceutical industries.[32] Figure 4.4 illustrates the fluorescence emission spectra and mean-centered spectra plots for 1.0×10^{-5} M α-pinene in the presence of 3.0×10^{-5} M poly-L-SUY (Figure 4.4A) and 3.0×10^{-5} M poly-L-SUF (Figure 4.4B). Hydrophobic compounds interact more strongly with the hydrophobic core of the micelle. One enantiomer of α-pinene may dissolve deeper into the hydrophobic pockets of poly-L-SUY and poly-L-SUF, resulting in chiral discrimination. For both FCMMs, the fluorescence emission spectra obtained for (−)-α-pinene had a higher emission intensity than (+)-α-pinene.
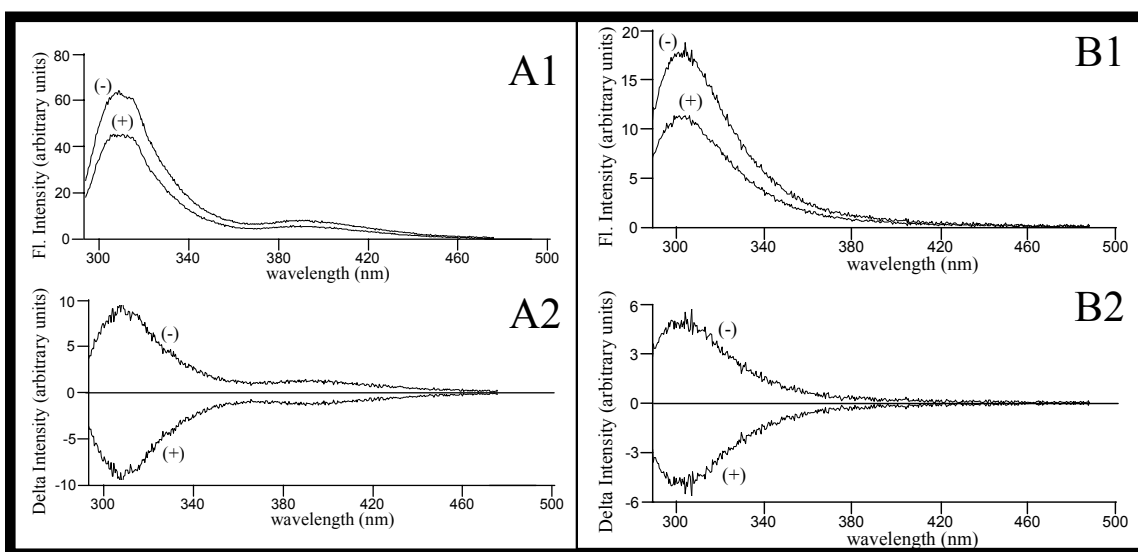
Figure 4.4   Fluorescence emission spectra (1) and mean-centered spectral plots (2) of 3.0×10^{-5} M (A) Poly-L-SUY [λex = 280 nm]; (B) Poly-L-SUF [λex = 260 nm] in the presence of 5.0×10^{-6} M enantiomers of α-pinene.

104

4.3.4 Determination of Enantiomeric Composition

As previously noted, poly-L-SUW exhibited the most spectral difference in the presence of analyte enantiomers for glucose, tartaric acid and serine. As a result, this FCMM was chosen for enantiomeric composition studies with these three analytes. Studies have shown enantiomeric purity can be determined by partial-least-square-regression modeling of steady-state fluorescence spectral data of fluorescent chiral analytes.[33,34] Multivariate regression modeling for enantiomeric composition prediction is a two-phase process. First, during the calibration phase, fluorescence emission spectra of a set of samples with known analyte enantiomer compositions in the presence of chiral selector are collected. The changes in the spectra are correlated to the known enantiomeric compositions and a regression model is developed.

Figure 4.5.IA illustrates the fluorescence emission spectra ($\lambda_{ex} = 280$ nm) of calibration solutions containing a fixed total glucose concentration (5.0×10^{-6} M) with various enantiomeric composition and fixed concentration of poly-L-SUW (3.0×10^{-5} M). As illustrated in Figure 4.3.1A, the fluorescence emission spectra for poly-L-SUW in the presence of 5.0×10^{-6} M D-glucose has a higher intensity than L-glucose. Although the glucose concentration was fixed, as the enantiomeric composition of L-glucose increased, the fluorescence emission intensity decreased.

The mean-centered spectra plots for the set of calibration solutions of various enantiomeric compositions of glucose in the presence of poly-L-SUW was obtained by subtracting the average spectra of all solutions from the spectrum of each individual sample (Figure 4.5.IIA). Additional information can be obtained from a mean-centered spectra plot when compared to the fluorescence emission spectra. Sample 6 contained 0.50 D- and 0.50 L-

and the mean-centered plot overlayed the origin. In Figure 4.5.IIA, the mean-centered plots of solutions containing more than 0.50 D- were above the origin and solutions containing less than 0.50 D- were below the origin. Quick screening of future samples containing an unidentified enantiomeric composition is possible by obtaining the fluorescence emission spectra of an unknown sample and incorporating the spectra into the mean-centered spectra plot. Using this strategy, one can determine if the sample is predominantly D-glucose, L-glucose, or racemic.
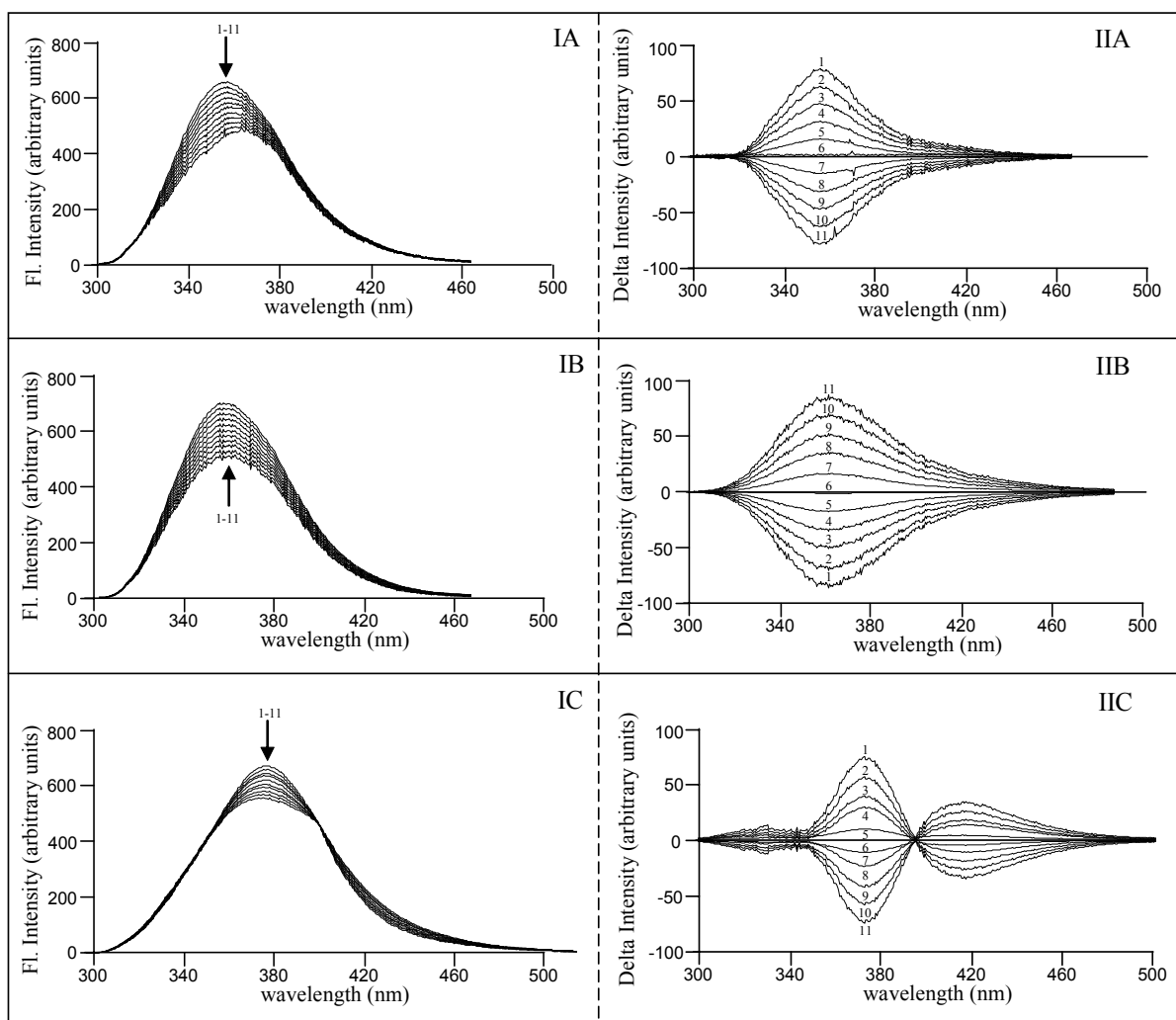
Figure 4.5   Fluorescence emission spectra (I) and mean-centered spectral plots (II) of 3.0×10^{-5} M Poly-L-SUW [λ_{ex} = 280 nm] in the presence of 5.0×10^{-6} M enantiomers of (A) Glucose; (B) Tartaric acid; (C) Serine with varied mole fractions: (1) 1.0 D; (2) 0.9 D; (3) 0.8 D; (4) 0.7 D; (5) 0.6 D; (6) 0.5 D; (7) 0.4 D; (8) 0.3 D; (9) 0.2 D; (10) 0.1 D; (11) 0.0 D.

Fluorescence emission spectra of poly-L-SUW (λ_{ex} = 280 nm) in the presence of a fixed total tartaric acid concentration (5.0×10^{-6} M) of eleven solutions with various enantiomeric compositions are illustrated in Figure 4.5.IB. In contrast to the fluorescence emission spectra obtained for glucose, the fluorescence emission spectra for poly-L-SUW in the presence of 5.0×10^{-6} M D-tartaric acid had lower emission intensity than L-tartaric acid. Likewise, the mean-centered spectra plot for the samples containing greater than 0.50 D-tartaric acid were below the origin and solutions containing less than 0.50 D-tartaric acid were above the origin (Figure 4.5.IIB).

Figure 4.5.IC illustrates the fluorescence emission spectra for eleven solutions of poly-L-SUW (λ_{ex} = 280 nm) in the presence of serine at a fixed concentration (5.0×10^{-6} M) with varying enantiomeric compositions. Similar to glucose, the fluorescence emission spectra for poly-L-SUW in the presence of 5.0×10^{-6} M D-serine has higher emission intensity than L-serine. As expected, the solution containing 0.50 D-serine and 0.50 L-serine is on the origin in the mean-centered spectral plot while solutions containing more than 0.50 D-serine are above the origin and solutions containing less than 0.50 D-serine are below (Figure 4.5.IIC). In addition, samples containing serine had a slight shift in maximum fluorescence emission (λ_{max} = 375 nm) as compared to the samples containing glucose or tartaric acid (λ_{max} = 370 nm).

The predictive ability of the calibration model can be tested by analyzing several figures of merit including the regression coefficient, the slope, and the offset from the PLS-1 regression modeling of the calibration samples. Table 4.2 summarizes the figures of merit for the regression models obtained for D-glucose, D-tartaric acid, and D-serine in the presence of poly-L-SUW. A perfect model would have a regression coefficient of 1, a slope of 1, and an offset of 0. A second phase in multivariate regression modeling is the validation phase, which follows the

calibration phase. During this phase, fluorescence emission spectra of a new set of samples having the same concentrations as the samples prepared in the calibration phase are collected. Although total analyte concentration of validation samples must be the same as calibration samples, enantiomeric compositions should be different. The enantiomeric compositions for the validation samples are predicted using the calibration regression model. The performance of the calibration model to accurately predict validation sample enantiomer composition is determined by the root-mean-square percent relative error (RMS%RE). A detailed equation for the calculation of the *RMS%RE* is found in Chapter 2. Ten validation samples having the same analyte concentration and various enantiomeric compositions were used to calculate RMS%RE. The *RMS%RE* values obtained for the ten validation samples of D-glucose, D-tartaric acid, and D-serine were 1.88%, 2.43% and 2.64%, respectively (Table 4.3). The *RMS%RE* for L-glucose (2.07%), L-tartaric acid (3.48%), and L-serine (3.60%) was slightly higher than the error obtained for the D-enantiomer of each analyte. Previously reported literature has shown that one enantiomer can bind more strongly to the chiral selector.[35,36] Fluorescence anisotropy measurements have concluded that the interaction between the chiral selector and the analyte are due to both stereoselective and nonstereoselective interactions.[35] The results indicated that the D-enantiomer of glucose, tartaric acid, and serine may form a more rigid and stronger complex with poly-L-SUW. Also, the difference in the chiral selectivity for each enantiomer can lead to a difference in predictive capability of the regression model.

Table 4.2   Figures of merit obtained from multivariate regression analysis of calibration samples for D-enantiomers of glucose, tartaric acid, and serine.

Analyte	Regression coefficient	Slope	Offset	Wavelength Range
Glucose	0.9999	0.9996	-1.10×10^{-4}	320-365
Tartaric Acid	0.9998	0.9993	5.09×10^{-4}	340-390
Serine	0.9997	0.9991	6.44×10^{-4}	360-400

Table 4.3 Actual and predicted mole fraction of 5.0×10^{-6} M D- and L- enantiomers of glucose, tartaric acid, and serine in 3.0×10^{-5} M Poly-L-SUW.

(D) Actual mole fraction	Glucose Predicted mole fraction	Relative error (%)	Tartaric Acid Predicted mole fraction	Relative error (%)	Serine Predicted mole fraction	Relative error (%)
0.950	0.947	0.316	0.951	-0.105	0.951	-0.105
0.850	0.851	-0.118	0.844	0.706	0.843	0.824
0.750	0.746	0.533	0.741	1.200	0.739	1.467
0.650	0.650	0.000	0.684	-5.231	0.681	-4.769
0.550	0.548	0.364	0.556	-1.091	0.557	-1.273
0.450	0.450	0.000	0.436	3.111	0.434	3.556
0.350	0.351	-0.286	0.353	-0.857	0.354	-1.143
0.250	0.248	0.800	0.244	2.400	0.243	2.800
0.150	0.153	-2.000	0.148	1.333	0.147	2.000
0.050	0.053	-5.500	0.048	3.220	0.048	4.100
RMS%RE		**1.88**		**2.43**		**2.64**

(L) Actual mole fraction	Glucose Predicted mole fraction	Relative error (%)	Tartaric Acid Predicted mole fraction	Relative error (%)	Serine Predicted mole fraction	Relative error (%)
0.050	0.053	-6.280	0.047	6.700	0.047	6.880
0.150	0.149	0.667	0.146	2.667	0.146	2.667
0.250	0.254	-1.600	0.240	4.000	0.239	4.400
0.350	0.350	0.000	0.356	-1.714	0.356	-1.714
0.450	0.452	-0.444	0.426	5.333	0.425	5.556
0.550	0.550	0.000	0.560	-1.818	0.561	-2.000
0.650	0.649	0.154	0.673	-3.538	0.672	-3.385
0.750	0.752	-0.267	0.734	2.133	0.734	2.133
0.850	0.847	0.353	0.840	1.176	0.839	1.294
0.950	0.947	0.316	0.952	-0.211	0.952	-0.211
RMS%RE		**2.07**		**3.48**		**3.60**

Studies in Chapter 3 of this dissertation demonstrated that the extent of spectral variation will determine the prediction accuracy for enantiomeric composition. Serine had the highest *RMS%RE* value and the lowest degree of spectral variation. This can possibly be due to a fewer number of hydroxyl groups on serine as compared to glucose and tartaric acid. It is also well known that the *%RE* is analyte dependent as a result of the diastereomeric complex formation between chiral selector and chiral analyte.[33,34] Studies evaluating the chiral interaction with dipeptide molecular micelle head groups have been reported.[37] Steady-state fluorescence anisotropy was used to explain chiral separation mechanisms for the separation of various analytes using poly-L-SULV. However, further studies are necessary to understand the details of

the diastereomeric interaction between the novel FCMMs and chiral analytes. The chiral analyses performed in this chapter were completed by use of non-fluorescent chiral analytes. In the next chapter, the investigation of the use of FCMMs for the enantiomeric composition prediction of fluorescent chiral analytes is reported.

4.4 Conclusions

The two enantiomers of three novel FCMM chiral selectors (poly-SUW, poly-SUY, and poly-SUF) were synthesized and characterized using several analytical techniques. Steady-state fluorescence spectroscopy was used as a rapid and sensitive technique for chiral analysis using FCMMs. These chiral selectors were capable of the recognition of non-fluorescent chiral analytes and offered several advantages as compared to current available selectors. Poly-L-SUW showed enhanced chiral recognition with analytes capable of hydrogen bonding, while poly-L-SUY and poly-L-SUF showed good chiral recognition with a more hydrophobic molecule. Conventional fluorescence instrumentation as opposed to specialized polarization instrumentation was used for the prediction of enantiomer composition of three non-fluorescent chiral analytes (glucose, tartaric acid, and serine). PLS-1 regression models of steady-state fluorescence emission spectral data for poly-L-SUW in the presence of the three analytes has been shown to have good prediction capability. Better predictions were obtained for the analytes with the greatest spectral variation in fluorescence emission. Previously, molecular micelles were limited to chiral recognition of fluorescent analytes; however, these FCMMs show promise as potential universal chiral selectors.

4. 5 References

[1] Hacksell, U.; Ahlenius, S. *Trends Biotechnol.* 1993, *11*, 73-74.

[2] Witte, D.; Ensing, K.; Franke, J. P.; De Zeeuw, R. A. *Pharm. World Sci.*1993, *15*, 10-16.

[3] Subramanian, G., Ed. *Chiral Separation Techniques: A Practical Approach,* 2nd Ed.; Wiley-VCH: Weinheim, 2001; Preface.

[4] Agranat, I.; Caner, H.; Caldwell, J. *Nat. Rev. Drug Discov.* 2002, *1*, 753-768.

[5] U.S. Food and Drug Administration; *Development of New Stereoisomeric Drugs* [policy statement] 1992; *22*, 249.

[6] Easton, C. J.; Lincoln, S. F. *Modified Cyclodextrins: Scaffolds and Templates for Supramolecular Chemistry*; Imperial College Press: London, 1999; Chapter 1.

[7] Xu, Y.; McCarroll, M. M. *J. Phys. Chem. B* 2005, *109*, 8144-8152.

[8] Wang, J.; Warner, I. M. *J. Chromatogr. A* 1995, *711*, 297-304.

[9] Chankvetadze, G.; Burjanadze, N.; Santi, M; Massolini, G. *J. Sep. Sci.* 2002, *25*, 733-740.

[10] Ward, T. J.; Hamburg, D. *Anal. Chem.* 2004, *76*, 4635-4644.

[11] Desiderio, C.; Fanali, S. *J. Chromotogr. A* 1998, *807*, 37-56.

[12] Reilly, J.; Sanchez-Felix, M.; Smith, N. W. *Chirality* 2003, *15*, 731-742.

[13] André, C.; Guillaume, Y.-C. *Electrophoresis* 2003, *24*, 1620-1626.

[14] Kang, J.; Wistuba, D.; Schurig, V. *Electrophoresis* 2003, *24*, 2674-2679.

[15] Tanaka, Y.; Otsuka, K.; Terabe, S. *J. Chromatogr. A* 2000, *875*, 323-330.

[16] Huang, W. X.; Xu, H.; Fazio, S. D.; Vivilecchia, R. V. *J. Chromatogr. A* 2000, *875*, 361-369.

[17] Hyun, M. H.; Jin, J. S.; Lee, W. *J. Chromatogr. A* 1998, *822*, 155-161.

[18] Wang, C.-Y.; Shang, Z.-C.; Mei, J.-H.; Yu, Q.-S. *Synth. Commun.* 2003, *33*, 3381-3386.

[19] Billiot, H. F.; Billiot, E. J.; Warner, I. M. *J. Chromatogr. A* 2001, *992*, 329-228.

[20] Shamsi, S. A.; Warner, I. M. *Electrophoresis* 1997, *18*, 853-872.

[21]   Nishi, H.; Tsumagari, N. *Anal. Chem.* 1989, *61*, 2434-2439.

[22]   Chiari, M.; Nesi, M.; Ottolina, G.; Righetti, P. G. *J. Chromatogr. A* 1994, *680*, 571-577.

[23]   Doshi, A.; Ono, T.; Hara, S.; Yamaguchi, J. *Anal. Chem.* 1989, *61*, 1984-1986.

[24]   Otsuka, K.; Terabe, S. *J. Chromatogr.* 1990, *515*, 221-226.

[25]   Rizvi, S. A.; Zheng, J.; Apkarian, R. P.; Dublin, S. N.; Shamsi, S. A. *Anal. Chem.* 2007, *79*, 879-898.

[26]   Pu, L. *Chem. Rev.* 2004, *104*, 1687-1716.

[27]   Macossay, J.; Shamsi, S. A.; Warner, I. M. *Tetrahedron Lett.* 1999, *40*, 577-580.

[28]   Du, H.; Fuh, R. C. A.; Li, J. Z.; Corkan, L. A.; Lindsey, J. S. *Photochem. Photobiol.* 1998, *68*, 141-142.

[29]   Williams, A. T. R.; Winfield, S. A.; Miller, J. N. *Analyst* 1983, *108*, 1067-1071.

[30]   Peres, L. O. *et al. Polymer* 2007, *48*, 98-104.

[31]   Liou, G.; Hsia, S.; Huang, N.; Yang, Y.-L. *Macromolecules* 2006, *39*, 5337-5346.

[32]   Allahverdiev, A.; Gündüz, G.; Murzin, D. Y. *Ind. Eng. Chem. Res.* 1998, *37*, 2373-2377.

[33]   Fakayode, S. O.; Busch, M. A.; Bellert D. J.; Busch, K. W. *Analyst* 2005, *130*, 233-241.

[34]   Tran, C. D.; Oliveira, D. *Anal. Biochem.* 2006, *356*, 51-58.

[35]   McCarroll, M. E.; Billiot, F. H.; Warner, I. M. *J. Am. Chem. Soc.* 2001, *123*, 3173-3174.

[36]   Kimaru, I. W.; Xu, Y.; McCarroll, M. E. *Anal. Chem.* 2006, *78*, 8485-8490.

[37]   Valle, B. V. *et al. Langmuir* 2007, *23*, 425-435.

CHAPTER 5

POLY(SODIUM *N*-UNDECANOYL-L-PHENYLALANINATE): A VERSATILE CHIRAL SELECTOR USING STEADY-STATE FLUORESCENCE SPECTROSCOPY

5.1 Introduction

It is well known that the determination of enantiomeric purity continues to receive growing interest due to the different activities or effects of the enantiomers of chiral compounds.[1-3] In general, one enantiomer may reverse or limit the desired effects of the therapeutic, active, or fragrant enantiomer. Therefore, chiral analysis continues to be a challenge because the number of chiral molecules and the demand for enantiomerically pure compounds continues to grow every year.[4] A versatile chiral selector is desired for the analysis of chiral molecules with a variety of functional groups and with or without fluorescent properties. In addition, fluorescent sensors with diverse molecular structures have been applied in chiral analysis and have received growing attention for their interaction with chiral molecules.[5]

Chiral fluorescent sensors, i.e. fluorescent chiral molecular micelles (FCMMs), should allow the enantioselective recognition of chiral molecules which may or may not contain a chromophore. Molecular micelle chiral selectors contain an apolar hydrocarbon tail and a polar head group. A pair of enantiomers (fluorescent or non-fluorescent) will interact with a chiral selector to form a complex. The interaction can vary depending on the extent of the host-guest complexation and binding between the enantiomer and chiral selector. As a result, variations of fluorescence emission spectra are expected.

Molecular micelles have proven to be successful chiral selectors in various applications with a variety of analytes.[6-11] In an effort to use an FCMM as a versatile chiral selector in steady-state fluorescence measurements, four fluorescent (1,1`-binaphthyl-2,2`-diamine (BNA), 1-(9-Anthryl)-2,2,2-trifluoroethanol (TFA), propranolol (PROP), and naproxen (NPRX)) and

four non-fluorescent (chloromethyl menthyl ether (CME), citramalic acid (CIT), tartaric acid (TAR), and limonene (LIM)) chiral molecules with diverse structure and hydrophobicity were chosen. These compounds have a variety of uses in several industries. BNA and CME are used in chiral compound synthesis and TFA is a chiral NMR solvating agent for the discrimination of enantiomeric purity of optically active compounds. PROP, a beta blocker used for the treatment of hypertension, and NPRX, an anti-inflammatory drug, are found in the pharmaceutical industry. CIT has been reported to be found in cerebrospinal fluid of humans with bacterial meningitis.[12] TAR is a known antioxidant, food additive, and an intermediate in chiral molecule synthesis and LIM is a terpene found in citrus fruit and a fragrance in cleaning products.

Although molecular micelles have been capable of chiral analysis for fluorescent and non-fluorescent techniques, the use of molecular micelles in spectroscopy has been limited to particular analytes. In Chapter 3, the use of non-fluorescent amino acid based molecular micelles for the chiral recognition and the determination of enantiomeric composition of fluorescent chiral analytes using steady-state fluorescence spectroscopy and regression modeling was reported. Novel FCMMs were synthesized and characterized in Chapter 4. Chiral analysis of non-fluorescent chiral analytes was investigated by use of three FCMMs. Regression modeling has proven to be a reliable method for determining the enantiomeric composition of chiral molecules using a spectroscopic technique.[13-18] Steady-state fluorescence spectroscopy is a rapid and relatively inexpensive analytical technique, allowing of fast screening and determination of the enantiomeric composition of chiral molecules. In this chapter, the use of poly-L-SUF as a chiral selector for the determination of the enantiomeric composition of four chiral fluorescent compounds and four chiral non-fluorescent compounds is reported.

114

5.2 Methods

5.2.1 Materials

 N-Hydroxysuccinimide, undecylenic acid, sodium bicarbonate, and dicyclohexylcarbodiimide were purchased from Fluka (Milwaukee, WI). Undecylenyl alcohol, monobasic sodium phosphate, dibasic sodium phosphate, sodium hydroxide, hydrochloric acid, ethyl acetate, and tetrahydrofuran were obtained from Sigma-Aldrich (Milwaukee, WI). Enantiomerically pure enantiomers of 1,1`-binaphthyl-2,2`-diamine (BNA), 1-(9-anthryl)-2,2,2-trifluoroethanol (TFA), propranolol (PROP), tartaric acid (TAR), citramalic acid (CIT), limonene (LIM), chloromethyl menthyl ether (CME), and S-naproxen (NPRX) were also purchased from Sigma-Aldrich (Milwaukee, WI). Enantiomerically pure R-naproxen was purchased from Albermarle (Baton Rouge, LA).   The amino acid L-phenylalanine was purchased from Bachem Bioscience Inc. (King of Prussia, PA). All chemicals were used as received. The purity of all analytes and reagents was 99% or higher.

5.2.2 Instrumentation

 Steady-state fluorescence spectra were acquired using a SPEX Fluorolog-3 spectrofluorometer (model FL3-22TAU3; Jobin Yvon, Edison, NJ) equipped with double excitation and emission monochromators (slit widths, 2 nm), a 400 W Xe-arc lamp, and a thermoelectrically cooled Hamamatsu R-928 photomultiplier tube. A 0.4 cm path length quartz fluorescence cuvet was used for fluorescence emission data collection.   Absorption and fluorescence emission were collected at room temperature and the blank was subtracted from each spectrum.   The blank consisted of the solvent medium for all experiments (buffer or methanol/water solution).

5.2.3 Synthesis of the Molecular Micelle

The monomer L-SUF was synthesized according a previously reported procedure[19] and details of the synthesis have been discussed in Chapter 4 of this dissertation. Polymerization was achieved by exposing a 40 mM aqueous solution to ^{60}Co γ-rays (0.7 krad/hr) for 168 hrs. H^{1}NMR was used to monitor complete polymerization of poly-L-SUF by the disappearance of the vinyl protons (6-5 ppm). Characterization of poly-L-SUF and its photophysical properties have also been reported in Chapter 4.

5.2.4 Sample Preparation

Poly-L-SUF samples for fluorescence study were prepared in 50 mM dibasic sodium phosphate buffer or a mixture of water and methanol. The buffer was filtered through a 0.45-μm nylon syringe filter (Nalgene, Rochester, NY) and the pH was adjusted using an ORION model 410A pH meter (Pulse Instruments, Van Nuys, CA) with 0.1 M NaOH or 0.1 M HCl prior to the addition of molecular micelle. Calibration and validation samples for steady-state fluorescence measurements were prepared from 1 M poly-L-SUF and 0.1 M analyte stock solutions dissolved in buffer or methanol. The structures of the fluorescent and non-fluorescent analytes are illustrated in Figure 5.1. Final concentrations were made by transferring appropriate volumes of poly-L-SUF and analyte to dry volumetric flasks and diluting with buffer solution or methanol and water. All solutions were sonicated 15 min to ensure proper dissolution and were allowed to equilibrate for 30 minutes.

5.2.5 Data Analysis

The Unscrambler, (CAMO, Inc., Corvallis, OR, version 9.1) chemometric software system was used for multivariate regression analysis of all fluorescence emission spectra.
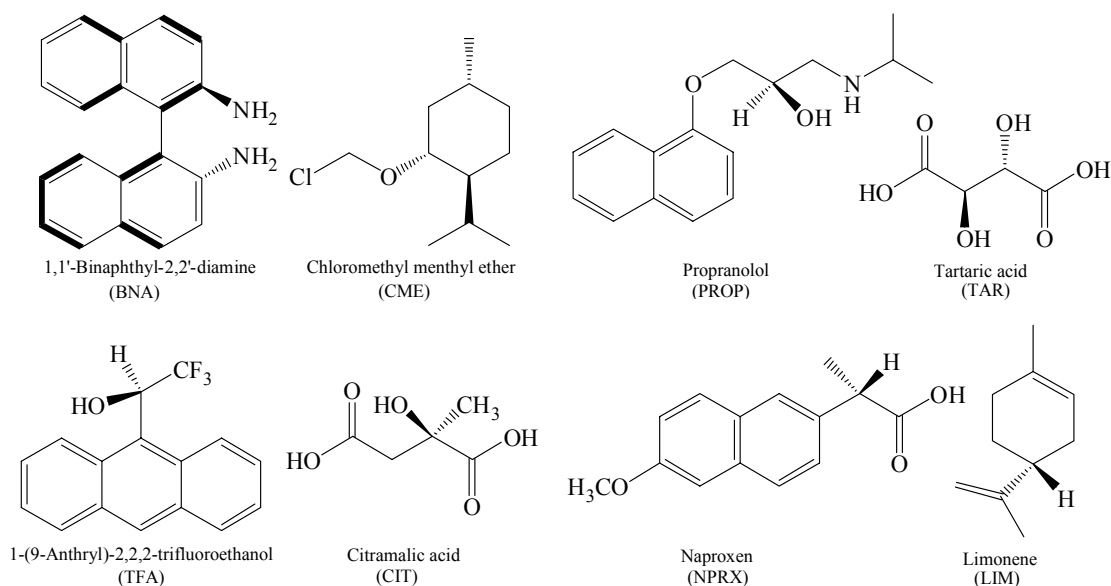
Figure 5.1 Molecular structures of the fluorescent and non-fluorescent analytes.

5.3 Results and Discussion

5.3.1 Effect of Poly-L-SUF Concentration

Figure 5.2.1 illustrates the effect of changing the poly-L-SUF concentration on the percent difference of fluorescence intensity at a particular wavelength for 1.0×10^{-5} M R- and S-fluorescent analyte. In this figure, the concentration of poly-L-SUF varies from 1 mM to 15 mM. The optimum concentration of poly-L-SUF is the concentration that maximizes the spectral difference of each enantiomer. The spectral difference is represented as fluorescence intensity percent difference at a particular wavelength and is found by taking the percent difference between the fluorescence intensity of the emission spectra containing one enantiomer from the fluorescence intensity of the emission spectra of the opposite enantiomer at the same wavelengths. It is clear that there is an optimum concentration of poly-L-SUF to achieve the highest fluorescence intensity percent difference of R- and S- analyte. The general trend of percent difference, while changing the chiral selector concentration is similar for all four

fluorescent compounds. Initially, increasing the poly-L-SUF concentration increased the differences in emission spectra for each enantiomer. At a particular optimum concentration, further increases in the concentration of poly-L-SUF led to a significant decrease of fluorescence intensity differences. BNA and PROP have maximum enantiomeric fluorescence spectra differences at 4 mM poly-L-SUF (Figure 5.2.1A and 5.2.1C). TFA and NPRX have maximum emission differences at 5 mM poly-L-SUF (Figure 5.2.1B and 5.2.1D). The fluorescence emission by use of optimum poly-L-SUF concentrations are illustrated in Figure 5.2.2 (A-D).
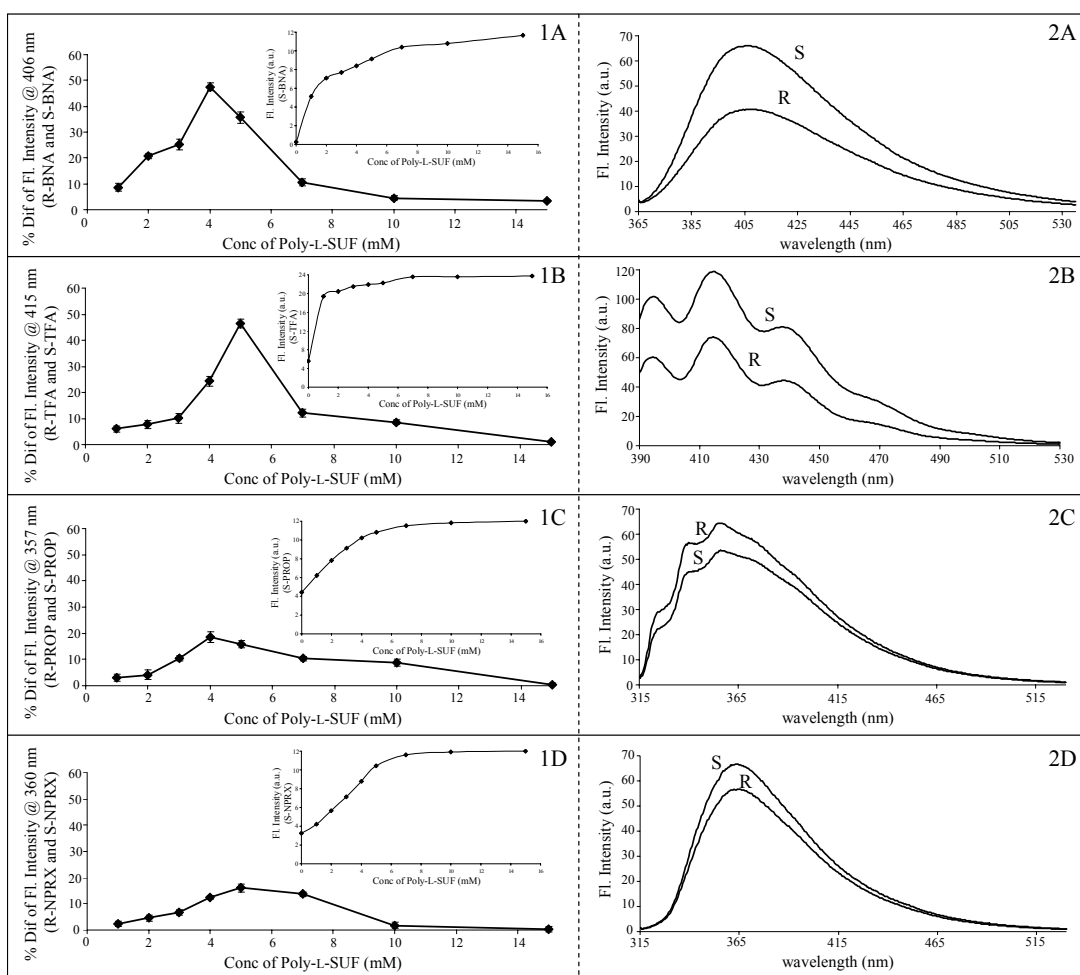
Figure 5.2 Concentration study of poly-L-SUF on the percent difference of fluorescence intensity for 1.0×10^{-5} M R- and S- BNA (1A), TFA (1B), PROP (1C), and NPRX (1D). The effect of changing the poly-L-SUF concentrations on the fluorescence intensity of BNA, TFA, PROP, and NPRX are shown in the insets of 1A-1D. Steady-state fluorescence emission spectra at optimum poly-L-SUF concentration for BNA (2A), TFA (2B), PROP (2C), and NPRX (2D).

118

As expected, the two enantiomers of each fluorescent compound have identical fluorescence emission spectra with a significantly lower intensity in the absence of chiral selector. Complexation of poly-L-SUF with fluorescent analytes increases the fluorescence intensity of analytes. These observations are well known and can be explained by several factors including the reduction of quenching modes, alteration of photophysical rates, and/or shielding mechanisms.[20] In addition, the ability of micelles to increase the fluorescence intensity of solutes has been used to lower the detection limits and increase the sensitivity of spectrofluorimetric methods for the determination of a variety of analytes.[21-23]

Figure 5.3.1 illustrates the effect of changing the concentration of poly-L-SUF on the percent difference of fluorescence intensity at 330 nm for 1.5×10^{-5} M of non-fluorescent analyte enantiomers. The concentration of poly-L-SUF varies from 2 mM to 20 mM and the optimum concentration of poly-L-SUF to achieve the highest fluorescence intensity percent difference was 12 mM for TAR, 7.5 mM for LIM, and 10.5 mM for CIT and CME. The same general trend of percent difference, while changing the concentration of poly-L-SUF is observed for the non-fluorescent analytes. The steady-state fluorescence emission spectra at optimum poly-L-SUF concentrations are illustrated in Figure 5.3.2 (A-D). The emission spectral differences of the enantiomers of CME and LIM are significantly less than TAR (Figure 5.3.2 C) and CIT (Figure 5.3.2 D) using poly-L-SUF as a chiral selector in buffer. The spectral variations depend on several possible factors including the solubility, size, charge and hydrophobicity of the analyte. The water solubility of CME and LIM is very low, which could possibly lead to less interaction with the chiral selector. In addition, the hydrophobic interactions between the molecular micelle chiral selector and CME and LIM analytes are weaker than the hydrophilic complexations with CIT and CME.
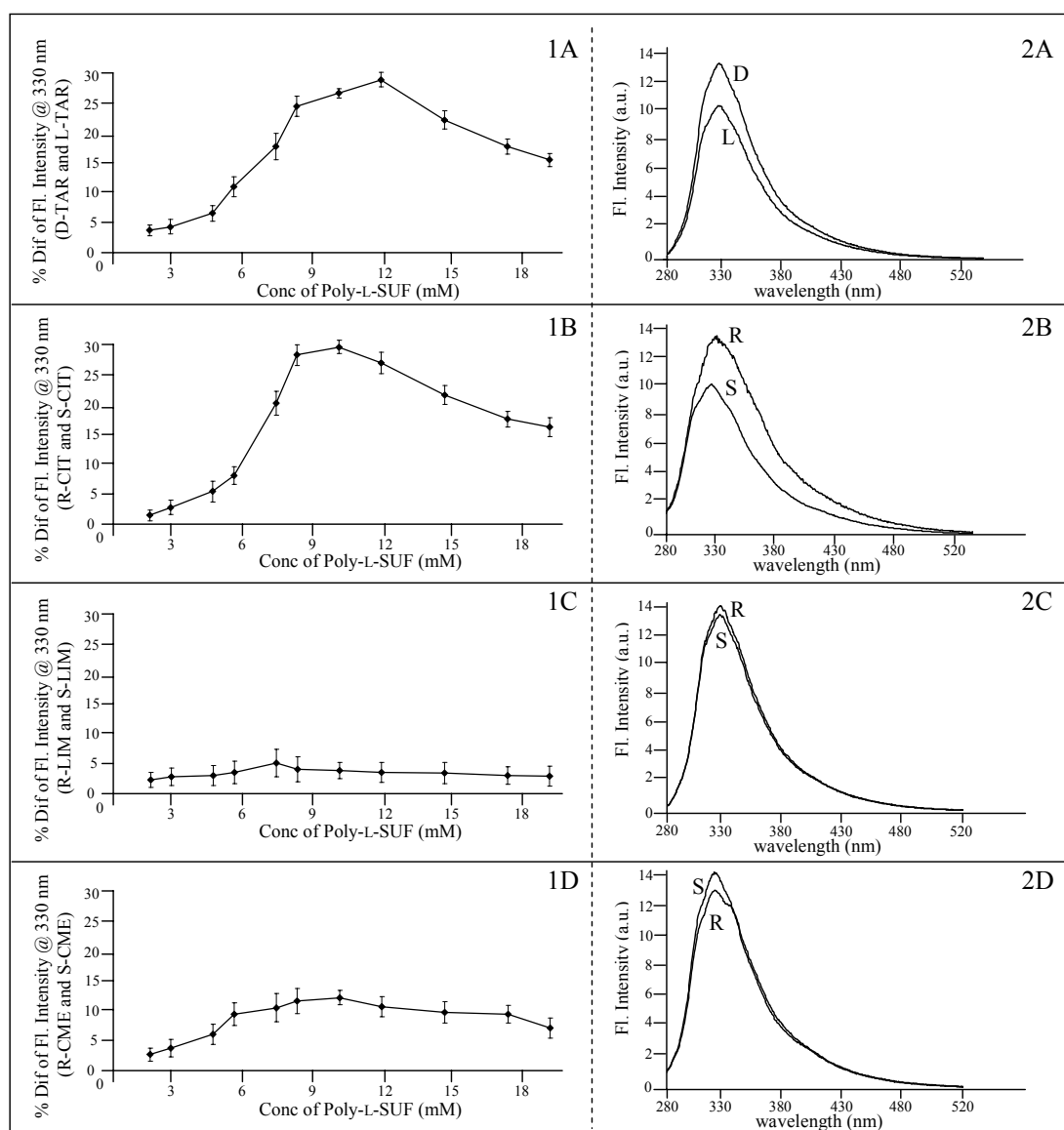
Figure 5.3 Concentration study of chiral selector on the percent difference of fluorescence intensity for poly-L-SUF in the presence of 1.0×10^{-5} M enantiomers of TAR (1A), CIT (1B), LIM (1C), and CME (1D). Steady-state fluorescence emission spectra at optimum poly-L-SUF concentration for TAR (2A), CIT (2B), LIM (2C), and CME (2D).

5.3.2 Effect of Different Buffer Solutions

In this study, the pH of the buffer plays a very important role. As illustrated in Figure 5.4, the spectral variation of the enantiomers for both fluorescent and non-fluorescent chiral analytes is higher at pH ≥ 7. This observation can be explained by the pH effects on

polymerized micelles reported by Chu and Thomas.[24] At acidic pH, the spectral variation may be reduced due to the compact conformation of the molecular micelle, allowing for less interaction between the enantiomer and chiral selector. As the pH increases, electrostatic repulsion may cause the molecular micelle to have a looser conformation which may provide better interactions with the enantiomers. It is noted that the percent difference of fluorescence intensity increased from pH 4 to pH 7 for all fluorescent and non-fluorescent analytes. Further increases in the pH did not change the spectral variation from pH 7 to pH 12. Therefore, the pH 7 buffer solution was selected for further studies of the enantiomeric composition predictions.
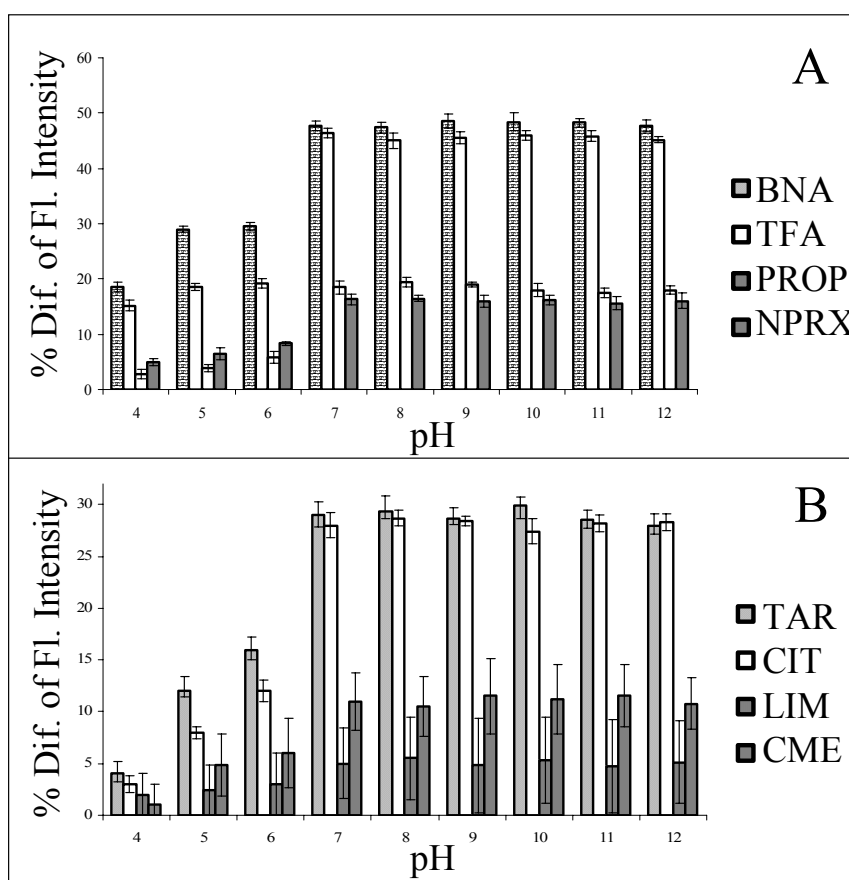
Figure 5.4 Effect of pH on the percent difference of fluorescence intensity for (A) 1.0×10^{-5} M of fluorescent analytes in the presence of poly-L-SUF at the optimum concentration and (B) optimum concentration of poly-L-SUF in the presence of 1.0×10^{-5} M for non-fluorescent analytes.

5.3.3 Determination of Enantiomeric Composition Using Optimized Conditions

Optimization studies, including the concentration of chiral selector and pH of the buffer, are necessary to develop a calibration model capable of predicting the enantiomeric composition of unknown samples. Previous studies in Chapter 3 of this dissertation with non-fluorescent chiral molecular micelles confirmed that the ability of the calibration model to accurately predict the enantiomeric composition of unknown samples depends upon the extent of the spectral variation. All analytes have the same total concentration (1.0×10^{-5} M) but different emission spectra with varying enantiomeric compositions in the presence of poly-L-SUF. Table 5.1 lists the compositions of 12 solutions for the calibration of all eight analytes. Figure 5.5 illustrates the spectra of the 12 solutions of each analyte in the optimum concentration of poly-L-SUF. It is interesting to observe that different enantiomeric compositions of each analyte led to relatively small changes in the emission spectra. As expected, the spectral differences are due to diastereomeric interactions between poly-L-SUF and both enantiomeric forms of each analyte.

Table 5.1   Compositions of 12 solutions used for calibration studies.

Sample	BNA S	BNA R	TFA S	TFA R	PROP S	PROP R	NPRX S	NPRX R	TAR D	TAR L	CIT,LIM,CME S	CIT,LIM,CME R
1	1.000	0.000	1.000	0.000	1.000	0.000	1.000	0.000	1.000	0.000	1.000	0.000
2	0.900	0.100	0.950	0.050	0.900	0.100	0.950	0.050	0.900	0.100	0.900	0.100
3	0.850	0.150	0.800	0.200	0.830	0.170	0.850	0.150	0.800	0.200	0.800	0.200
4	0.700	0.300	0.750	0.250	0.750	0.250	0.750	0.250	0.700	0.300	0.700	0.300
5	0.600	0.400	0.600	0.400	0.600	0.400	0.650	0.350	0.600	0.400	0.600	0.400
6	0.500	0.500	0.500	0.500	0.500	0.500	0.500	0.500	0.500	0.500	0.500	0.500
7	0.400	0.600	0.450	0.550	0.430	0.570	0.400	0.600	0.400	0.600	0.400	0.600
8	0.350	0.650	0.350	0.650	0.350	0.650	0.300	0.700	0.300	0.700	0.300	0.700
9	0.300	0.700	0.300	0.700	0.200	0.800	0.200	0.800	0.250	0.750	0.250	0.750
10	0.200	0.800	0.200	0.800	0.150	0.850	0.150	0.850	0.200	0.800	0.200	0.800
11	0.100	0.900	0.100	0.900	0.100	0.900	0.100	0.900	0.100	0.900	0.100	0.900
12	0.000	1.000	0.000	1.000	0.000	1.000	0.000	1.000	0.000	1.000	0.000	1.000
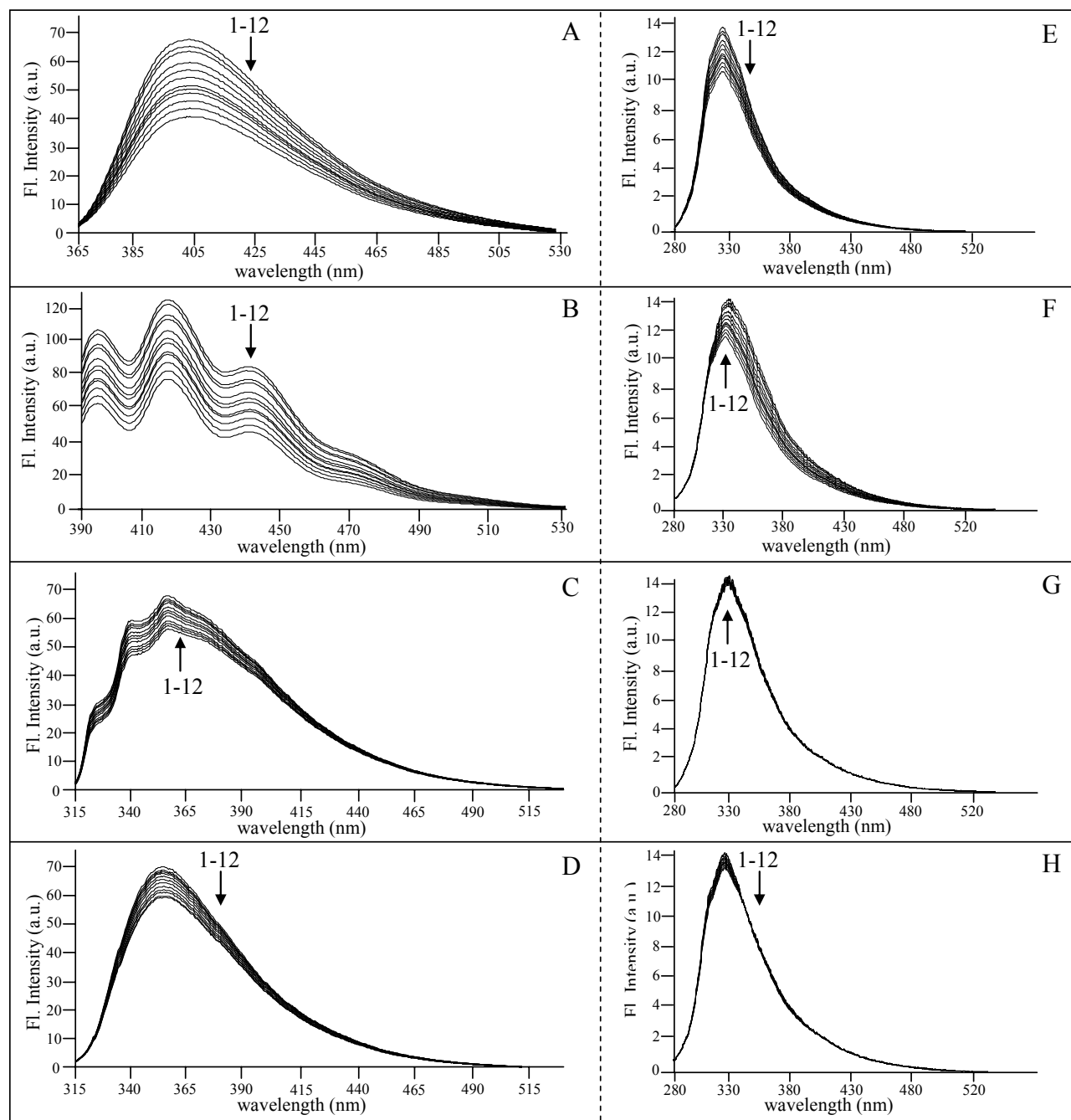
Figure 5.5 Fluorescence emission spectra of 12 solutions containing optimum concentration of poly-L-SUF and 1.0×10^{-5} M of (A) BNA, (B) TFA, (C) PROP, (D) NPRX, (E) TAR, (F) CIT, (G) LIM, and (H) CME.

A multivariate method of analysis, partial least-square-regression modeling (PLS-1), was used to correlate the small spectral changes with known compositional changes to form a calibration model. Calibrations were performed on emission spectra of the 12 samples of poly-L-SUF in the presence of analyte and better regressions between spectral data and enantiomeric composition were obtained for each analyte in the wavelength regions with the most variation (see Table 5.2). A perfect calibration model would have a regression coefficient and slope of 1 and an offset of 0. Table 5.2 lists the figures of merit within the given spectral range. The regression parameters for 6 of the analytes are very close to a perfect model; however, the regression models for LIM and CME have a lower regression coefficient and slope and a higher offset than the other analytes.

Table 5.2   Figures of merit obtained from multivariate regression analysis of calibration samples in buffered solution.

Analyte	Regression Coefficient	Slope	Offset	Wavelength Range
BNA	0.9976	0.9984	2.88×10^{-3}	385-485
TFA	0.9947	0.9923	6.78×10^{-3}	390-450
PROP	0.9952	0.9941	8.01×10^{-3}	320-400
NPRX	0.9979	0.9988	4.08×10^{-3}	350-405
TAR	0.9946	0.9937	9.87×10^{-3}	300-350
CIT	0.9968	0.9979	2.74×10^{-3}	300-350
LIM	0.9401	0.9121	9.17×10^{-2}	300-350
CME	0.9780	0.9486	5.15×10^{-2}	300-350

To evaluate the prediction ability of the calibration models, 10 independently prepared validation samples with the same analyte concentration as the calibration set but different enantiomeric compositions were evaluated over the same wavelength region used for the regression models. Figure 5.6 illustrates the plots for all fluorescent (Figure 5.6 A-D) and non-fluorescent compounds (Figure 5.6 E – H), where the actual mole fraction was plotted against the

124

predicted mole fraction. The predicted mole fractions for each analyte enantiomer were plotted separately and as expected, were linearly related with regression coefficients ranging from 0.9834 – 0.9999. In addition, the linear relationship still exists when predicted and actual mole fractions were plotted together for both enantiomers with regression coefficients ranging from 0.9834 – 0.9989. As expected from a small spectral variation, the regression for LIM and CME are lower than the other analytes.

The prediction ability of the calibration models for the validation samples was evaluated by use of the root-mean-square percent relative error (RMS%RE), which was introduced in Chapter 2 of this dissertation. The *RMS%RE* for the ten validation samples for S-BNA, S-TFA, S-PROP, and S-NPRX were 1.77, 2.95, 3.17, and 2.90%, respectively, while the values for R-BNA, R-TFA, R-PROP, and R-NPRX were 2.31, 2.57, 3.03, and 3.20, respectively (Table 5.3). The results indicate that the validation studies depend on the analyte. Furthermore, it is known that one enantiomer can bind more strongly to the chiral selector, leading to different enantiomeric validation results.[25, 26]

Table 5.4 lists the *RMS%RE* for the non-fluorescent analytes. As listed, the values for S-LIM and S-CME (14.53 and 15.80%) are much higher than the values for D-TAR and S-CIT (4.37 and 3.79%). The same trend is observed for the opposite enantiomer and once again, the results indicate that the validation is analyte dependent. As previously noted, the extent of the spectral variation obtained during the calibration phase plays an important role in the prediction ability of the model. Spectral differences are based on diastereomeric interactions between the analyte and the chiral selector. Several factors including solubility of the analyte in the molecular micelle, hydrophobicity of the analyte, charge of the analyte, and size of the analyte determine the extent of the interactions. TAR and CIT are more soluble in water as compared to

LIM and CME. As a result, there may be less interaction between enantiomer and chiral selector for the more hydrophobic molecules. Less interaction will lead to lower spectral variation as seen in the calibration studies for these two molecules.

5.3.4 Study of Guest-Host Complexation in Buffer and Methanol/Water Medium

To study the influence of the solvent on the chiral discrimination and enantiomeric prediction by use of molecular micelles, a series of experiments was performed using methanol and water mixtures.   Although it is well known that the water solubility of many terpenes and ethers is very poor[27] the solubility of the hydrophobic compounds LIM and CME was expected to increase with the use of methanol. In addition, the following experiments demonstrated that the method is not limited to water only. It would be expected that better chiral discrimination would result with a solvent medium that allows for increased solubility of chiral selector and analyte.

Samples were prepared as described previously and the multiple regression modeling was performed. Once again, the enantiomeric composition of 12 calibration samples was varied from 1.0 to 0.0 mol fraction. All experiments were performed using the same analyte concentration (1×10^{-5} M) and the optimum concentration of poly-L-SUF in the buffer medium. However, in this study, the calibration and validation samples were prepared in 25:75 methanol/water and 75:25 methanol/water. As expected, the use of organic solvent increased the solubility of the hydrophobic molecules, which also increased the interaction between the chiral selector and the analyte. As a result, the observed figures of merit for the calibration models improved as compared to those obtained in buffer (Appendix IV). This was an indication that the validation results would be better (lower *RMS%RE*) using methanol in the solvent medium.
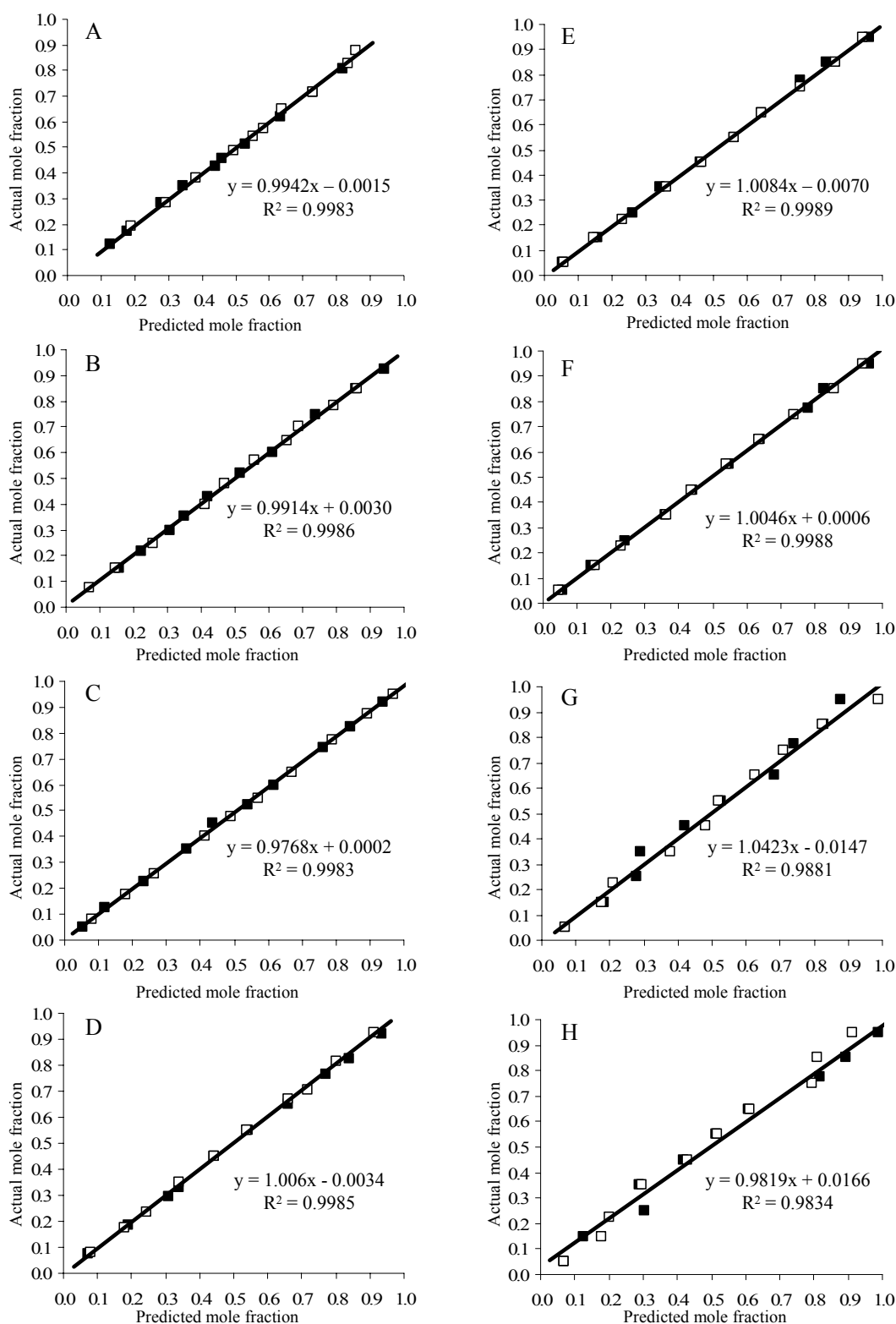
Figure 5.6 Actual mole fraction composition versus predicted mole fraction composition for optimum concentration of poly-L-SUF and (A) BNA, (B) TFA, (C) PROP, (D) NPRX, (E) TAR, (F) CIT, (G) LIM, and (H) CME. □, S or D enantiomer; ■, R or L enantiomer.

127

Table 5.3   Actual and predicted mole fraction of 1.0×10^{-5} M enantiomers of fluorescent analytes with optimum concentration of poly-L-SUF in buffered solution.

Act S BNA mol frac	Pred S BNA mol frac	S BNA rel error %	Act S TFA mol frac	Pred S TFA mol frac	S TFA rel error %
0.877	0.859	2.05	0.850	0.862	-1.41
0.826	0.835	-1.09	0.783	0.791	-1.02
0.715	0.728	-1.82	0.700	0.687	1.86
0.650	0.638	1.85	0.645	0.652	-1.09
0.575	0.582	-1.22	0.570	0.559	1.93
0.545	0.554	-1.65	0.480	0.471	1.88
0.487	0.496	-1.85	0.400	0.413	-3.25
0.380	0.384	-1.05	0.250	0.256	-2.40
0.285	0.292	-2.46	0.150	0.145	3.33
0.192	0.188	2.08	0.075	0.070	6.67
RMS%RE		*1.77*	*RMS%RE*		*2.95*
Act R BNA mol frac	Pred R BNA mol frac	R BNA rel error %	Act R TFA mol frac	Pred R TFA mol frac	R TFA rel error %
0.123	0.127	-3.25	0.150	0.158	-5.33
0.174	0.176	-1.15	0.217	0.223	-2.64
0.285	0.279	2.11	0.300	0.308	-2.67
0.350	0.342	2.29	0.355	0.349	1.69
0.425	0.440	-3.53	0.430	0.418	2.79
0.455	0.461	-1.32	0.520	0.514	1.15
0.513	0.528	-2.92	0.600	0.612	-2.00
0.620	0.632	-1.94	0.750	0.738	1.60
0.715	0.728	-1.82	0.850	0.859	-1.06
0.808	0.819	-1.36	0.925	0.942	-1.84
RMS%RE		*2.31*	*RMS%RE*		*2.57*
Act S PROP mol frac	Pred S PROP mol frac	S PROP rel error %	Act S NPRX mol frac	Pred S NPRX mol frac	S NPRX rel error %
0.950	0.971	-2.21	0.924	0.911	1.41
0.874	0.892	-2.06	0.815	0.801	1.72
0.772	0.791	-2.46	0.705	0.719	-1.99
0.650	0.671	-3.23	0.670	0.662	1.19
0.550	0.570	-3.64	0.550	0.538	2.18
0.475	0.489	-2.95	0.450	0.442	1.78
0.400	0.415	-3.75	0.350	0.339	3.14
0.255	0.264	-3.53	0.236	0.246	-4.24
0.175	0.181	-3.43	0.175	0.181	-3.43
0.078	0.081	-3.85	0.078	0.082	-5.13
RMS%RE		*3.17*	*RMS%RE*		*2.90*
Act R PROP mol frac	Pred R PROP mol frac	R PROP rel error %	Act R NPRX mol frac	Pred R NPRX mol frac	R NPRX rel error %
0.050	0.052	-4.00	0.076	0.071	6.58
0.126	0.120	4.76	0.185	0.192	-3.78
0.228	0.234	-2.63	0.295	0.308	-4.41
0.350	0.362	-3.43	0.330	0.341	-3.33
0.450	0.438	2.67	0.450	0.442	1.78
0.525	0.540	-2.86	0.550	0.542	1.45
0.600	0.616	-2.67	0.650	0.662	-1.85
0.745	0.761	-2.15	0.764	0.772	-1.05
0.825	0.841	-1.94	0.825	0.838	-1.58
0.922	0.939	-1.84	0.922	0.934	-1.30
RMS%RE		*3.03*	*RMS%RE*		*3.20*

Table 5.4   Actual and predicted mole fraction of 1.0×10^{-5} M enantiomers of non-fluorescent analytes with optimum concentration of poly-L-SUF in buffered solution.

Act D TAR mol frac	Pred D TAR mol frac	D TAR rel error %	Act S CIT mol frac	Pred S CIT mol frac	S CIT rel error %
0.950	0.942	0.84	0.950	0.941	0.95
0.850	0.861	-1.29	0.850	0.859	-1.06
0.750	0.759	-1.20	0.750	0.738	1.60
0.650	0.641	1.38	0.650	0.636	2.15
0.550	0.563	-2.36	0.550	0.542	1.45
0.450	0.464	-3.11	0.450	0.437	2.89
0.350	0.360	-2.86	0.350	0.363	-3.71
0.225	0.231	-2.67	0.225	0.229	-1.78
0.150	0.145	3.33	0.150	0.154	-2.67
0.050	0.056	-12.00	0.050	0.045	10.00
RMS%RE		*4.37*	*RMS%RE*		*3.79*
Act L Tar mol frac	Pred L TAR mol frac	L TAR rel error %	Act R CIT mol frac	Pred R CIT mol frac	R CIT rel error %
0.050	0.055	-10.00	0.050	0.056	-12.00
0.150	0.157	-4.67	0.150	0.143	4.67
0.250	0.262	-4.80	0.250	0.243	2.80
0.350	0.342	2.29	0.350	0.361	3.14
0.450	0.461	-2.44	0.450	0.439	2.44
0.550	0.562	-2.18	0.550	0.546	0.73
0.650	0.641	1.38	0.650	0.638	1.85
0.775	0.759	2.06	0.775	0.782	-0.90
0.850	0.834	1.88	0.850	0.829	2.47
0.950	0.961	-1.16	0.950	0.962	-1.26
RMS%RE		*4.14*	*RMS%RE*		*4.49*
Act S LIM mol frac	Pred S LIM mol frac	S LIM rel error %	Act S CME mol frac	Pred S CME mol frac	S CME rel error %
0.950	0.988	-4.00	0.950	0.911	4.11
0.850	0.824	3.06	0.850	0.808	4.94
0.750	0.710	5.33	0.750	0.793	-5.73
0.650	0.625	3.85	0.650	0.614	5.54
0.550	0.519	5.64	0.550	0.518	5.82
0.450	0.482	-7.11	0.450	0.429	4.67
0.350	0.377	-7.71	0.350	0.295	15.71
0.225	0.210	6.67	0.225	0.201	10.67
0.150	0.174	-16.00	0.150	0.179	-19.33
0.050	0.070	-40.00	0.050	0.070	-40.00
RMS%RE		*14.53*	*RMS%RE*		*15.80*
Act R LIM mol frac	Pred R LIM mol frac	R LIM rel error %	Act R CME mol frac	Pred R CME mol frac	R CME rel error %
0.050	0.067	-34.00	0.050	0.068	-36.00
0.150	0.184	-22.67	0.150	0.124	17.33
0.250	0.278	-11.20	0.250	0.304	-21.60
0.350	0.290	17.14	0.350	0.290	17.14
0.450	0.419	6.89	0.450	0.420	6.67
0.550	0.526	4.36	0.550	0.512	6.91
0.650	0.684	-5.23	0.650	0.609	6.31
0.775	0.742	4.26	0.775	0.817	-5.42
0.850	0.828	2.59	0.850	0.895	-5.29
0.950	0.879	7.47	0.950	0.988	-4.00
RMS%RE		*15.05*	*RMS%RE*		*16.01*

The summary of the results obtained from the validation studies are illustrated in Figure 5.7 (and in Appendix V), where the *RMS%RE* values decreased for all analytes as the amount of methanol increased. The most significant changes were observed for the regression models for poly-L-SUF in the presence of LIM and CME. As previously reported in Table 5.4, the *RMS%RE* obtained for LIM using buffer was 14.43%. Addition of methanol resulted in a significant difference in the spectral difference for poly-L-SUF in the presence of each enantiomer and ultimately lowers the *RMS%RE* values. The *RMS%RE* for LIM and CME using 25:75 methanol/water was 7.95 and 6.18%, respectively, while it decreased further using 75:25 methanol/water to 4.28 and 2.54%, respectively.
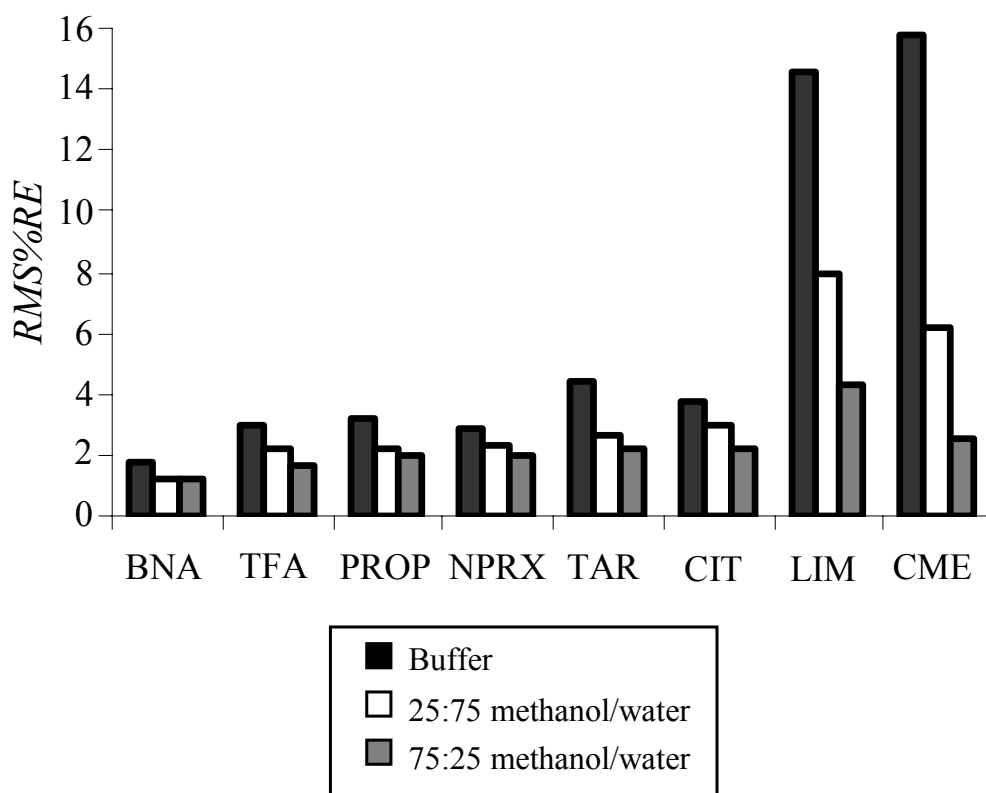
Figure 5.7 *RMS%RE* obtained for all analytes with optimum poly-L-SUF concentration in buffered solutions, 25:75 methanol/water, and 75:25 methanol/water.

5.4 Conclusions

PLS-1 regression analysis of fluorescence spectral data obtained for poly-L-SUF in the presence of fluorescent and non-fluorescent chiral analytes has demonstrated the versatility of the present method. The use of fluorescence spectroscopy allowed for the enantiomeric determination of analytes with varying functionally groups, solubility, size and hydrophobicity at low concentrations. Analysis of non-fluorescent analytes is possible because a fluorescent chiral selector was used for chiral recognition studies. The ability of the chiral selector to differentiate between analyte enantiomers is based on diastereomeric interactions. Spectral variation was found to depend on the concentration of poly-L-SUF and the pH of the buffer used. The calibration models for more hydrophobic compounds were found to have poor prediction capabilities using a buffer medium. Addition of organic solvent demonstrated the versatility of the method and better predictions were obtained when methanol/water mixtures were used as a solvent medium for guest-host complexation. Furthermore, poly-L-SUF has proven to be a versatile chiral selector for the enantiomeric determination of fluorescent and non-fluorescent molecules.

5.5 References

[1]   Armstrong, D. W.; Han, S. H. *CRC Crit. Rev. Anal. Chem.* (1988) *19*, 175.

[2]   Jamali, F.; Mehvar, R.; Pasutto, F. *J. Pharm. Sci.* (1989) *78*, 695-715.

[3]   Caldwell, J. *J. Chromatogr A* (1996) *719*, 3-13.

[4]   Rouhi, A. *Chem. Eng. News* (2003) *81*, 45-55.

[5]   Pu, L. *Chem. Rev.* (2004) *104*, 1687-1716.

[6]   Wang, J.; Warner, I. *Anal. Chem.* (1994) *66*, 3773-3776.

[7]   Edward, S.; Shamsi, S. *J. Chromatogr A* (2000) *903*, 227-236.

[8]   Shamsi, S.; Valle, B.; Billiot, F.; Warner I. *Anal. Chem.* (2003) *75*, 379-387.

[9]   Kamande, M.; Zhu, X.; Kapnissi-Christodoulou, C.; Warner, I. *Anal. Chem.* (2004) *76*, 6681-6692.

[10]   Xu, Y.; McCarroll, M. *J. Phys. Chem. B* (2005) *109*, 8144-8152.

[11]   Fakayode, S.; Williams, A.; Busch, M.; Busch, K.; Warner, I. *J. Fluoresc.* (2006) *16*, 659-670.

[12]   Perlman, S.; Carr, S. *Clin. Chem.* (1984) *30*, 1209-1212.

[13]   Fakayode, S.; Busch, M; Bellert, D.; Busch, K. *Analyst* (2005) *130*, 233-241.

[14]   Fakayode, S.; Busch, M.; Busch, K. *Talanta* (2006) *68*, 1574-1583.

[15]   Fakayode, S.; Swamidoss, I.; Busch, M.; Busch, K. *Talanta* (2005) *65*, 838-845.

[16]   Busch, K. *et al., Anal. Chim. Acta* (2004) *525*, 53-62.

[17]   Busch, K. *et al., J. Am. Chem. Soc*. (2003) *125*, 1690-1691.

[18]   Tran, C.; Oliveira, D. *Anal. Biochem.* (2006) *356*, 51-58.

[19]   Macossay, J.; Shamsi, S. A.; Warner, I. M. *Tetrahedron Lett.* (1999) *40*, 577-580.

[20]   Hinze, W.; *et al. Trends in Anal. Chem.* (1984) *3*, 193-199.

[21]   Ishibashi, N.; Kina, K. *Anal. Lett.* (1972) *5*, 637.

[22]   Sabry, S.; *Anal. Chim. Acta* (1998) *367*, 41-53.

[23]   Garcia-Campana, A.; Aaron, J.; Bosque-Sendra, J. *Talanta* (2001) *55*, 531-539.

[24]   Chu, D.; Thomas, T. *Macromolecules* (1991) *24*, 2212-2216.

[25]   McCarroll, M.; Billiot, F.; Warner, I. *J. Am. Chem. Soc.* (2001) *123*, 3173-3174.

[26]   Kimaru, I.; Xu, Y.; McCarroll, M. *Anal. Chem.* (2006) *78*, 8485-8490.

[27]   Goodman, M.; Morehouse, F. *Organic Molecules in Action*, (1973) Gordon and Breach.

CHAPTER 6

CONCLUSIONS AND FUTURE STUDIES

In this dissertation, chiral analysis by use of molecular micelles and experimental design techniques using chromatographic and spectroscopic methods is described. Molecular micelles are proven to be versatile chiral selectors because the studies include a variety of chiral analytes with varying size, solubility, hydrophobicity, and compound class. The significance of chiral analysis, types of chiral selectors, experimental design, and instrumental theory including CE as well as fluorescence spectroscopy were introduced in Chapter 1.

In Chapter 2, MEKC separation parameters (molecular micelle concentration, applied voltage, pH, and operating temperature) were optimized by use of multiple regression analysis for the calibration of migration time and resolution of achiral and chiral analytes. Several multiple regression techniques including MLR, PCR, and PLS-1 were used for prediction studies. As expected, the validation of independently prepared samples was similar for each analyte using all regression techniques.

The dipeptide molecular micelle poly-L-SULV proved to be a good chiral selector for the resolution of chiral analytes in MEKC as well as for the chiral recognition studies using a spectroscopic technique. In Chapter 3, steady-state fluorescence spectroscopy was employed to investigate the use of poly-L-SULV, poly-L-SUL, or poly-L-SUV for the chiral analysis of BOH, BNA, and TFA. Better chiral discrimination of the analytes was obtained for studies using poly-L-SULV as the chiral selector. PLS-1 was used to correlate changes in the fluorescence spectral data of the chiral analytes as the enantiomeric composition was varied. The regression models produced from the spectral data were validated by determining the enantiomeric composition of independently prepared test solutions. The *RMS%RE* ranged between 1.57 and 6.10 %. In

addition, chiral analyte concentrations as low as 5 x 10^{-6} M were found to give regression models with good predictability.

In Chapter 4, novel FCMMs including poly-SUW, poly-SUY, and poly-SUF were synthesized and characterized using a variety of analytical techniques. In addition, the L-form of each FCMM was used for the chiral analysis of glucose, tartaric acid and serine. Poly-L-SUW had a significant fluorescence emission spectral difference as compared to poly-L-SUY and poly-L-SUF for the enantiomeric recognition of glucose, tartaric acid, and serine. Studies with the hydrophobic molecule α-pinene suggested that poly-L-SUY and poly-L-SUF had better chiral discrimination ability for hydrophobic analytes as compared to hydrophilic analytes. Chemometric modeling by PLS-1 regression analysis of steady-state fluorescence emission spectral data for the enantiomeric composition prediction of the chiral hydrophilic analytes in the presence of poly-L-SUW was reported. The sensitivity of the fluorescence technique allowed for investigation of low concentrations of chiral selector (3.0×10^{-5} M) and analyte (5.0×10^{-6} M) to be used in these studies. Validation of the calibration regression models was determined by use of a set of independently prepared samples of the same concentration of chiral selector and analyte with varying enantiomeric composition and the *RMS%RE* was found to range from 2.04% to 4.06%.

FCMMs have an inherent advantage over non-fluorescent molecular micelles. The chiral recognition of four fluorescent and four non-fluorescent molecules by use of poly-L-SUF chiral selector was reported in Chapter 5. The influence of FCMM concentration, buffer pH and complexation medium on FCMM-analyte host-guest complexation and the emission spectral properties of the resulting complexes were investigated. The figures of merit obtained from the PLS-1 regression modeling of the calibration samples suggested good prediction ability for the

validation of six of the eight chiral analytes. Better host-guest complexation of the more hydrophobic molecules, CME and LIM was obtained in methanol/water mixtures, resulting in better predictability of the regression models. The *RMS%RE* for all eight chiral analytes was found to range from 1.77 to 15.80% (buffer), 1.26 to 7.95% (25:75 methanol/water), and 1.21 to 4.28% (75:25 methanol/water).

Dipeptide molecular micelles have proven to have good chiral recognition ability in chromatographic (Chapter 2) and spectroscopic (Chapter 3) techniques. As noted in Chapter 2, enantiomeric resolution of chiral analytes is a big challenge in separation science and the conventional method of determining the optimum separation conditions of analytes may be time consuming and labor intensive. Thus, development of dipeptide FCMMs may have increased chiral selectivity of fluorescent and non-fluorescent chiral molecules. Additional studies pertinent to MEKC can be extended to the investigation of the use of dipeptide FCMMs as chiral selectors. In addition, a more sensitive detection method (indirect laser-induced fluorescence detection) other than conventional UV-absorbance detection may be used with FCMMs as the additive in the background electrolyte. This approach would allow for the rapid detection of analytes without derivatization using a fluorescent probe.

Multiple regression modeling of spectral data of a one-component solution is the simplest form of enantiomeric determination. Chapters 3 through 5 reported the enantiomeric composition prediction of a one-component chiral solution including only the enantiomers of one chiral molecule. Additional studies can be extended to accurate and simultaneous determination of multi-component fluorescent or non-fluorescent solutions by use of FCMMs. The chiral analysis of several mixtures of two different chiral molecules can be monitored simulating the progress of an asymmetric synthesis chemical reaction over time.

ORTHOGONAL ARRAY DATA SETS FOR MLR REGRESSION MODELING

Expt	Voltage (kV)	Temp (°C)	pH	Poly-L-SULV (%w/v)	Ave. Migration Time (t) (min)	Rs	Rs/t (per min)
1	15	15	7.2	1.00	21.424	1.52	0.07
2	20	25	7.2	0.75	9.314	0.92	0.10
3	25	15	7.2	1.00	10.521	1.59	0.15
4	15	15	7.5	0.75	18.399	1.14	0.06
5	20	15	7.2	0.75	12.895	1.32	0.10
6	25	15	7.2	0.50	8.284	0.96	0.12
7	25	20	7.5	0.75	8.865	0.83	0.09
8	30	20	7.5	1.00	7.632	0.92	0.12
9	30	20	7.5	0.75	7.345	0.68	0.09
10	20	20	7.5	0.50	10.651	0.70	0.07
11	20	15	7.2	0.50	11.351	0.88	0.08
12	30	15	7.2	0.50	6.270	0.94	0.15
13	25	20	7.2	1.00	8.610	1.20	0.14
14	20	25	7.5	1.00	16.966	0.88	0.05
15	30	15	7.5	0.75	7.400	1.06	0.14
16	30	15	7.5	0.50	6.751	0.77	0.11
17	25	20	7.5	0.50	8.132	0.45	0.06
18	20	20	7.2	1.00	11.631	1.18	0.10
19	30	25	7.2	1.00	5.860	0.99	0.17
20	30	20	7.2	1.00	6.531	1.29	0.20
21	30	20	7.2	0.50	5.412	0.79	0.15
22	15	15	7.2	0.75	18.696	1.18	0.06
23	20	25	7.5	0.50	11.004	0.47	0.04
24	25	15	7.5	0.75	10.088	0.96	0.10
25	15	20	7.5	1.00	19.490	0.98	0.05
26	15	20	7.5	0.50	15.039	0.56	0.04
27	25	25	7.2	1.00	7.643	1.11	0.15
28	15	20	7.2	0.75	15.032	0.95	0.06
29	20	15	7.5	0.75	13.185	1.20	0.09
30	20	25	7.2	0.50	8.395	0.74	0.09
31	25	25	7.5	0.50	8.829	0.33	0.04
32	25	25	7.5	1.00	10.623	0.82	0.08
33	15	25	7.2	0.50	11.721	0.62	0.05
34	20	15	7.5	0.50	12.001	1.04	0.09
35	25	15	7.5	0.50	8.979	0.77	0.09
36	20	15	7.5	1.00	14.875	1.32	0.09
37	25	15	7.5	1.00	11.388	1.04	0.09
38	15	25	7.5	1.00	27.274	0.93	0.03
39	20	20	7.2	0.75	10.508	1.08	0.10
40	30	15	7.2	1.00	7.802	1.35	0.17
41	30	20	7.2	0.75	5.892	1.21	0.21
42	30	25	7.5	1.00	8.758	0.54	0.06
43	20	25	7.2	1.00	10.227	1.02	0.10
44	15	25	7.5	0.50	19.404	0.59	0.03
45	30	25	7.2	0.50	4.923	0.60	0.12
46	30	25	7.5	0.50	6.482	0.24	0.04
47	15	15	7.2	1.00	21.424	1.52	0.07

Appendix I.A Calibration of benzoin.

Expt	Voltage (kV)	Temp (°C)	pH	poly-L-SULV (%w/v)	Ave. Migration Time (t) (min)	Rs	Rs/t (per min)
1	15	20	7.5	0.50	13.539	0.31	0.02
2	20	25	7.2	0.50	7.692	0.28	0.04
3	25	25	7.2	1.00	6.663	1.06	0.16
4	15	25	7.2	0.75	11.664	0.48	0.04
5	30	20	7.2	1.00	5.706	0.59	0.10
6	20	20	7.2	0.75	9.317	0.56	0.06
7	20	15	7.5	1.00	12.530	0.72	0.06
8	30	15	7.2	0.75	6.217	1.04	0.17
9	20	15	7.2	0.75	11.250	0.62	0.06
10	30	15	7.5	1.00	7.090	0.68	0.10
11	20	20	7.5	0.50	9.609	0.29	0.03
12	30	15	7.2	1.00	6.721	0.80	0.12
13	30	25	7.2	1.00	5.157	0.77	0.15
14	15	15	7.2	0.50	14.617	0.41	0.03
15	30	20	7.2	0.50	4.972	0.36	0.07
16	25	25	7.2	0.75	6.257	0.49	0.08
17	15	20	7.5	0.75	14.881	0.51	0.03
18	25	15	7.5	0.75	8.775	0.64	0.07
19	15	20	7.2	1.00	14.667	0.63	0.04
20	25	15	7.2	1.00	8.990	0.77	0.09
21	25	25	7.2	0.50	5.821	0.39	0.07
22	25	20	7.5	0.75	7.798	0.32	0.04
23	15	15	7.2	1.00	17.981	0.72	0.04
24	15	15	7.5	0.75	16.026	0.46	0.03
25	20	15	7.2	0.50	10.263	0.45	0.04
26	25	20	7.2	1.00	7.487	0.64	0.09
27	25	15	7.5	0.50	8.073	0.38	0.05
28	15	20	7.2	0.75	13.315	0.45	0.03
29	25	15	7.2	0.50	7.533	0.43	0.06
30	20	15	7.5	0.50	10.773	0.54	0.05
31	25	20	7.5	1.00	8.534	0.38	0.04
32	20	20	7.2	1.00	10.076	0.67	0.07
33	20	15	7.5	0.75	11.490	0.59	0.05
34	30	15	7.2	0.50	5.721	0.44	0.08
35	15	20	7.5	0.50	13.539	0.31	0.02

Appendix I.B   Calibration of hydrobenzoin.

Expt	Voltage (kV)	Temp (°C)	pH	poly-L-SULV (%w/v)	Ave. Migration Time (t) (min)	Rs	Rs/t (per min)
1	20	20	7.5	0.50	14.149	1.21	0.09
2	30	25	7.5	0.75	7.073	0.57	0.08
3	15	20	7.0	0.75	20.555	0.57	0.03
4	30	15	7.0	0.75	9.887	0.47	0.05
5	20	20	7.0	1.00	20.649	0.40	0.02
6	15	20	7.0	0.50	19.205	0.28	0.01
7	25	25	7.5	0.75	9.807	0.96	0.10
8	30	15	7.5	0.50	8.677	1.14	0.13
9	15	15	7.5	0.75	27.229	1.83	0.07
10	30	15	7.0	1.00	12.613	0.42	0.03
11	30	15	7.5	0.75	10.796	1.35	0.13
12	30	15	7.0	0.50	9.333	0.27	0.03
13	20	15	7.5	0.75	16.891	1.86	0.11
14	25	15	7.0	1.00	17.969	0.64	0.04
15	25	15	7.5	0.75	12.226	1.69	0.14
16	20	25	7.0	1.00	14.610	0.26	0.02
17	15	25	7.5	0.75	18.598	1.26	0.07
18	15	20	7.0	1.00	29.882	0.59	0.02
19	30	20	7.5	1.00	8.596	1.35	0.16
20	15	15	7.5	1.00	26.622	1.96	0.07
21	15	15	7.0	1.00	44.759	0.98	0.02
22	20	25	7.0	0.75	11.612	0.21	0.02
23	15	25	7.5	1.00	20.463	1.38	0.07
24	25	20	7.5	0.50	10.528	1.13	0.11
25	15	15	7.0	0.75	33.037	0.96	0.03
26	20	20	7.5	1.00	15.560	1.66	0.11
27	15	25	7.5	0.50	15.045	0.81	0.05
28	25	20	7.0	0.50	9.697	0.22	0.02
29	25	15	7.0	0.50	13.006	0.49	0.04
30	20	15	7.0	0.50	18.957	0.66	0.03
31	25	20	7.5	0.75	10.963	1.49	0.14
32	15	20	7.5	0.50	19.342	1.21	0.06
33	25	20	7.0	0.75	10.131	0.33	0.03
34	30	25	7.5	0.50	7.023	0.80	0.11
35	25	15	7.0	0.75	14.052	0.75	0.05

Appendix I.C   Calibration of coumachlor.

Expt	Voltage (kV)	Temp (°C)	pH	poly-L-SULV (%w/v)	Ave. Migration Time (t) (min)	Rs	Rs/t (per min)
1	20	20	7.5	1.00	13.567	0.80	0.06
2	20	25	7.5	1.00	12.441	0.40	0.03
3	15	20	7.5	1.00	19.210	0.80	0.04
4	25	20	7.5	0.75	9.844	0.54	0.05
5	30	25	7.5	1.00	6.882	0.32	0.05
6	30	15	7.5	1.00	8.608	0.76	0.09
7	30	20	7.5	1.00	7.713	0.39	0.05
8	25	25	7.5	1.00	9.447	0.33	0.03
9	25	15	7.5	0.75	10.806	0.75	0.07
10	20	25	7.5	0.75	12.026	0.34	0.03
11	15	20	7.5	0.75	18.269	0.66	0.04
12	25	25	7.5	0.75	8.932	0.25	0.03
13	25	20	7.5	1.00	10.225	0.96	0.09
14	30	15	7.5	0.50	8.008	0.27	0.03
15	20	20	7.5	0.50	12.895	0.32	0.02

Appendix I.D   Calibration of warfarin.

Expt	Voltage (kV)	Temp (°C)	pH	poly-L-SULV (%w/v)	Ave. Migration Time (t) (min)	Rs	Rs/t (per min)
1	30	25	9	0.75	13.521	0.95	0.07
2	25	15	8	1.00	34.082	0.60	0.02
3	30	15	8	0.50	24.087	0.49	0.02
4	20	15	9	0.50	32.174	0.85	0.03
5	20	25	8	1.00	37.356	0.40	0.01
6	15	20	9	0.50	40.786	0.78	0.02
7	25	20	9	0.75	26.110	0.82	0.03
8	20	25	9	0.50	25.216	0.71	0.03
9	25	15	9	0.75	38.776	0.86	0.02
10	30	15	8	1.00	27.594	0.40	0.01
11	15	25	9	0.50	35.999	0.72	0.02
12	30	15	9	0.50	19.124	0.86	0.04
13	25	25	9	0.50	18.141	0.72	0.04
14	15	20	8	1.00	60.212	0.66	0.01
15	20	20	9	1.00	33.998	0.97	0.03
16	30	15	9	0.75	18.712	0.99	0.05
17	30	20	9	0.75	15.770	0.98	0.06
18	20	15	8	0.75	52.247	0.55	0.01
19	20	20	9	0.75	31.291	0.95	0.03
20	25	20	9	1.00	24.150	1.02	0.04
21	30	20	8	0.50	19.711	0.60	0.03
22	25	15	9	1.00	37.462	0.62	0.02
23	25	20	9	0.50	20.339	0.77	0.04
24	25	15	8	0.50	32.464	0.53	0.02

Appendix I.E   Calibration of lorazepam.

Expt	Voltage (kV)	Temp (°C)	pH	poly-L-SULV (%w/v)	Ave. Migration Time (t) (min)	Rs	Rs/t (per min)
1	15	25	8.0	1.00	30.552	0.77	0.03
2	25	15	8.0	0.50	17.203	0.47	0.03
3	20	25	8.0	1.00	20.984	0.55	0.03
4	15	15	9.0	0.50	31.922	0.80	0.03
5	30	20	9.0	0.75	11.026	0.45	0.04
6	25	15	8.0	1.00	19.940	0.98	0.05
7	15	25	9.0	0.50	24.575	0.37	0.02
8	30	15	9.0	1.00	16.380	0.53	0.03
9	20	15	9.0	0.50	22.923	0.83	0.04
10	15	20	8.0	0.75	43.785	0.64	0.01
11	15	20	9.0	0.50	28.285	0.63	0.02
12	20	20	8.0	0.75	28.533	0.42	0.01
13	20	20	8.0	1.00	23.842	0.73	0.03
14	20	20	9.0	0.75	21.388	0.74	0.03
15	20	15	9.0	0.75	26.255	0.94	0.04
16	30	15	9.0	0.75	13.253	0.72	0.05
17	15	15	8.0	1.00	42.533	0.96	0.02
18	20	25	9.0	1.00	20.941	0.38	0.02
19	30	20	8.0	1.00	11.959	0.36	0.03
20	15	20	9.0	1.00	48.303	0.65	0.01
21	20	15	8.0	0.50	34.833	0.50	0.01
22	30	20	9.0	1.00	11.856	0.39	0.03
23	25	15	9.0	1.00	21.806	0.84	0.04
24	20	20	9.0	0.50	19.681	0.53	0.03
25	25	20	9.0	1.00	16.316	0.62	0.04
26	15	25	9.0	1.00	28.871	0.53	0.02

Appendix I.F   Calibration of temazepam.

Expt	Voltage (kV)	Temp (°C)	pH	poly-L-SULV (%w/v)	Ave. Migration Time (t) (min)	Rs	Rs/t (per/min)
1	30	20	9.0	0.50	10.921	25.37	2.32
2	15	15	10.0	0.50	33.263	29.13	0.88
3	30	15	10.0	0.75	12.515	21.63	1.73
4	20	15	9.0	0.75	31.594	24.52	0.78
5	20	15	10.0	0.50	21.445	29.28	1.37
6	20	25	10.0	0.75	19.901	42.50	2.14
7	30	20	9.0	0.75	12.011	27.47	2.29
8	25	25	10.0	1.00	18.460	41.64	2.26
9	20	25	9.0	0.50	18.765	25.00	1.33
10	15	25	10.0	0.50	22.759	22.37	0.98
11	30	15	9.5	0.75	12.250	30.58	2.50
12	15	20	9.0	1.00	45.630	28.71	0.63
13	20	25	9.5	0.75	16.993	23.44	1.38
14	20	20	9.0	0.50	21.112	24.45	1.16
15	15	15	10.0	0.75	36.719	27.03	0.74
16	20	15	9.0	0.50	28.013	19.40	0.69
17	25	20	9.0	0.75	18.035	27.63	1.53
18	15	25	10.0	0.75	28.863	22.57	0.78
19	20	15	9.5	0.50	19.588	31.94	1.63
20	15	15	9.0	0.75	45.354	22.25	0.49
21	20	15	10.0	1.00	28.763	30.72	1.07
22	30	20	10.0	1.00	17.181	21.12	1.23
23	20	25	9.5	0.50	14.787	27.69	1.87
24	30	15	9.0	0.50	13.366	21.79	1.63
25	20	20	9.5	1.00	23.421	42.32	1.81
26	25	15	9.0	1.00	34.204	20.60	0.60
27	15	25	9.5	1.00	31.171	54.94	1.76
28	30	25	9.5	0.50	8.016	24.73	3.09
29	25	20	9.5	1.00	18.211	51.24	2.81
30	30	20	9.0	1.00	14.428	20.48	1.42
31	20	15	9.0	1.00	47.726	35.40	0.74
32	25	25	9.0	1.00	16.870	15.17	0.90
33	15	25	9.5	0.75	24.222	23.34	0.96
34	15	15	9.5	0.50	27.896	27.70	0.99
35	25	15	9.5	1.00	22.370	27.96	1.25
36	15	20	9.5	0.75	28.649	26.06	0.91
37	15	15	9.0	0.50	41.200	20.26	0.49
38	15	25	9.0	0.50	25.505	24.49	0.96
39	30	15	10.0	0.50	10.916	27.96	2.56
40	30	15	9.5	0.50	10.668	23.97	2.25
41	15	25	9.5	0.50	21.392	27.93	1.31
42	25	15	10.0	0.75	18.282	23.87	1.31
43	25	25	10.0	0.50	11.968	28.43	2.38
44	20	25	9.5	1.00	21.207	55.86	2.63
45	25	20	10.0	0.75	15.859	28.48	1.80
46	30	25	10.0	0.50	8.715	23.20	2.66
47	20	25	9.0	0.75	21.378	27.20	1.27
48	25	20	9.0	1.00	20.723	30.96	1.49
49	30	15	9.0	0.75	14.304	24.84	1.74
50	25	15	9.5	0.75	17.357	25.94	1.49

51	15	20	10.0	1.00	44.866	33.63	0.75
52	15	20	9.5	0.50	24.796	27.96	1.13
53	25	25	10.0	0.75	14.658	37.15	2.53
54	30	15	9.5	1.00	14.084	25.30	1.80
55	25	15	9.0	0.50	19.336	20.85	1.08
56	30	25	10.0	0.75	10.816	49.23	4.55
57	25	20	9.0	0.50	14.736	22.88	1.55
58	30	25	9.0	0.75	10.217	26.03	2.55
69	20	15	10.0	0.75	25.881	24.77	0.96
60	15	20	9.0	0.50	30.529	24.53	0.80
61	20	20	9.0	0.75	25.730	24.95	0.97
62	20	25	10.0	1.00	26.895	51.64	1.92
63	15	20	9.5	1.00	35.415	44.95	1.27
64	20	25	10.0	0.50	16.448	26.87	1.63
65	30	25	9.5	0.75	9.182	24.72	2.69
66	20	20	9.5	0.75	19.952	23.80	1.19
67	25	20	10.0	0.50	13.314	26.35	1.98
68	15	15	9.5	0.75	35.669	21.84	0.61
69	25	20	10.0	1.00	20.807	25.31	1.22
70	20	15	9.5	1.00	30.805	26.68	0.87
71	30	15	10.0	1.00	15.026	32.79	2.18

Appendix I.G   Calibration of achiral chlorophenols.

Expt	Voltage (kV)	Temp (°C)	pH	poly-L-SULV (%w/v)	Ave. Migration Time (t) (min)	Rs	Rs/t (per min)
1	15	25	10.0	1.00	44.940	34.63	0.77
2	15	20	9.0	0.75	31.928	15.08	0.47
3	15	25	9.0	1.00	36.113	23.40	0.65
4	25	25	9.0	0.50	22.661	28.71	1.27
5	25	15	9.0	0.75	26.040	24.38	0.94
6	20	20	10.0	0.75	28.557	28.38	0.99
7	15	20	10.0	0.75	30.622	20.33	0.66
8	25	25	9.5	0.50	19.481	25.30	1.30
9	20	20	9.5	0.50	25.534	29.16	1.14
10	20	20	9.0	1.00	33.694	28.21	0.84
11	30	20	10.0	0.50	19.674	26.99	1.37
12	30	20	9.5	0.75	19.111	25.36	1.33
13	30	25	9.0	0.50	20.200	29.19	1.45
14	30	20	9.5	0.50	18.879	26.53	1.41
15	30	15	9.0	1.00	27.221	31.56	1.16
16	25	25	9.0	0.75	20.999	23.10	1.10
17	25	20	9.5	0.50	22.156	28.65	1.29
18	15	15	10.0	1.00	39.133	20.14	0.51
19	20	15	9.5	0.75	27.256	23.24	0.85
20	30	20	10.0	0.75	19.407	23.48	1.21
21	25	15	10.0	0.50	25.385	30.84	1.21
22	25	15	9.5	0.50	20.671	23.81	1.15
23	25	20	9.5	0.75	23.125	28.15	1.22
24	20	20	10.0	1.00	32.518	24.93	0.77
25	15	20	10.0	0.50	25.555	19.95	0.78
26	30	25	9.0	1.00	22.098	24.34	1.10
27	20	25	9.0	1.00	25.551	15.15	0.59
28	25	25	9.5	0.75	20.828	25.92	1.24
29	20	20	10.0	0.50	25.003	25.95	1.04
30	25	25	9.5	1.00	39.149	58.06	1.48
31	15	25	9.0	0.75	29.797	21.07	0.71
32	25	15	10.0	1.00	27.050	25.07	0.93
33	15	25	10.0	1.00	44.940	34.63	0.77
34	15	20	9.0	0.75	31.928	15.08	0.47
35	15	25	9.0	1.00	36.113	23.40	0.65

Appendix I.H   Calibration of achiral benzodiazepines.

APPENDIX II
VALIDATION STUDIES: MIGRATION TIME, RESOLUTION, AND RESOLUTION
PER UNIT TIME FOR CHIRAL AND ACHIRAL ANALYTES

Exp	Average Migration Time (t) (min)			Resolution (Rs)			Rs/t (per min)		
	Exp	Pred	Pred-Exp	Exp	Pred	Pred-Exp	Exp	Pred	Pred-Exp
1	9.350	10.728	1.378	0.72	0.86	0.14	0.08	0.08	0.00
2	14.539	15.753	1.214	1.04	1.11	0.07	0.07	0.07	0.00
3	16.523	16.616	0.093	0.98	0.88	-0.10	0.06	0.05	-0.01
4	14.564	13.948	-0.616	1.66	1.48	-0.18	0.11	0.11	0.00
5	9.405	9.363	-0.042	1.24	1.24	0.00	0.13	0.13	0.00
6	5.394	4.436	-0.958	0.97	0.79	-0.18	0.18	0.18	0.00
7	7.048	5.997	-1.051	1.35	1.20	-0.15	0.19	0.20	-0.01
8	13.107	14.533	1.426	0.86	0.90	0.04	0.07	0.06	-0.01
9	17.117	17.056	-0.061	0.85	0.88	0.03	0.05	0.05	0.00
10	11.844	13.690	1.846	0.99	0.84	-0.15	0.08	0.06	-0.02
11	13.466	14.910	1.444	0.95	1.05	0.10	0.07	0.07	0.00
12	7.825	8.582	0.757	1.12	1.03	-0.09	0.14	0.12	-0.02
13	12.616	12.910	0.294	0.63	0.63	0.00	0.05	0.05	0.00
14	6.729	6.179	-0.550	0.53	0.56	0.03	0.08	0.09	0.01
15	8.365	8.960	0.595	1.02	1.18	0.16	0.12	0.13	0.01
16	6.329	6.582	0.253	0.63	0.62	-0.01	0.10	0.09	-0.01
17	10.044	11.545	1.501	0.90	1.01	0.11	0.09	0.09	0.00
18	20.577	19.056	-1.521	1.20	1.29	0.09	0.06	0.07	0.01
19	10.188	9.544	-0.644	0.63	0.60	-0.03	0.06	0.06	0.00
20	7.006	7.802	0.796	0.92	0.83	-0.09	0.13	0.11	-0.02
21	7.008	7.362	0.354	0.82	0.83	0.01	0.12	0.11	-0.01
RMS%RE		**9.82**			**10.16**				**10.35**

Appendix II.A   Validation of benzoin.

Exp	Average Migration Time (t) (min)			Resolution (Rs)			Rs/t (per min)		
	Exp	Pred	Pred-Exp	Exp	Pred	Pred-Exp	Exp	Pred	Pred-Exp
1	6.958	7.484	0.526	0.63	0.53	-0.10	0.09	0.07	-0.02
2	16.212	14.340	-1.872	0.57	0.59	0.02	0.04	0.04	0.00
3	14.830	14.177	-0.653	0.34	0.38	0.04	0.02	0.03	0.01
4	8.304	9.145	0.841	0.50	0.45	-0.05	0.06	0.05	-0.01
5	16.370	14.358	-2.012	0.92	0.58	-0.34	0.06	0.04	-0.02
6	5.640	4.643	-1.000	0.59	0.54	-0.05	0.10	0.12	-0.02
7	6.020	5.655	-0.365	0.39	0.40	0.01	0.06	0.07	0.01
8	8.934	9.827	0.893	0.66	0.59	-0.07	0.07	0.06	-0.01
9	11.409	11.517	0.108	0.70	0.59	-0.11	0.06	0.05	-0.01
10	9.569	9.852	0.283	0.81	0.67	-0.14	0.08	0.07	-0.01
11	10.358	10.839	0.481	0.41	0.45	0.04	0.04	0.04	0.00
12	17.328	15.533	-1.795	0.59	0.65	0.06	0.03	0.04	0.01
13	6.489	6.333	-0.156	0.60	0.54	-0.06	0.09	0.09	0.00
14	8.559	9.646	1.087	0.36	0.39	0.03	0.04	0.04	0.00
15	12.345	12.177	-0.168	0.78	0.74	-0.04	0.06	0.06	0.00
RMS%RE			**9.06**			**14.27**			**21.31**

Appendix II.B   Validation of hydrobenzoin.

Exp	Average Migration Time (t) (min)			Resolution (Rs)			Rs/t (per min)		
	Exp	Pred	Pred-Exp	Exp	Pred	Pred-Exp	Exp	Pred	Pred-Exp
1	13.323	13.740	0.417	1.27	1.07	-0.20	0.10	0.08	-0.02
2	11.619	13.853	2.234	1.70	1.41	-0.29	0.15	0.10	-0.05
3	14.829	16.827	1.998	1.62	1.39	-0.23	0.11	0.08	-0.03
4	7.898	5.024	-2.874	1.01	0.98	-0.03	0.13	0.12	-0.01
5	11.600	13.036	1.436	1.42	1.43	0.01	0.12	0.11	-0.01
6	14.009	15.692	1.683	1.26	1.22	-0.04	0.09	0.08	-0.01
7	20.943	20.658	-0.285	0.94	0.73	-0.21	0.04	0.04	0.00
8	9.797	12.015	2.218	1.72	1.60	-0.12	0.18	0.13	-0.05
9	16.544	19.410	2.866	0.26	0.21	-0.05	0.02	0.01	-0.01
10	14.795	16.940	2.145	1.81	1.73	-0.08	0.12	0.10	-0.02
11	15.561	17.962	2.401	1.55	1.56	0.01	0.10	0.09	-0.01
12	22.246	23.704	1.458	1.64	1.67	0.03	0.07	0.07	0.00
13	10.552	10.766	0.214	1.29	1.09	-0.20	0.12	0.10	-0.02
14	26.820	22.887	-3.933	1.30	1.69	0.39	0.05	0.07	0.02
15	12.747	11.788	-0.959	0.83	0.92	0.09	0.07	0.08	0.01
16	28.589	22.610	-5.979	0.78	0.88	0.10	0.03	0.04	0.01
17	20.666	21.752	1.086	1.58	1.52	-0.06	0.08	0.07	-0.01
RMS%RE			**15.77**			**13.62**			**23.60**

Appendix II.C   Validation of coumachlor.

Exp	Average Migration Time (t) (min)			Resolution (Rs)			Rs/t (per min)		
	Exp	Pred	Pred-Exp	Exp	Pred	Pred-Exp	Exp	Pred	Pred-Exp
1	22.650	18.721	-3.929	0.88	0.92	0.04	0.04	0.05	0.01
2	14.688	15.150	0.462	0.83	0.81	-0.02	0.06	0.05	-0.01
3	17.866	16.658	-1.208	0.59	0.63	0.04	0.04	0.04	0.00
4	22.141	19.345	-2.796	1.04	1.14	0.10	0.05	0.06	0.01
5	7.387	6.040	-1.347	0.11	0.12	0.01	0.01	0.02	0.01
6	13.180	13.810	0.630	0.68	0.56	-0.12	0.05	0.04	-0.01
7	16.701	16.034	-0.667	0.39	0.42	0.03	0.02	0.03	0.01
8	12.533	12.202	-0.331	0.83	0.91	0.08	0.07	0.07	0.00
9	13.990	14.526	0.536	0.55	0.59	0.04	0.04	0.04	0.00
10	9.465	8.001	-1.464	0.49	0.58	0.09	0.05	0.07	0.02
11	9.719	9.611	-0.108	0.24	0.23	-0.01	0.02	0.02	0.00
12	7.631	6.663	-0.968	0.34	0.33	-0.01	0.04	0.05	0.01
13	22.647	18.098	-4.549	0.60	0.71	0.11	0.03	0.04	0.01
14	17.611	16.754	-0.857	0.42	0.45	0.03	0.02	0.03	0.01
15	10.551	10.955	0.404	0.50	0.48	-0.02	0.05	0.04	-0.01
RMS%RE			**15.77**			**13.62**			**23.60**

Appendix II.D   Validation of warfarin.

Exp	Average Migration Time (t) (min)			Resolution (Rs)			Rs/t (per min)		
	Exp	Pred	Pred-Exp	Exp	Pred	Pred-Exp	Exp	Pred	Pred-Exp
1	44.933	44.383	-0.550	0.86	0.86	0.00	0.02	0.02	0.00
2	20.770	24.893	4.127	0.58	0.58	0.00	0.03	0.02	-0.01
3	18.756	19.571	0.815	0.92	0.85	-0.07	0.05	0.04	-0.01
4	23.656	27.385	3.729	0.87	0.87	0.00	0.04	0.03	-0.01
5	43.177	46.835	3.658	0.78	0.84	0.06	0.02	0.02	0.00
6	49.311	49.705	0.394	0.62	0.59	-0.03	0.01	0.01	0.00
7	59.368	42.931	-16.437	0.88	0.97	0.09	0.01	0.02	0.01
8	53.178	49.746	-3.432	0.87	0.89	0.02	0.02	0.02	0.00
9	26.756	29.256	2.500	0.41	0.52	0.11	0.02	0.02	0.00
10	37.667	40.020	2.353	0.89	0.91	0.02	0.02	0.02	0.00
11	14.967	12.297	-2.670	0.85	0.84	-0.01	0.06	0.07	0.01
12	22.081	24.933	2.852	0.95	0.89	-0.06	0.04	0.04	0.00
13	45.142	41.932	-3.210	0.81	0.88	0.07	0.02	0.02	0.00
14	29.297	34.618	5.321	0.55	0.56	0.01	0.02	0.02	0.00
15	53.350	48.706	-4.644	0.34	0.49	0.15	0.01	0.01	0.00
16	28.453	31.748	3.295	0.79	0.81	0.02	0.03	0.03	0.00
17	17.546	18.119	0.573	0.94	0.96	0.02	0.05	0.05	0.00
18	26.275	30.296	4.021	0.78	0.93	0.15	0.03	0.03	0.00
RMS%RE			**12.83**			**13.78**			**26.26**

Appendix II.E   Validation of lorazepam.

Exp	Average Migration Time (t) (min)			Resolution (Rs)			Rs/t (per min)		
	Exp	Pred	Pred-Exp	Exp	Pred	Pred-Exp	Exp	Pred	Pred-Exp
1	18.514	19.760	1.246	0.87	0.71	-0.16	0.05	0.04	-0.01
2	17.969	18.787	0.818	0.48	0.39	-0.09	0.03	0.02	-0.01
3	38.459	38.753	0.294	0.83	0.89	0.06	0.02	0.02	0.00
4	26.278	26.533	0.255	0.57	0.50	-0.07	0.02	0.02	0.00
5	30.902	30.892	-0.010	0.79	0.72	-0.07	0.03	0.02	-0.01
6	28.778	32.684	3.906	0.95	0.89	-0.06	0.03	0.03	0.00
7	16.763	18.083	1.320	0.76	0.60	-0.16	0.05	0.03	-0.02
8	37.487	35.252	-2.235	0.95	0.93	-0.02	0.03	0.03	0.00
9	35.079	36.071	0.992	0.80	0.78	-0.02	0.02	0.02	0.00
10	12.980	11.041	-1.939	0.33	0.27	-0.06	0.03	0.02	-0.01
11	14.211	13.723	-0.488	0.42	0.38	-0.04	0.03	0.03	0.00
12	16.929	20.580	3.651	0.61	0.56	-0.05	0.04	0.03	-0.01
13	15.248	15.400	0.152	0.66	0.49	-0.17	0.04	0.03	-0.01
14	26.735	31.007	4.272	0.73	0.78	0.05	0.03	0.03	0.00
15	24.412	24.971	0.559	0.36	0.46	0.10	0.01	0.02	0.01
16	14.992	15.515	0.523	0.41	0.55	0.14	0.03	0.04	0.01
17	12.992	10.336	-2.656	0.56	0.49	-0.07	0.04	0.05	0.01
18	14.922	16.220	1.298	0.33	0.34	0.01	0.02	0.02	0.00
19	45.145	37.076	-8.069	0.64	0.79	0.15	0.01	0.02	0.01
20	32.552	29.182	-3.370	1.09	0.93	-0.16	0.03	0.03	0.00
RMS%RE			**10.61**			**16.63**			**37.63**

Appendix II.F   Validation of temazepam.

Exp	Average Migration Time (t) (min)			Resolution (Rs)			Rs/t (per min)		
	Exp	Pred	Pred-Exp	Exp	Pred	Pred-Exp	Exp	Pred	Pred-Exp
1	35.059	35.295	0.236	26.91	34.89	7.98	0.77	0.76	-0.01
2	13.152	15.239	2.087	30.03	24.95	-5.08	2.28	2.50	0.21
3	21.368	21.548	0.180	26.52	23.94	-2.58	1.24	1.29	0.05
4	21.787	22.548	0.761	30.56	31.38	0.82	1.40	1.49	0.09
5	10.958	11.958	1.001	26.40	27.00	0.60	2.41	2.97	0.56
6	17.556	15.239	-2.317	30.92	25.03	-5.89	1.76	1.97	0.21
7	29.447	33.548	4.102	31.15	31.56	0.41	1.06	1.65	0.59
8	10.243	11.485	1.243	26.38	27.97	1.59	2.58	2.98	0.40
9	9.127	9.219	0.092	27.44	23.67	-3.77	3.01	3.21	0.20
10	17.211	20.395	3.185	33.28	27.56	-5.72	1.93	1.95	0.01
11	14.711	16.493	1.782	24.57	29.24	4.67	1.67	1.29	-0.38
12	12.605	14.389	1.785	29.91	24.35	-5.56	2.37	2.87	0.50
13	24.697	25.485	0.788	25.71	26.68	0.97	1.04	1.06	0.02
14	11.484	13.210	1.726	24.63	30.02	5.39	2.14	2.50	0.35
15	15.374	17.590	2.216	32.38	23.76	-8.62	2.11	2.96	0.85
16	14.305	14.395	0.090	25.24	21.70	-3.54	1.76	2.14	0.37
17	14.321	15.340	1.019	29.58	28.65	-0.93	2.07	2.05	-0.01
18	29.420	29.596	0.176	27.87	35.67	7.80	0.95	1.35	0.40
19	24.787	30.493	5.707	22.43	27.77	5.34	0.90	1.39	0.49
20	13.681	14.398	0.717	25.71	32.86	7.15	1.88	2.98	1.10
21	12.263	12.495	0.233	27.15	31.30	4.15	2.21	2.60	0.38
22	18.412	22.495	4.083	27.79	27.09	-0.70	1.51	1.97	0.46
23	30.311	34.590	4.279	24.10	30.60	6.50	0.80	1.39	0.60
24	22.052	24.609	2.557	27.28	32.34	5.06	1.24	1.55	0.31
RMS%RE			**11.97**			**17.92**			**31.08**

Appendix II.G   Validation of achiral chlorophenols.

Exp	Average Migration Time (t) (min)			Resolution (Rs)			Rs/t (per min)		
	Exp	Pred	Pred-Exp	Exp	Pred	Pred-Exp	Exp	Pred	Pred-Exp
1	42.289	43.294	1.005	38.47	38.19	-0.28	0.91	1.24	0.33
2	38.299	38.298	-0.001	18.91	19.29	0.38	0.49	0.59	0.10
3	35.059	35.392	0.333	26.91	34.39	7.48	0.77	0.94	0.17
4	13.152	16.492	3.340	30.03	31.29	1.26	2.28	2.39	0.11
5	21.368	24.345	2.977	26.52	29.39	2.87	1.24	1.59	0.35
6	21.787	25.395	3.609	30.56	39.29	8.73	1.40	1.59	0.18
7	31.316	33.482	2.166	23.46	20.29	-3.17	0.75	0.93	0.18
8	10.958	12.220	1.262	26.40	29.39	2.99	2.41	2.59	0.18
9	17.556	15.385	-2.171	30.92	35.39	4.47	1.76	1.94	0.18
10	29.447	32.495	3.048	31.15	39.29	8.14	1.06	1.50	0.44
11	9.500	9.284	-0.216	27.94	28.39	0.45	2.94	3.29	0.35
12	10.243	12.492	2.250	26.38	29.39	3.01	2.58	2.85	0.27
13	9.069	9.492	0.423	30.10	30.19	0.09	3.32	3.20	-0.11
14	9.127	9.293	0.166	27.44	21.39	-6.05	3.01	3.45	0.44
15	17.211	18.393	1.182	33.28	38.48	5.20	1.93	2.21	0.28
16	14.711	14.296	-0.415	24.57	28.49	3.92	1.67	1.84	0.17
17	12.605	13.248	0.644	29.91	35.49	5.58	2.37	2.94	0.57
18	44.504	45.395	0.891	24.59	28.49	3.90	0.55	0.69	0.14
19	24.697	25.394	0.697	25.71	25.28	-0.43	1.04	1.40	0.36
20	11.484	11.592	0.108	24.63	25.39	0.76	2.14	2.35	0.20
21	15.374	16.394	1.020	32.38	34.29	1.91	2.11	2.39	0.29
22	14.305	15.292	0.987	25.24	27.49	2.25	1.76	1.39	-0.37
23	14.321	16.393	2.072	29.58	31.29	1.71	2.07	2.49	0.43
24	29.420	32.194	2.774	27.87	29.39	1.52	0.95	1.39	0.45
25	24.787	25.308	0.522	22.43	26.49	4.06	0.90	1.49	0.59
RMS%RE			**10.12**			**14.37**			**25.63**

Appendix II.H   Validation of achiral benzodiazepines.

^{1}H-NMR (undecanoyl-L-tryptophan)
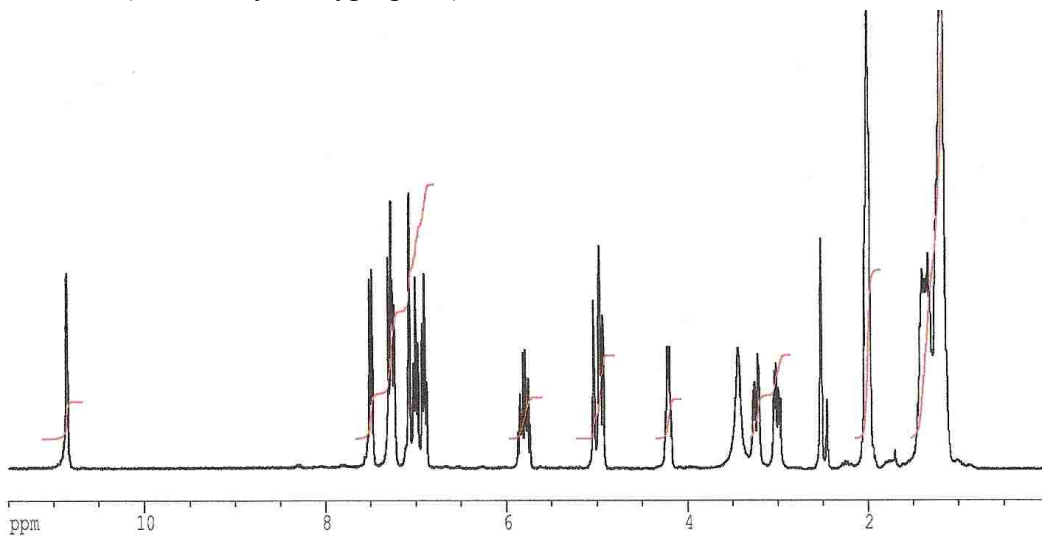
^{13}C-NMR (undecanoyl-L-tryptophan)
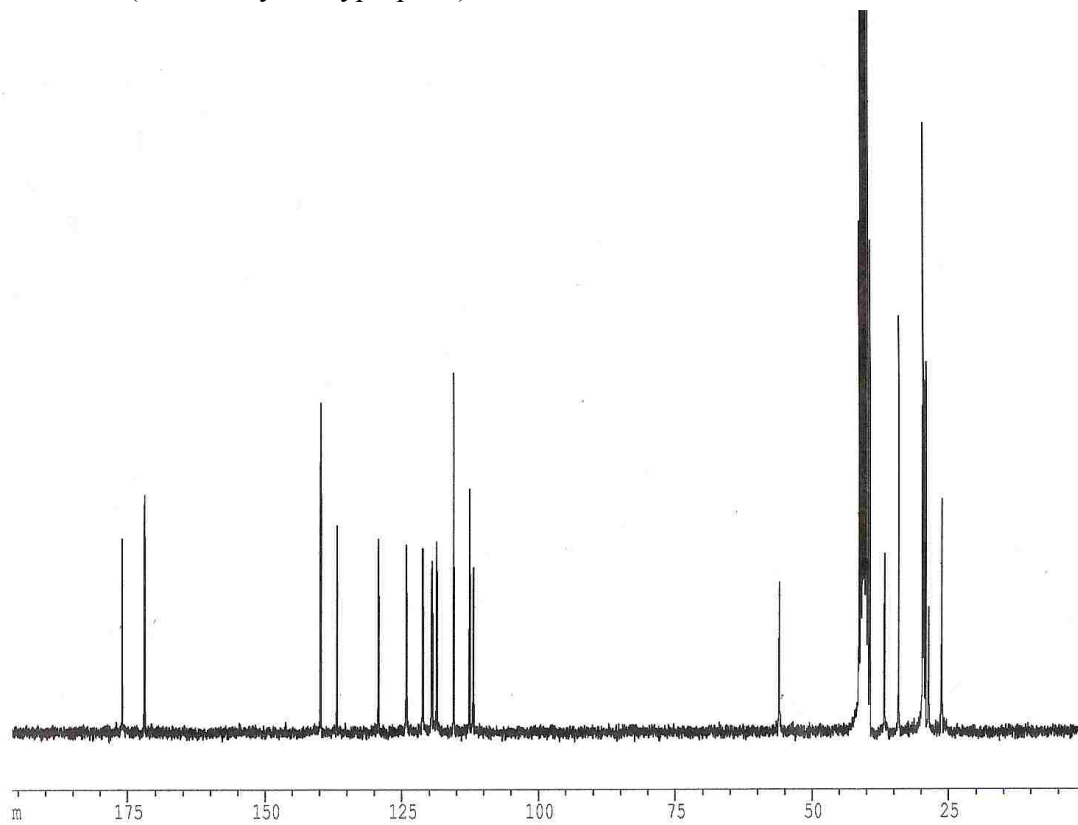
¹H-NMR (undecanoyl-L-tyrosine)

¹³C-NMR (undecanoyl-L-tyrosine)

154
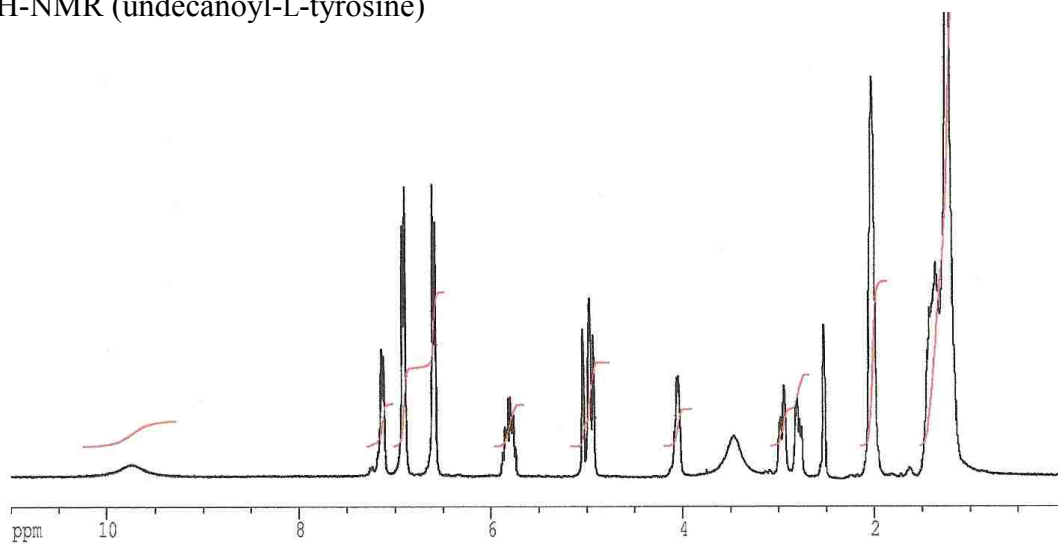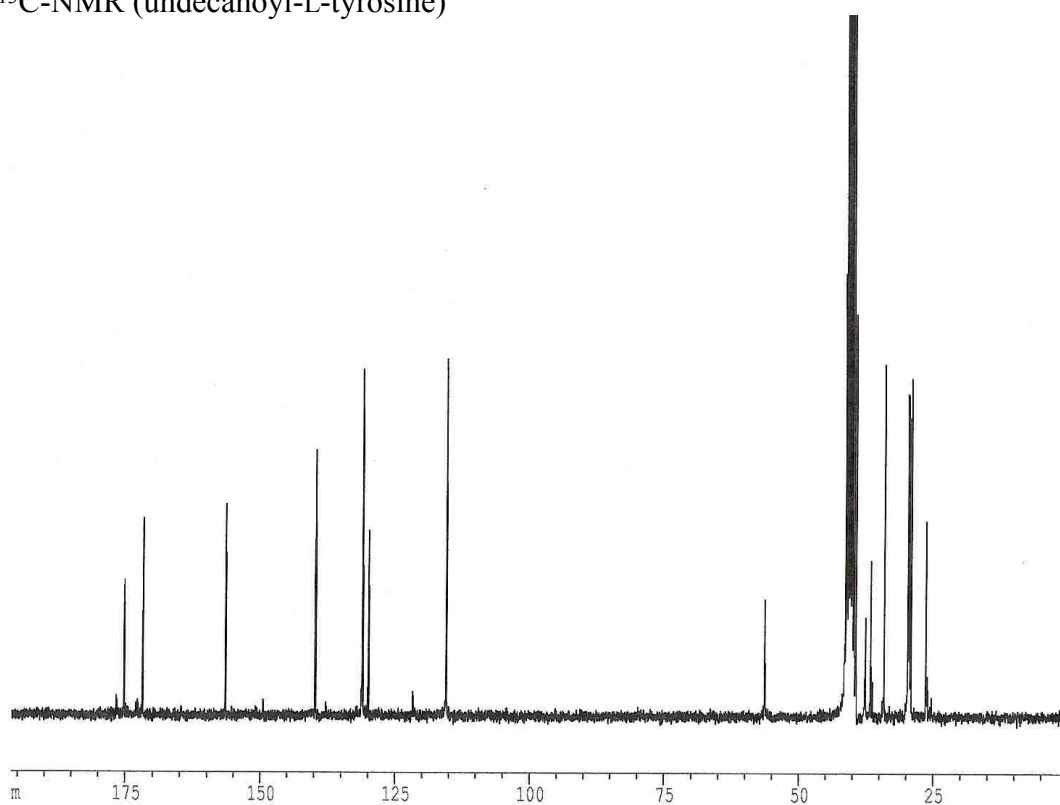
1H-NMR (undecanoyl-L-phenylalanine)
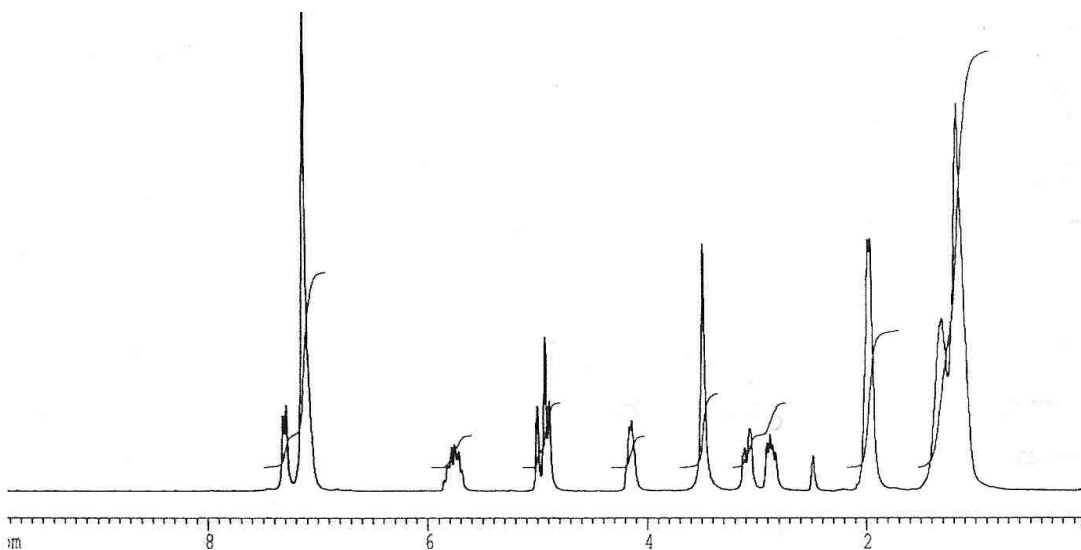
13C-NMR (undecanoyl-L-phenylalanine)
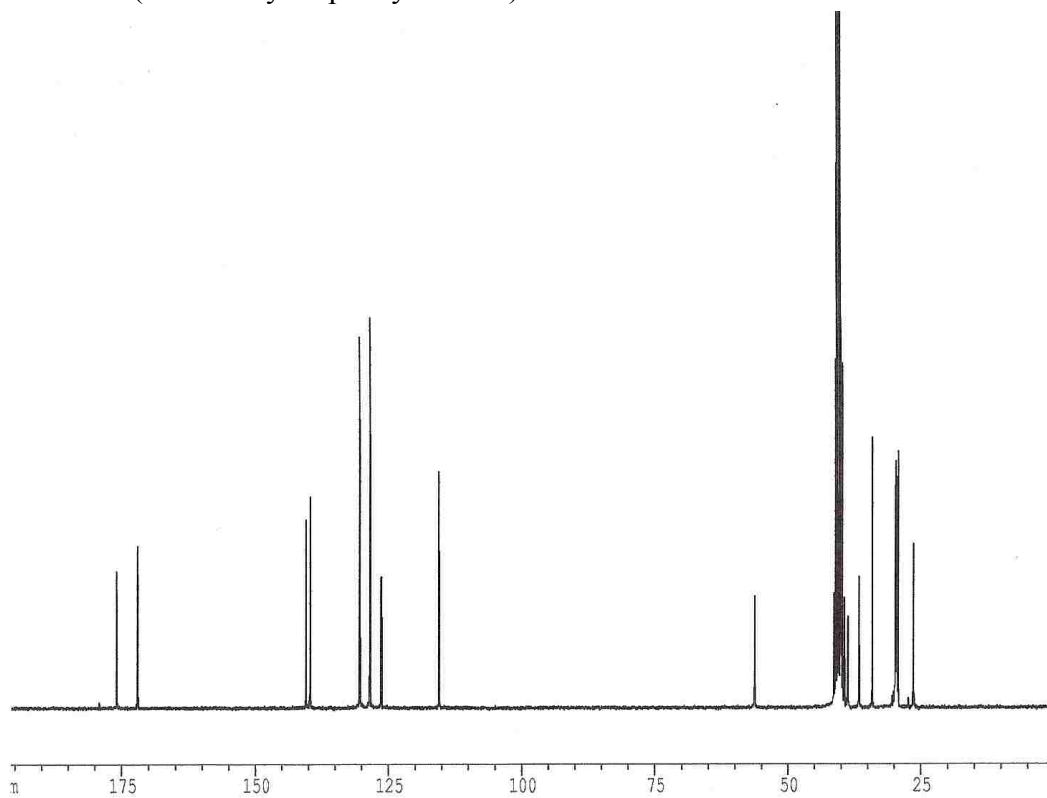
APPENDIX IV
FIGURES OF MERIT OBTAINED FROM MULTIPLE REGRESSION ANALYSIS OF CALIBRATION SAMPLES IN METHANOL/WATER MEDIUM

Analyte	Regression coefficient	Slope	Offset	Wavelength range
BNA (25:75 MeOH/H$_2$0)	0.9989	0.9972	8.10×10^{-3}	385-485
BNA (75:25 MeOH/H$_2$0)	0.9995	0.9974	7.22×10^{-3}	385-485
TFA (25:75 MeOH/H$_2$0)	0.9989	0.9934	4.23×10^{-3}	390-450
TFA (75:25 MeOH/H$_2$0)	0.9992	0.9927	6.14×10^{-3}	390-450
PROP (25:75 MeOH/H$_2$0)	0.9989	0.9967	7.41×10^{-3}	320-400
PROP (75:25 MeOH/H$_2$0)	0.9990	0.9967	7.44×10^{-3}	320-400
NPRX (25:75 MeOH/H$_2$0)	0.9985	0.9989	4.05×10^{-3}	350-405
NPRX (75:25 MeOH/H$_2$0)	0..9993	0.9986	6.74×10^{-3}	350-405
TAR (25:75 MeOH/H$_2$0)	0.9987	0.9948	5.51×10^{-3}	300-350
TAR (75:25 MeOH/H$_2$0)	0.9989	0.9944	7.24×10^{-3}	300-350
CIT (25:75 MeOH/H$_2$0)	0.9982	0.9971	1.49×10^{-3}	300-350
CIT (75:25 MeOH/H$_2$0)	0.9986	0.9972	5.68×10^{-3}	300-350
LIM (25:75 MeOH/H$_2$0)	0.9902	0.9802	7.62×10^{-3}	300-350
LIM (75:25 MeOH/H$_2$0)	0.9923	0.9914	5.14×10^{-3}	300-350
CME (25:75 MeOH/H$_2$0)	0.9938	0.9966	7.01×10^{-3}	300-350
CME (75:25 MeOH/H$_2$0)	0.9967	0.9972	4.26×10^{-3}	300-350

VALIDATION STUDIES USING METHANOL/WATER MEDIUM

Act S BNA mol frac	Pred S BNA mol frac	S BNA rel error %	Act S TFA mol frac	Pred S TFA mol frac	S TFA rel error %
0.877	0.868	1.03	0.850	0.842	0.94
0.826	0.829	-0.36	0.783	0.791	-1.02
0.715	0.722	-0.98	0.700	0.694	0.86
0.650	0.646	0.62	0.645	0.655	-1.55
0.575	0.565	1.74	0.570	0.578	-1.40
0.545	0.539	1.10	0.480	0.472	1.67
0.487	0.481	1.23	0.400	0.406	-1.50
0.380	0.372	2.11	0.250	0.247	1.20
0.285	0.281	1.40	0.150	0.146	2.67
0.192	0.190	1.04	0.075	0.071	5.33
RMS%RE		*1.26*	*RMS%RE*		*2.21*
Act R BNA mol frac	Pred R BNA mol frac	R BNA rel error %	Act R TFA mol frac	Pred R TFA mol frac	R TFA rel error %
0.123	0.125	-1.63	0.150	0.155	-3.33
0.174	0.173	0.57	0.217	0.212	2.30
0.285	0.288	1.05	0.300	0.306	-2.00
0.350	0.355	-1.43	0.355	0.359	-1.13
0.425	0.435	-2.35	0.430	0.425	1.16
0.455	0.460	-1.10	0.520	0.514	1.15
0.513	0.505	1.56	0.600	0.596	0.67
0.620	0.616	0.65	0.750	0.742	1.07
0.715	0.720	-0.70	0.850	0.844	0.71
0.808	0.802	0.74	0.925	0.932	-0.76
RMS%RE		*1.29*	*RMS%RE*		*1.64*
Act S PROP mol frac	Pred S PROP mol frac	S PROP rel error %	Act S NPRX mol frac	Pred S NPRX mol frac	S NPRX rel error %
0.950	0.966	-1.68	0.924	0.918	0.65
0.874	0.862	1.37	0.815	0.811	0.49
0.772	0.761	1.42	0.705	0.713	-1.13
0.650	0.664	-2.15	0.670	0.661	1.34
0.550	0.565	-2.73	0.550	0.540	1.82
0.475	0.480	-1.05	0.450	0.444	1.33
0.400	0.405	-1.25	0.350	0.342	2.29
0.255	0.261	-2.35	0.236	0.245	-3.81
0.175	0.180	-2.86	0.175	0.180	-2.86
0.078	0.075	3.85	0.078	0.081	-3.85
RMS%RE		*2.24*	*RMS%RE*		*2.27*
Act R PROP mol frac	Pred R PROP mol frac	R PROP rel error %	Act R NPRX mol frac	Pred R NPRX mol frac	R NPRX rel error %
0.050	0.052	-4.00	0.076	0.073	3.95
0.126	0.122	3.17	0.185	0.191	-3.24
0.228	0.233	-2.19	0.295	0.305	-3.39
0.350	0.344	1.71	0.330	0.328	0.61
0.450	0.442	1.78	0.450	0.461	-2.44
0.525	0.532	-1.33	0.550	0.541	1.64
0.600	0.605	-0.83	0.650	0.661	-1.69
0.745	0.753	-1.07	0.764	0.760	0.52
0.825	0.818	0.85	0.825	0.834	-1.09
0.922	0.931	-0.98	0.922	0.925	-0.33
RMS%RE		*2.06*	*RMS%RE*		*2.26*

Appendix V. A   Actual and predicted mole fraction of 1.0×10^{-5} M enantiomers of fluorescent analytes with optimum concentration of poly-L-SUF in 25:75 methanol/water.

Act D TAR mol frac	Pred D TAR mol frac	D TAR rel error %	Act S CIT mol frac	Pred S CIT mol frac	S CIT rel error %
0.950	0.925	2.63	0.950	0.943	0.74
0.850	0.841	1.06	0.850	0.839	1.29
0.750	0.742	1.07	0.750	0.741	1.20
0.650	0.661	-1.69	0.650	0.664	-2.15
0.550	0.560	-1.82	0.550	0.545	0.91
0.450	0.459	-2.00	0.450	0.442	1.78
0.350	0.358	-2.29	0.350	0.355	-1.43
0.225	0.221	1.78	0.225	0.223	0.89
0.150	0.146	2.67	0.150	0.154	-2.67
0.050	0.047	6.00	0.050	0.054	-8.00
RMS%RE		*2.66*	*RMS%RE*		*2.94*
Act L Tar mol frac	Pred L TAR mol frac	L TAR rel error %	Act R CIT mol frac	Pred R CIT mol frac	R CIT rel error %
0.050	0.047	6.00	0.050	0.054	-8.00
0.150	0.153	-2.00	0.150	0.145	3.33
0.250	0.244	2.40	0.250	0.258	-3.20
0.350	0.344	1.71	0.350	0.359	-2.57
0.450	0.458	-1.78	0.450	0.446	0.89
0.550	0.546	0.72	0.550	0.567	-3.09
0.650	0.643	1.08	0.650	0.642	1.23
0.775	0.760	1.94	0.775	0.770	0.65
0.850	0.868	-2.12	0.850	0.838	1.41
0.950	0.959	-0.95	0.950	0.971	-2.21
RMS%RE		*2.50*	*RMS%RE*		*3.33*
Act S LIM mol frac	Pred S LIM mol frac	S LIM rel error %	Act S CME mol frac	Pred S CME mol frac	S CME rel error %
0.950	0.929	2.21	0.950	0.932	1.29
0.850	0.834	1.88	0.850	0.815	4.12
0.750	0.737	1.73	0.750	0.772	-2.93
0.650	0.669	-2.92	0.650	0.635	2.31
0.550	0.572	-4.00	0.550	0.571	-3.82
0.450	0.435	3.33	0.450	0.460	-2.22
0.350	0.366	-4.57	0.350	0.339	3.14
0.225	0.230	-2.22	0.225	0.212	5.78
0.150	0.163	-8.67	0.150	0.142	5.33
0.050	0.061	-22.00	0.050	0.042	16.00
RMS%RE		*7.95*	*RMS%RE*		*6.18*
Act R LIM mol frac	Pred R LIM mol frac	R LIM rel error %	Act R CME mol frac	Pred R CME mol frac	R CME rel error %
0.050	0.060	-20.00	0.050	0.059	-18.00
0.150	0.169	-12.67	0.150	0.139	7.33
0.250	0.239	4.40	0.250	0.240	4.00
0.350	0.334	4.57	0.350	0.368	-5.14
0.450	0.437	2.89	0.450	0.431	4.22
0.550	0.535	2.73	0.550	0.525	4.54
0.650	0.672	-3.38	0.650	0.623	4.15
0.775	0.743	4.13	0.775	0.808	-4.26
0.850	0.877	-3.18	0.850	0.834	1.88
0.950	0.921	3.05	0.950	0.972	-2.32
RMS%RE		*8.15*	*RMS%RE*		*7.09*

Appendix V.B Actual and predicted mole fraction of 1.0×10^{-5} M enantiomers of non-fluorescent analytes with optimum concentration of poly-L-SUF in 25:75 methanol/water.

Act S BNA mol frac	Pred S BNA mol frac	S BNA rel error %	Act S TFA mol frac	Pred S TFA mol frac	S TFA rel error %
0.877	0.866	1.25	0.850	0.845	0.59
0.826	0.825	0.12	0.783	0.772	1.40
0.715	0.713	0.28	0.700	0.710	-1.43
0.650	0.644	0.92	0.645	0.651	-0.30
0.575	0.581	-1.04	0.570	0.562	1.40
0.545	0.540	0.92	0.480	0.473	1.46
0.487	0.482	1.03	0.400	0.398	0.50
0.380	0.375	1.32	0.250	0.253	-1.20
0.285	0.290	-1.75	0.150	0.148	1.33
0.192	0.188	2.08	0.075	0.072	4.00
RMS%RE		*1.21*	*RMS%RE*		*1.70*

Act R BNA mol frac	Pred R BNA mol frac	R BNA rel error %	Act R TFA mol frac	Pred R TFA mol frac	R TFA rel error %
0.123	0.126	-2.44	0.150	0.152	-1.33
0.174	0.169	2.87	0.217	0.221	-1.84
0.285	0.287	-0.70	0.300	0.296	1.33
0.350	0.351	-0.29	0.355	0.348	1.97
0.425	0.419	1.41	0.430	0.439	-2.09
0.455	0.452	0.66	0.520	0.522	-0.38
0.513	0.515	-0.39	0.600	0.606	-1.00
0.620	0.624	-0.65	0.750	0.758	-1.07
0.715	0.711	0.56	0.850	0.847	0.35
0.808	0.803	0.62	0.925	0.930	-0.54
RMS%RE		*1.36*	*RMS%RE*		*1.34*

Act S PROP mol frac	Pred S PROP mol frac	S PROP rel error %	Act S NPRX mol frac	Pred S NPRX mol frac	S NPRX rel error %
0.950	0.958	-0.84	0.924	0.919	0.54
0.874	0.869	0.57	0.815	0.819	-0.49
0.772	0.784	-1.55	0.705	0.710	-0.71
0.650	0.641	1.38	0.670	0.664	0.90
0.550	0.556	-1.09	0.550	0.542	1.45
0.475	0.463	2.53	0.450	0.449	0.22
0.400	0.395	1.25	0.350	0.358	-2.29
0.255	0.250	1.96	0.236	0.229	2.96
0.175	0.171	2.29	0.175	0.180	-2.86
0.078	0.081	-3.85	0.078	0.075	3.85
RMS%RE		*1.96*	*RMS%RE*		*2.02*

Act R PROP mol frac	Pred R PROP mol frac	R PROP rel error %	Act R NPRX mol frac	Pred R NPRX mol frac	R NPRX rel error %
0.050	0.052	-4.00	0.076	0.078	-2.63
0.126	0.123	2.38	0.185	0.181	2.16
0.228	0.231	-1.32	0.295	0.287	2.71
0.350	0.358	-2.29	0.330	0.321	2.72
0.450	0.457	-1.56	0.450	0.439	2.44
0.525	0.520	0.95	0.550	0.545	0.91
0.600	0.592	1.33	0.650	0.637	2.00
0.745	0.738	0.94	0.764	0.759	0.65
0.825	0.837	-1.45	0.825	0.830	-0.61
0.922	0.926	-0.43	0.922	0.929	-0.76
RMS%RE		*1.92*	*RMS%RE*		*1.96*

Appendix V.C   Actual and predicted mole fraction of 1.0×10^{-5} M enantiomers of fluorescent analytes with optimum concentration of poly-L-SUF in 75:25 methanol/water.

Act D TAR mol frac	Pred D TAR mol frac	D TAR rel error %	Act S CIT mol frac	Pred S CIT mol frac	S CIT rel error %
0.950	0.932	1.89	0.950	0.961	-1.16
0.850	0.844	0.71	0.850	0.843	0.82
0.750	0.746	0.53	0.750	0.759	-1.20
0.650	0.652	-0.31	0.650	0.661	-1.69
0.550	0.543	1.27	0.550	0.542	1.45
0.450	0.445	1.11	0.450	0.447	0.67
0.350	0.358	-2.29	0.350	0.346	1.14
0.225	0.230	-2.22	0.225	0.228	-1.33
0.150	0.144	4.00	0.150	0.148	1.33
0.050	0.052	-4.00	0.050	0.047	6.00
RMS%RE		*2.22*	*RMS%RE*		*2.23*
Act L Tar mol frac	Pred L TAR mol frac	L TAR rel error %	Act R CIT mol frac	Pred R CIT mol frac	R CIT rel error %
0.050	0.047	6.00	0.050	0.053	-6.00
0.150	0.152	-1.33	0.150	0.154	-2.67
0.250	0.247	1.20	0.250	0.246	1.60
0.350	0.346	1.14	0.350	0.355	-1.43
0.450	0.452	-0.44	0.450	0.448	0.44
0.550	0.559	-1.64	0.550	0.538	2.18
0.650	0.648	0.31	0.650	0.644	0.92
0.775	0.771	0.52	0.775	0.769	0.77
0.850	0.860	-1.18	0.850	0.861	-1.29
0.950	0.961	-1.16	0.950	0.942	0.84
RMS%RE		*2.16*	*RMS%RE*		*2.38*
Act S LIM mol frac	Pred S LIM mol frac	S LIM rel error %	Act S CME mol frac	Pred S CME mol frac	S CME rel error %
0.950	0.941	0.95	0.950	0.941	0.95
0.850	0.861	-1.29	0.850	0.837	1.53
0.750	0.737	1.73	0.750	0.760	-1.33
0.650	0.641	1.38	0.650	0.642	1.23
0.550	0.537	2.36	0.550	0.539	2.00
0.450	0.436	3.11	0.450	0.462	-2.67
0.350	0.341	2.57	0.350	0.337	3.71
0.225	0.232	-3.11	0.225	0.235	-4.44
0.150	0.140	6.67	0.150	0.145	3.33
0.050	0.055	-10.00	0.050	0.044	12.00
RMS%RE		*4.28*	*RMS%RE*		*4.54*
Act R LIM mol frac	Pred R LIM mol frac	R LIM rel error %	Act R CME mol frac	Pred R CME mol frac	R CME rel error %
0.050	0.056	-12.00	0.050	0.044	12.00
0.150	0.158	-5.33	0.150	0.142	5.33
0.250	0.241	3.60	0.250	0.239	4.40
0.350	0.339	3.14	0.350	0.363	-3.71
0.450	0.435	3.33	0.450	0.462	-2.67
0.550	0.531	3.45	0.550	0.538	2.18
0.650	0.667	-2.62	0.650	0.643	1.08
0.775	0.751	3.10	0.775	0.764	1.42
0.850	0.870	-2.35	0.850	0.860	-1.18
0.950	0.933	1.79	0.950	0.962	-1.26
RMS%RE		*4.93*	*RMS%RE*		*4.73*

Appendix V.D Actual and predicted mole fraction of 1.0×10^{-5} M enantiomers of non-fluorescent analytes with optimum concentration of poly-L-SUF in 75:25 methanol/water.

VITA

Alicia was born in Lafayette, Louisiana, to Paul and Pemella Williams. She attended St. Ignatius School in Grand Coteau, Louisiana, before moving to Sts. Leo-Seton in Lafayette, Louisiana, for the remainder of her elementary education. Her high school education was in Arnaudville, Louisiana, at Beau Chene High School, where she graduated in 1998 at the top of her senior class. During high school, she attended summer school programs at Xavier University of Louisiana in New Orleans, Louisiana, including *Stress on Analytical Reasoning-Project SOAR* (summer of 1996) and *Howard Hughes* (summer of 1997). Thereafter, she received her Bachelor of Science (*Summa Cum Laude*) in chemistry with a minor in mathematics and a concentration in German from Xavier University (May 2002). As an undergraduate student, Alicia began her career as a research assistant while participating in the *Minority Access to Research Careers (MARC) Program*. She received numerous awards and honors during her undergraduate study, one of the most notable being the *Rohm & Haas Undergraduate Research Award*. During one of her undergraduate summer research programs, she met Dr. Isiah M. Warner, who later became her graduate school adviser at Louisiana State University in Baton Rouge, Louisiana. In June 2002, Alicia began her graduate studies as an analytical chemist and she received several honors during her graduate career, including the *Graduate Alliance for Education in Louisiana Dissertation Writing Fellowship (GAELA)*, *Procter & Gamble Research and Technical Careers in Industry (RTCI)* recipient, *Procter & Gamble Enhancement Award*, *Southern Regional Education Board (SREB)* scholar, *David & Lucile Packard Foundation* grant recipient, *Huel Perkins Fellowship* recipient. Before completing her graduate studies, Alicia was presented with the *James W. Robinson Outstanding Research in Analytical Sciences Award* by the Louisiana State University department of chemistry. Alicia graduated with the degree of

Doctor of Philosophy in chemistry from Louisiana State University in December 2007.

Publications and conference presentations during her graduate career include:

Williams, Alicia A.; Fakayode, Sayo O.; Huang, Xiaodong; Warner, Isiah M.; "Use of Multivariate Analysis for Optimization of Separation Parameters and Prediction of Migration Time, Resolution and Resolution Normalized Migration Time in Micellar Electrokinetic Chromatography"; Electrophoresis (2006), 27, 4127-4140.

Fakayode, Sayo O.; **Williams, Alicia A.**; Busch, Marianna A.; Busch, Kenneth W.; and Warner, Isiah M.; :The Use of Poly(sodium *N*-Undecanoyl-L-leucylvalinate), Poly(sodium *N*-Undecanoyl-L-leucinate) and Poly(sodium *N*-Undecanoyl-L-valinate) Surfactants as Chiral Selectors For Determination of Enantiomeric Composition of Samples by Multivariate Regression Modeling of Fluorescence Spectral Data"; Journal of Fluorescence (2006), 16(5), 659-670.

Williams, Alicia A.; Fakayode, Sayo O.; Alptürk, Onur; Jones, Christina M.; Lowry, Mark; Strongin, Robert M.; Warner, Isiah M.; "Determination of Enantiomeric Compositions of Analytes Using Novel Fluorescent Chiral Molecular Micelles and Steady State Fluorescence Measurements"; Journal of Fluorescence, *accepted September 2007*.

Williams, Alicia A.; Fakayode, Sayo O; Warner, Isiah M.; "Poly(sodium *N*-undecanoyl-L-phenylalaninate): A Versatile Chiral Selector for the Determination of Enantiomeric Composition of Fluorescent and non-Fluorescent Chiral Molecules Using Steady-State Fluorescence Spectroscopy"; Chirality, *submitted October 2007*.

2006 – July 15th Oral Presentation "Use of Multivariate Analysis for Optimization of Separation Parameters and Prediction of Migration Time, Resolution and Resolution Normalized Migration Time in Micellar Electrokinetic Chromatography"; **Alicia A. Williams**, Sayo O. Fakayode; Xiaodong Huang; Isiah M. Warner – American Association for the Advancement of Science (AAAS) – Washington DC.

2005 – August 28th Oral Presentation "Use of Experimental Design to Model Separation Parameters in Micellar Electrokinetic Chromatography"; **Alicia A. Williams**, Sayo O. Fakayode, Isiah M. Warner **-** American Chemical Society Meeting & Exposition - Washington DC.

2005 – February 25th Poster Presentation "Separation of Phenolic Acid Standards and Plant Phenolic Compounds Using HPLC and Ionic Liquids as Modifiers in MEKC"; **Alicia A. Williams**, Jane I. Murungi, Isiah M. Warner - Pittsburgh Conference (PITTCON® 2005) – Orlando, FL.

2004 – July 17th Poster Presentation, "Optimization of Extraction Methods for *Maytenus obscura*"; **Alicia A. Williams**, Unique J. Luna, Jane I. Murungi, Isiah M. Warner - David and Lucille Packard Foundation/American Association for the Advancement of Science (AAAS) - Washington DC.